Development and Application of Embedded Methods to Strongly and Weakly Correlated Systems

Von der Fakultät Chemie der Universität Stuttgart zur Erlangung der Würde eines Doktors der Naturwissenschaften (Dr. rer. nat.) genehmigte Abhandlung

Vorgelegt von

Eugenio Vitale

aus Rom, Italien

Hauptberichter:	Prof. Dr. Ali Alavi
Mitberichter:	P.D. Dr. Daniel Kats
Mitberichter:	Prof. Dr. Andreas Köhn
Prüfungsvorsitzender:	Prof. Dr. Rainer Niewa

Tag der mündlichen Prüfung: 20. Juli 2022

Max-Planck Institut für Festkörperforschung

Institut für Theoretische Chemie
der Universität Stuttgart

2022

Contents

List of Acronyms

CAS	Complete Active Space
CAS-CI	Complete Active Space - Configuration Interaction
CASPT2	Complete Active Space with second-order Perturbation Theory
CASSCF	Complete Active Space Self Consistent Field
CC	Coupled Cluster
CCD	Coupled Cluster with doubles
CCSD	Coupled Cluster with singles and doubles
CCSD(T)	Coupled Cluster with singles and doubles plus perturbative triples
CI	Configuration Interaction
DC	Distinguishable Cluster
DCSD	Distinguishable Cluster with singles and doubles
DFT	Density Functional Theory
FCC	Full Coupled Cluster
FCI	Full Configuration Interaction
FCIQMC	Full Configuration Interaction Quantum Monte Carlo
FeP	Iron(II)-Porphyrin
GTO	Gaussian Type Orbital
HF	Hartree Fock
LMCT	Ligand to Metal Charge Transfer
MO	Molecular Orbital
MR	Multi Reference
MRCI	Multi Reference Configuration Interaction
MRCI+Q	Multi Reference Configuration Interaction with Davidson correction
MRCISD	Multi Reference Configuration Interaction with singles and doubles
NO	Natural Orbital
NPE	Non-Parallelity Error
PEC	Potential Energy Curve
QC	Quantum Chemistry

QMC	Quantum Monte Carlo
RHF	Restricted Hartree Fock
ROHF	Restricted Open-shell Hartree Fock
SD	Slater Determinant
SR	Single Reference
STO	Slater Type Orbital
TCC	Tailored Coupled Cluster
TCCSD	Tailored Coupled Cluster with singles and doubles
TCCSD(T)	Tailored Coupled Cluster with singles and doubles plus perturbative triples
TDC	Tailored Distinguishable Cluster
TDCSD	Tailored Distinguishable Cluster with singles and doubles
TM	Transition Metal

Abstract

Coupled cluster (CC) theory is a popular and reliable tool in quantum chemistry due to its improvable hierarchy of methods able to rapidly converge to the full configuration interaction (FCI) limit in weakly correlated systems. Although it represents one of the most efficient single reference (SR) methods to treat many-body correlations with high accuracy and reliable outcomes, it yields qualitatively erroneous results when applied to strongly correlated systems (e.g., at molecular dissociations or in other highly degenerate situations).

The conventional approach employed in such strongly correlated problems is the multi-reference (MR) methods. The latter give the possibility to provide qualitatively correct results giving a good description of the static correlation energy. The conventional first step in MR strategies is represented by the complete active space self consistent field (CASSCF). In the latter method, a FCI is applied on a fragment of the total orbitals of the system, the so called active space, together with a self-consistent orbital optimization. However, the complexity and computational cost of MR methodologies are comparably high and makes the SR-based approaches more appealing. An interesting option is given by the corrected CC methods. The latter consist of modifications of the canonical CC approach, where specific corrections are applied. These corrections can be divided into two categories, *internally* (*ic*) and *externally* (*ec*) corrected CC methods. In the present work, a focus on one *ic*CC method is given in combination with an *ec*CC method. The *ic*CC technique is given by the Distinguishable Cluster (DC) method. This DC approach was first established a decade ago as a small modification of the CC with dobules (CCD) amplitude equations and it has been shown to reach a qualitatively correct description in strongly correlated systems. Besides that, DC increases also the accuracy in weakly correlated regimes in comparison with CC. The *ec*CC technique is represented by the tailored CC (TCC) method. This TCC approach was also established some years back in order to decrease the CC sensitivity to static correlation. The idea is to make use of the typical split-amplitude ansatz of CC to introduce external cluster amplitudes, which take care of the static correlation energy of the system. This separation is done at the orbital level, as in CASSCF.

Within this thesis, the Distinguishable Cluster method is combined with FCI Quantum Monte Carlo (FCIQMC) in order to present a new tailored approach, the tailored DC (TDC). The reasons which support this new TDC approach are given by two considerations. First, the enhanced stability and accuracy of DC are expected also in the tailored formalism. Second, the large CI solver provided by FCIQMC can be useful to alleviate the two main known drawbacks of the tailored approach, i.e. the bias towards a single reference determinant and the missing relaxation of the external amplitudes.

The resulting approach is more accurate than the corresponding tailored coupled cluster and the pure distinguishable cluster. To demonstrate this, the method is first benchmarked with a variety of test cases and then further evaluated with spin gaps computation in a few Fe(II) complexes. The systematic improvability of the TDC method is shown as the active space is increased. Further, a perturbative F12 correction is considered, which remarkably enhances the basis set convergence.

Additionally, the inclusion of triple excitations in the tailored DC approach has been studied. The further correction given by the triple external amplitudes speeds up the convergence with respect to the active-space size.

In the last part of the thesis, a further embedding scheme to treat strong correlation effects is evaluated. Specifically, the development and application of a screened Coulomb formalism is discussed. Here, a subsystem is again defined at the orbital level and its integrals are screened as a result of the introduction of a screened fluctuation density. This simple approach inspired by Random Phase approximation (RPA) shows to be extremely efficient in the dissociation of one- and two-dimensional hydrogen systems.

Zusammenfassung

Die Coupled Cluster (CC) Theorie ist ein beliebtes und zuverlässiges Werkzeug in der Quantenchemie, da sie eine verbesserte Hierarchie von Methoden bietet, die in schwach korrelierten Systemen schnell zur Grenze der Full Configuration Interaction (FCI) konvergieren können. Obwohl es eine der effizientesten Single Reference (SR) Methoden darstellt, um Vielteilchenkorrelationen mit hoher Genauigkeit und zuverlässigen Ergebnissen zu behandeln, liefert es qualitativ fehlerhafte Ergebnisse, wenn es auf stark korrelierte Systeme angewendet wird (z. B. bei molekularen Dissoziationen oder in anderen hochgradig entarteten Situationen).

Die konventionellen Ansätze, welche bei solchen stark korrelierten Problemen angewendet wird, sind die multi reference (MR) Methoden. Letztere bieten die Möglichkeit, qualitativ korrekte Ergebnisse zu liefern, die eine gute Beschreibung der statischen Korrelationsenergie liefern. Der konventionelle erste Schritt in MR-Strategien wird durch das Complete Active Space Self Consistent Field (CASSCF) dargestellt. Bei letzterem Verfahren wird ein FCI auf ein Fragment der Gesamtorbitale des Systems, dem sogenannten aktiven Raum, zusammen mit einer selbstkonsistenten Orbitaloptimierung angewendet. Die Komplexität und der Rechenaufwand von MR-Methoden sind jedoch vergleichsweise hoch und machen die SR-basierten Ansätze attraktiver. Eine interessante Option bieten die korrigierten CC-Methoden. Diese bestehen aus Modifikationen des kanonischen CC-Ansatzes, bei denen spezifische Korrekturen vorgenommen werden. Diese Korrekturen können in zwei Kategorien unterteilt werden, *internally* (*ic*) und *externally* (*ec*) korrigierte CC-Methoden. In der vorliegenden Arbeit wird ein Fokus auf eine *ic*CC Methode in Kombination mit einer *ec*CC Methode gelegt. Die *ic*CC-Technik wird durch die Distinguishable Cluster (DC) Methode gegeben. Dieser DC-Ansatz wurde erstmals vor einem Jahrzehnt als kleine Modifikation der CC with doubles (CCD) Amplitudengleichungen etabliert und erreicht nachweislich eine qualitativ korrekte Beschreibung in stark korrelierten Systemen. Außerdem erhöht DC auch die Genauigkeit in schwach korrelierten Regimen im Vergleich zu CC. Die *ec*CC-Technik wird durch die Tailored CC (TCC) -Methode dargestellt. Dieser TCC-Ansatz wurde auch vor einigen Jahren etabliert, um die CC-Sensitivität gegenüber statischer Korrelation zu verringern. Die Idee ist, den typischen Split-Amplitude-Ansatz von

CC zu nutzen, um externe Clusteramplituden einzuführen, die sich um die statische Korrelationsenergie des Systems kümmern. Diese Trennung erfolgt wie bei CASSCF auf Orbitalebene.

In dieser Arbeit wird die Distinguishable Cluster-Methode mit FCI Quantum Monte Carlo (FCIQMC) kombiniert, um einen neuen maßgeschneiderten Ansatz, den Tailored DC (TDC), vorzustellen. Die Gründe, die diesen neuen TDC-Ansatz unterstützen, werden durch zwei Überlegungen gegeben. Erstens wird die verbesserte Stabilität und Genauigkeit von DC auch im maßgeschneiderten Formalismus erwartet. Zweitens kann der von FCIQMC bereitgestellte große CI-Löser nützlich sein, um die beiden bekannten Hauptnachteile des maßgeschneiderten Ansatzes zu mildern, nämlich die Tendenz zu einer einzelnen Referenzdeterminante und die fehlende Relaxation der externen Amplituden.

Der resultierende Ansatz ist genauer als das entsprechende maßgeschneiderte gekoppelte Cluster und das rein unterscheidbare Cluster. Um dies zu demonstrieren, wird die Methode zunächst mit einer Vielzahl von Testfällen verglichen und anschließend mit Spinlücken-Berechnungen einiger Fe(II)-Komplexe weiter evaluiert. Die systematische Verbesserbarkeit der TDC-Methode wird gezeigt, je mehr der aktive Raum vergrößert wird. Ferner wird eine störende F12-Korrektur in Betracht gezogen, die die Basissatzkonvergenz bemerkenswert verbessert.

Zusätzlich wurde die Einbeziehung von Dreifachanregungen in dem maßgeschneiderten DC-Ansatz untersucht. Die weitere Korrektur durch die dreifachen externen Amplituden beschleunigt die Konvergenz in Bezug auf die Aktivraumgröße.

Im letzten Teil der Arbeit wird ein weiteres Einbettungsschema zur Behandlung starker Korrelationseffekte evaluiert. Konkret wird die Entwicklung und Anwendung eines gerasterten Coulomb-Formalismus diskutiert. Hier wird wiederum ein Subsystem auf Orbitalebene definiert und dessen Integrale durch die Einführung einer gerasterten Fluktuationsdichte untersucht. Dieser einfache Ansatz, der von der Random Phase approximation (RPA) inspiriert ist, erweist sich als äußerst effizient bei der Dissoziation von ein- und zweidimensionalen Wasserstoffsystemen.

Acknowledgements

First and foremost, I want to express my deep and sincere gratitude to Daniel Kats for his constant support and guidance during my PhD. His availability for spontaneous discussions resulted in countless scientific talks, where I could always admire his clear logical thinking. All of this gave me great support to carry on with my research and made the last four years an enjoyable time.

I would also like to thank Ali Alavi, whose passion and deep knowledge of our research field have been inspiring for me. I am very grateful for the opportunity to join an outstanding research environment such as our group. Here, I felt welcome from the very first moment and for this, I would like to thank all the group members. The innumerable conversations triggered at the coffee corner made me laugh and learn a lot. Especially, I would like to mention Werner Dobrautz and Kai Guther, whose help during my first steps as PhD and the first approach to the NECI code has been invaluable, and Giovanni Li Manni, whose explanations gave me many insights into chemistry throughout my time here. Further, the additional involvement in conferences or experiences out of the office were made memorable by people such as Oskar, Kesha, Thomas, Niklas and Ke. Thanks also to the colleagues who gave me suggestions and spent time proofreading my thesis, such as Pradipta and Thomas. Particular recognition goes to Thomas, who helped me in this PhD thesis's last important bureaucratic step.

Last but not least, I want to thank my family, who always supported me throughout all my studies, especially my mother, and my new family, whose recent new member gave me countless days (and nights) to take my mind away from my PhD. All of this would not have been possible without my better half. This is for you.

Part I

Introduction

"*It was almost three o'clock in the morning before the final result of my computations lay before me. The energy principle had held for all the terms, and I could no longer doubt the mathematical consistency and coherence of the kind of quantum mechanics to which my calculations pointed. At first, I was deeply alarmed. [...] I was far too excited to sleep and so, as a new day dawned, I made for the southern tip of the island, where I had been longing to climb a rock jutting out into the sea. I now did so without too much trouble, and waited for the sun to rise.* " [1, 2] These are the thoughts of Werner Heisenberg in 1925 on the Helgoland island in the North Sea, after he had just developed the basis of a new quantum mechanical formalism [3].

Until that moment, this young physicist, and the world of modern physics, had been continuously trying to devise a new theory able to describe nature at the atomic level. Indeed, in those critical years it became undeniable how the old Newtonian mechanics was not rigorously applicable to processes at the atomic scale. This was made evident at the beginning of the twentieth century through different studies. One of all, considered the birth of Quantum Theory, was proposed in the famous lecture by Max Planck on 14th of December 1900 before the "Physikalische Gesellschaft" (i.e. Physical Society). For the first time, the black-body radiation was explained by emission and absorption of discrete portions of energy [4]. From that moment on, many different scientists, such as Einstein (with his photoelectric effect interpretation [5]), Rutherford (with his explanation of the atomic structure [6, 7]), or Bohr (with his synthesis of Rutherford's atom model with Planck's quantum hypothesis [8–10]), to name a few, shed light on the path toward a new mechanics, which saw a turning point with Heisenberg in 1925.

After that trip to Helgoland, the work on the theory was further encouraged by Heisenberg's colleague Wolfgang Pauli. In Göttingen, together with Max Born and Pascual Jordan, this theory began to take shape [11]. At the same time, in Cambridge, Paul Dirac developed the same theory with a more general mathematical formalism [12]. In only a few months, these concentrated efforts led to a new coherent mathematical framework, which was then ready to be applied. A formal proof was demonstrated by Pauli [13], showing that the matrix theory of Heisenberg, Born and Jordan gives energy values that match the hydrogen spectrum as supposed by Bohr [14]. Finally, the results were perfect. The "Knabenphysik" (i.e. the Boys Physics, so called in Göttingen because the main authors, except Max Born, are all about twenty years old) proved its power and convinced most physicists that the new theory is correct.

The next fundamental step forward was given by Erwin Schrödinger in 1926 [15]. He introduced the wave-particle duality into quantum mechanics, giving rise to the

best known differential formalism [a] and he demonstrated that his wave mechanics was mathematically equivalent to Heisenberg's matrix theory. Although the Schrödinger equation can be seen as the quantum counterpart of Newton's second law, the accurate predictions obtained in classical mechanics are far from being also maintained in the quantum realm. Indeed, solving exactly this equation is an exponentially hard problem. Analytic solutions of it are only possible in a limited number of quantum systems [17]. Hence, numerical solutions are to be found by means of approximated methods, whose goal is to keep the crucial physical character of the system, whereas the computational cost decreases to an acceptable expense. Computational Quantum Chemistry (QC) is the branch that is concerned with producing these approximate numerical solutions with, in principle, any desired degree of accuracy.

The fundamental goal of QC is to solve the time-independent Schrödinger equation in order to provide reliable information about the properties of molecules and their reactions. QC can grant a number of advantages over experimental techniques. For example, in cases where the experiments can be difficult or even dangerous (due to materials that might need to be cautiously handled). However, the combination with experiments remains crucial. On the one hand, QC can be a key validation of experimental results with no obvious interpretation. On the other hand, it can play an important role in understanding chemical mechanisms which arise too fast for experiments to follow. The bottom line shows a field able to help explain the endless chemical questions emerging from different systems of interest.

Numerical solutions of the time-independent Schrödinger equation are obtained by means of several different approximations. The best known was introduced by Born and Oppenheimer [18]. The latter considers the motion of electrons and nuclei decoupled. The physical basis is the fact that the mass of an atomic nucleus is much larger than the mass of an electron (more than 1000 times). Consequently, the electronic problem can first be solved with nuclei positions as fixed parameters and the nuclei problem can then be determined in a subsequent step. However, even with this approximation in place, the task of solving the Schrödinger equation remains arduous.

$Ab-initio$ methods, or first principles, are those approaches that try to solve the electronic Schrödinger equation with no inputs but physical constants, such as positions of nuclei and number of electrons. The most straightforward $ab-initio$ calculation is given by the Hartree-Fock (HF) method [19–22], where an N-electron wave function is

[a] Legend has it that Schrödinger devised this new formalism while he was in a chalet in the Swiss Alps, where he secretly went with his affair. There he studied the thesis about matter waves of Louis de Broglie [16], which was suggested by Einstein.

described by a single reference (SR) configuration given by a Slater determinant, which is one convenient way to ensure the antisymmetric nature of the wave function. HF theory represents a landmark in the QC field. Indeed, a straightforward but efficient idea makes the HF method already qualitatively correct for a wide range of systems. Here, the problematic electron-electron interaction is approximated by a mean-field potential. The many-body problem is turned into a many one-body problem. Hence, the computational cost is dramatically reduced.

Despite its validity, the HF method was little used until 1950s. Indeed, since the very first quantum chemical application [b], QC received the necessary support only with the advent of computers. However, HF could still lead to large deviations from experimental results due to its neglect of electron correlation. The missing instantaneous Coulombic electron-electron repulsion gives the so called dynamic correlation. Nevertheless, a variety of different approaches have been developed using HF as a reasonable starting point. The latter are commonly known as post-HF methods.

The natural improvement upon HF regards the construction of the many electron wave function by a mix of different Slater determinants. The latter are generated on top of the HF wave function taken as a reference, so they are called SR methods. Two of the most representative post-HF SR methods are certainly configuration interaction (CI) [24] and coupled cluster (CC) [25–28] techniques. The former presents a wave function that is comprised of a linear combination of several Slater determinants, obtained as excitations from a reference determinant, usually HF. The latter makes use of an exponential *ansatz*, where an excitation operator gives rise to the excited functions of the reference determinant. These two different approaches lead to a formally equivalent wave function, if all possible excitations from the reference determinant are considered, i.e. full CI (FCI) and full CC (FCC). Indeed, the exact wave function is supposed to be the same, regardless of the parametrization used. However, these full methods are quite impractical unless small systems are under study. For this reason, usual quantum chemical applications adopt truncated CI/CC methods, i.e. those where the number of excited determinants is intentionally reduced to achieve a computationally affordable calculation. In that respect, CC is advantageous with its products of excitations, because, in comparison with the CI wave function, it accounts for additional terms at every excitation level. Indeed, CC became popular for its hierarchy of methods able to rapidly converge to the FCI limit in weakly correlated systems. For instance, CC with

[b] The conventional beginning of QC is set by the study from Heitler and London in 1927 [23], where the potential energy curve of the hydrogen molecule is calculated using the Schrödinger equation.

singles and doubles plus perturbative triples, CCSD(T) [29], is considered the "gold standard" in QC for its accurate prediction of properties in small systems.

Although CC seems to achieve already good accuracy, there is a class of chemical systems where truncated CC is not able to recover the necessary electron correlation. The latter is usually characterized by the so called static (or non-dynamic) correlation, which is a typical lack of SR methods. These systems need to be supported by qualitatively correct reference wave functions, where the complexity of similarly weighted most-important configurations can be adequately represented.

These multi-reference (MR) systems constitute one of the challenging problems of QC. Conventionally, they are addressed by approaches that rely on multiple determinants as reference wave functions, i.e. MR methods. The ability of the single determinant HF method to give a qualitatively correct description (in weakly correlated systems) is here extended to strongly correlated environments. MR methods do not aim to recover large fractions of the correlation energy of a given system, but rather to include the important additional determinants. One of the conventional first steps in MR strategies is the Complete Active Space Self-Consistent Field method [30–34]. Here, a selection of electronic configurations is obtained by the definition of an active orbital space, where not only the CI coefficients are optimized (such as FCI), but the orbitals used to build the determinants are also optimized. Indeed, if the multiconfiguration is reduced to only one determinant, the method would simply correspond to HF. However, the exponential scaling makes the computational cost unbearable already at small active spaces (approximately 18 electrons in 18 orbitals), as for FCI. The latter is the main limit of such a methodology and it has been the object of several studies focused on the development of approximations able to maintain the same accurate MR description at a lower computational cost. The density matrix renormalization group (DMRG) [35–41] and the full configuration interaction quantum Monte Carlo (FCIQMC) [42–46] are representatives of such approximate methods with their CASSCF versions, i.e. DMRG-SCF [47–49] and Stochastic-CASSCF [50].

Nevertheless, the idea of treating both kind of correlation effects without leaving the inexpensive SR CC framework has been very attractive in the past years. This research branch saw the very first attempts almost forty years ago but recently showed a renewed interest. Generally, these approaches can be divided into two main classes, *internally* and *externally* corrected CC methods [51].

The *internally* corrected CC (*ic*CC) methods are based on possible modifications of certain cluster components, such as cancellations or additions of terms in the amplitude

equations. Several different *ic*CC methods have been developed since the first attempts. For example, approximate coupled pair (ACP) [52], approximate coupled-cluster doubles (ACCD) [53], ACP with quadruples (ACPQ) [54–57], *n*CC hierarchy [58], parametrized coupled-cluster (pCCSD) [59], quasi-variational CC [60] or distinguishable cluster (DC) [61–63] methods. The latter is the only *ic*CC method treated in the present work. It has been introduced as a small modification of the double amplitude equation. In the last decade, it has been established as a helpful approach able to qualitatively describe strongly correlated systems. Further, it has been shown in numerous studies that DC with singles and doubles (DCSD) outperforms CCSD in both weakly and strongly correlated systems [64–70].

The *externally* corrected CC (*ec*CC) methods are based on the inclusion of an external source of cluster amplitudes, such as the one- and two-body clusters, or higher than pair clusters. This class of approximated methods is supported by the fact that the CC wave function can be expressed in the split-amplitude *ansatz* [71, 72]. They rely on a high accuracy calculation as an external source in order to alleviate the lack of static correlation typical in CC. Many different *ec*CC methods have been established in the past years, giving rise to further applicability of approximated SR CC methods. To name a few, valence-bond corrected CC [73, 74], reduced MR CCSD (RMR-CCSD) [75, 76], CAS-CI and CASSCF based ecCCSD [77–79] or tailored CC (TCC) [80]. The latter is also treated extensively in the present work in combination with the DC approach. It has been introduced as a convenient method to describe potential energy curves (PECs) of simple molecules in a far more accurate way than conventional truncated CC [80]. At first, TCC defines an active space where an FCI is performed. In the subsequent step, the resulting CAS amplitudes for singles and doubles are kept frozen, while all the amplitudes of the remaining orbitals are relaxed using the CC amplitude equations. Finally, its affordable computational cost and generally improvable approach make this method an interesting candidate for further studies.

In the present work, the main focus is on the development and application of the tailored distinguishable cluster (TDC) approach. The latter is obtained by the combination of the icCC method DC and the ecCC method TCC. In this new approach, the two typical drawbacks that usually afflict the tailored formalism, i.e. the bias towards a specific reference determinant and the missing relaxation of the CAS amplitudes, are tried to be alleviated. On the one hand, the qualitatively correct description of strong electron correlation by DCSD can be beneficial for the former drawback. On the other hand, mitigation of these disadvantages can be obtained by the inclusion of

large active spaces, which is especially indicated when multiple bonds are broken [51]. In that respect, different solutions have been proposed to adjust TCC. One among all, showing promising outcomes, involves the DMRG as the external source [81–83]. Our method of choice is FCIQMC, which guarantees the possibility of studying active spaces well beyond a deterministic FCI would allow [84].

Finally, the DCSD method merged with a competitive external source such as FCIQMC makes the new approach able to extend the applicability of the tailored formalism to a wide class of systems. Further, including always larger active spaces allows to consistently obtain more accurate results, as long as computationally possible.

Part of the present work is also focused on a screened embedding formalism inspired by the random phase approximation (RPA). The introduction of screened integrals into an embedded system enables to get additional information regarding the entire system. This formalism is applied to the DCSD and TDCSD methods in order to study molecular dissociation through PECs. Indeed, dissociated geometries produce quasi-degenerate electronic configurations, which are not properly described by a SR wave function. Simplified models have been devised in order to study strong correlation effects, such as various configurations of hydrogen atoms in simple H_n molecules. These benchmark quantum chemical systems have a crucial influence in further understanding the leading physical mechanisms behind these effects. They are here analyzed to assess the validity of the proposed screened embedding.

This thesis adopts the following structure. In Part II, the basic concepts regarding the theory and methods relevant to this thesis are explained. In Part III, the results coming from the newly developed embedded methods are presented and discussed. In Part IV, a summary of the main achievements of this thesis is outlined. In Part V, an Appendix with details related to further theoretical concepts is given.

Part II

Theory

Chapter 1

Quantum Many-Body Problem

The advent of quantum mechanics made clear how light particles, namely smaller than the mass of a proton, behave differently than heavier objects. Indeed, at the atomic size, the matter-wave duality becomes significant [a]. This duality is remarkably expressed by the Schrödinger equation (the non-relativistic version is shown, since no particles moving at a meaningful fraction of the speed of light are considered in this work),

$$i\hbar\frac{\partial}{\partial t}\Psi(\mathbf{x},t) = \hat{H}\Psi(\mathbf{x},t) \tag{1.1}$$

where i is the imaginary unit, $\hbar$ is the Planck's constant divided by 2π and $\hat{H}$ is the corresponding operator of the classical Hamiltonian which characterizes the energy of the system. Indeed, these linear Hermitian operators are the replacements of classical functions of coordinate and momentum. $\Psi(\mathbf{x},t)$ is the position-space wave function that completely describes a quantum system. This function, which depends on space, spin coordinates and time, carries all the physical information about the system. It replaces the classical notion of trajectories with the probabilistic interpretation of quantum mechanics. Indeed, $|\Psi(\mathbf{x},t)|^2$ represents the probability to find the system in a certain configuration $\mathbf{x}$ at a specific time t (so not anymore an exact prediction of where the particles are at a certain time). However, only the stationary states, such as the ground state, are of interest in this study, so the time-independent Schrödinger equation will be assumed throughout this work unless otherwise noted,

$$\hat{H}\Psi(\mathbf{x}) = E\Psi(\mathbf{x}). \tag{1.2}$$

Here, E represents the energy eigenvalue associated with the eigenstate $\Psi(\mathbf{x})$.

[a] As suggested by the De Broglie hypothesis, $\lambda = h/p$ (where λ is the wavelength, h the Planck constant and p the momentum), for macroscopic particles the mass is usually so large that the short wavelengths do not show prevalent wave properties.

QC problems consist of interactions between atoms or molecules, namely between electrons and nuclei. Therefore, the resulting eigenvalue problem can be defined with the non-relativistic molecular Hamiltonian written as the summation of kinetic and potential energy of these two type of particles,

$$\hat{H} = -\sum_i \frac{1}{2}\nabla^2_{\mathbf{r}_i} - \sum_I \frac{1}{2m_I}\nabla^2_{\mathbf{R}_J} + \sum_{i,j>i} \frac{1}{|\mathbf{r}_i - \mathbf{r}_j|} + \sum_{I,J>I} \frac{Z_I Z_J}{|\mathbf{R}_I - \mathbf{R}_J|} - \sum_{i,J} \frac{Z_J}{|\mathbf{r}_i - \mathbf{R}_J|}. \quad (1.3)$$

The lower and the upper case letter r represent the position of electrons and nuclei, respectively. Further, m_I and Z_I correspond to the mass and charge of a nucleus (while the mass and charge of the electron are not explicitly shown since atomic units [85] are in place here and in the rest of this work).

1.1 Born-Oppenheimer Approximation

The Born-Oppenheimer approximation was introduced in 1927 [18] and represents a cornerstone in QC. In this approximation the degrees of freedom of electrons and nuclei are decoupled based on the large difference between their mass. Indeed, the nuclei are sufficiently heavy that quantum effects are very small, while electrons are too light to be described by classical mechanics. This difference in mass would then correspond to electrons so much faster than nuclei that they could adjust almost immediately to every change in the nuclear geometry. From this follows a convenient way to represent the wave function into a nuclear (subscript n) and electronic (subscript e) part,

$$\Psi(\mathbf{r}, \mathbf{R}) = \Psi_e(\mathbf{r})\Psi_n(\mathbf{R}). \quad (1.4)$$

However, the electronic wave function will still depend on nuclear coordinates but as parameters instead of variables. In the same way the Hamiltonian operator can be split into the electronic and nuclear parts giving rise to the following equations,

$$\left[-\sum_i \frac{1}{2}\nabla^2_{\mathbf{r}_i} + \sum_{i,j>i} \frac{1}{|\mathbf{r}_i - \mathbf{r}_j|} - \sum_{i,J} \frac{Z_J}{|\mathbf{r}_i - \mathbf{R}_J|}\right] \Psi_e(\mathbf{r}) = E_e(\mathbf{R})\Psi_e(\mathbf{r}) \quad (1.5)$$

$$\left[-\sum_I \frac{1}{2m_I}\nabla^2_{\mathbf{R}_J} + \sum_{I,J>I} \frac{Z_I Z_J}{|\mathbf{R}_I - \mathbf{R}_J|} + E_e(\mathbf{R})\right] \Psi_n(\mathbf{R}) = E_{tot}\Psi_n(\mathbf{R}). \quad (1.6)$$

These two equations must be solved in the shown order such that the electronic energy, $E_e(\mathbf{R})$, is assumed as an external potential in the nuclear equation 1.6. Further, the

latter equation would then provide with the final total energy of the system.

The electronic Schrödinger equation (1.5) with fixed nuclei positions contains the major computational cost with its electron-electron interaction. Methods designed to solve Eq. 1.5 are indicated as *electronic structure calculations*. The latter are performed in all the present study by means of different methods. So from now on $\Psi(\mathbf{r})$ will simply represent the N-electron wave function, $\Psi_e(\mathbf{r})$, and $\hat{H}$ the electronic Hamiltonian, $\hat{H}_e$.

Before the rest of the theory is further explained, it is convenient to introduce the Dirac notation, which will be often used throughout this work. The equivalences are as follows:

$$\begin{aligned} \Psi \equiv |\Psi\rangle, \quad \Psi^* \equiv \langle\Psi|, \\ \int \Psi^*\Psi d\mathbf{r} = \langle\Psi|\Psi\rangle, \\ \int \Psi^*\hat{H}\Psi d\mathbf{r} = \langle\Psi|\hat{H}|\Psi\rangle. \end{aligned} \tag{1.7}$$

The *bra* $\langle\Psi|$ represents the complex conjugate wave function and the conjugation with the *ket* $|\Psi\rangle$ indicates an integration over all coordinates. The so called *bracket* is also referred as overlap element, or matrix element when an operator is involved, such as in the last line of Eq. 1.7.

1.2 Hartree-Fock Theory

The solution of a many-electron system remains still arduous after the Born-Oppenheimer approximation and requires elaborate computational methods. An important simplification can be introduced with the concept of independent particles. In this view, the motion of one electron is considered independent from all the other electrons. Thus, the electronic wave function can be obtained as a product of single electron functions. A milestone in QC is given by the Hartree-Fock theory [19–22], which represents this independent particle model with an average electron-electron interaction.

Briefly after the publication of the Schrödinger equation, the physicist D. R. Hartree devised a way to solve Eq. 1.5 based only on fundamental physical principles [19, 20], giving rise to the so called *ab-initio* methods. He derived an equation for the single independent electron which would move in a mean field potential generated by all the other electrons. This method was first characterized by the idea of representing a complex many-electron wave function as a simple product of 1-electron wave functions. However, it would not be satisfactory for fermions (such as electrons), which obey the antisymmetry principle. This lack in the Hartree method was noticed in 1930 by the

two physicists V. A. Fock [21] and J. C. Slater [22], who independently introduced this property into the wave function.

1.2.1 Antisymmetry of the wave function

The key idea for an antisymmetric wave function was introduced by Pauli in 1925 [86] with his concept of spin for all fundamental particles. The spin is characterized by a spin quantum number, s, which would get different values for different types of particles. For example, non-integer values of s correspond to fermions (s=1/2 for electrons), while integer values represent bosons. Experiments would show that electrons in a magnetic field would align either parallel or antiparallel to it. The latter results in two possible orientations described by the spin magnetic quantum number $m_s = +1/2$ and m_s = -1/2 and, in turn, led to the famous Pauli exclusion principle: "*The wave function describing any state of an N-electron system must be antisymmetric under any permutation of the electronic coordinates*". This means that the principal quantum number, n, the angular quantum number, l, the magnetic quantum number, m_l, and the spin quantum number, m_s, can never be the same for two electrons. In other words, two electrons in the same atomic orbital must have antiparallel spins. However, the electronic Schrödinger equation shown so far has no yet reference to spin. The latter is introduced in the orbital description with the spin-orbitals, $\phi(\mathbf{x})$:

$$\phi(\mathbf{x}) = \phi(\mathbf{r})\omega(s), \tag{1.8}$$

where $\phi(\mathbf{r})$ represents the spatial orbital and $\omega(s)$ the spin function. If we assume that $\langle\phi_{\mathbf{r}_i}|\phi_{\mathbf{r}_j}\rangle = \delta_{ij}$ (i.e. the overlap between two spatial orbitals is zero unless the same orbital is considered) and $\langle\omega_i|\omega_j\rangle = \delta_{ij}$ (i.e. the overlap is zero unless parallel spins are considered), then we obtain a basis of orthonormal spin orbitals.

A many-electron wave function can be conveniently represented as a product of 1-electron functions (spin orbitals) in a relatively simple scheme which ensures antisymmetry. That is a Slater determinant (SD), where an N-electron wave function in N spin orbitals is written as

$$|\Psi(\mathbf{x}_1, \mathbf{x}_2, \ldots, \mathbf{x}_N)\rangle = \frac{1}{\sqrt{N!}} \begin{vmatrix} \phi_1(\mathbf{x}_1) & \phi_2(\mathbf{x}_1) & \ldots & \phi_N(\mathbf{x}_1) \\ \phi_1(\mathbf{x}_2) & \phi_2(\mathbf{x}_2) & \ldots & \phi_N(\mathbf{x}_2) \\ \vdots & \vdots & \ddots & \vdots \\ \phi_1(\mathbf{x}_N) & \phi_2(\mathbf{x}_N) & \ldots & \phi_N(\mathbf{x}_N) \end{vmatrix}; \langle\phi_i|\phi_j\rangle = \delta_{ij}. \tag{1.9}$$

Indeed, each permutation of any two rows in the determinant would change the sign of $|\Psi\rangle$. This guarantees the wave function to be antisymmetric with respect to the exchange of any pairs of electrons. The factor $1/\sqrt{N!}$ ensures normalization of the resulting determinant, i.e. $\langle\Psi|\Psi\rangle = 1$. A shorthand notation for the SD is given by the diagonal elements with implicit electron order, $|\Psi(\mathbf{x}_1, \mathbf{x}_2, \ldots, \mathbf{x}_N)\rangle = |\phi_1(\mathbf{x}_1)\phi_2(\mathbf{x}_2)\ldots\phi_N(\mathbf{x}_N)\rangle = |\phi_1\phi_2\ldots\phi_N\rangle$.

1.2.2 Energy of a single Slater Determinant

In the HF method a single SD is considered to describe an electron configuration of N electrons. The energy associated to it can be conveniently expressed when the SD is given by N orthonormal spin orbitals and can be written as an expectation value of the Hamiltonian operator. Further, the expansion of the N-electron wave function $|\Psi\rangle$ (Eq. 1.9) can be included in it.

$$E = \frac{\langle\Psi|\hat{H}|\Psi\rangle}{\langle\Psi|\Psi\rangle} = \langle\phi_1\phi_2\ldots\phi_N|\hat{H}|\phi_1\phi_2\ldots\phi_N\rangle, \tag{1.10}$$

where the denominator given by the norm of the wave function is ensured to be equal to 1 by the normalization introduced in Eq. 1.9. Each SD generates N! permutations, so the latter equation would be characterized by $(N!)^2$ integrals.

In the HF equations the Hamiltonian operator is typically collected according to the number of electron indices. Thus, the operator in Eq. 1.5 can be written as

$$\hat{H} = \sum_i \hat{h}_1(\mathbf{x}_i) + \sum_{i,j>i} \hat{h}_2(\mathbf{x}_i, \mathbf{x}_j). \tag{1.11}$$

$\hat{h}_1$ represents the one-electron energy operator describing the kinetic energy of electron i and its attraction to all the nuclei and $\hat{h}_2$ represents the two-electron energy operator describing the electron-electron repulsion.

The complex energy expression resulting from the large number of terms arising in the expectation value of the Hamiltonian operator can be simplified thanks to the orthonormality conditions of spatial orbitals and spin functions (see Appendix A for further details about the derivation of the energy expression). The final energy of a single SD in a system with N electrons can be written as:

$$\langle\Psi|\hat{H}|\Psi\rangle = \sum_i^N h_{ii} + \frac{1}{2}\sum_{i,j}^N (J_{ij} - K_{ij}) + E_{nuc}, \tag{1.12}$$

where the indices i and j run over all the electrons in the system. Further, the nuclear energy is also added as the last term since its expression is trivially obtained. Indeed, it does not have any dependence on the electronic coordinates (i.e. $\langle\Psi|\hat{V}_{nuc}|\Psi\rangle = E_{nuc}\langle\Psi|\Psi\rangle = E_{nuc}$) and can be added as a constant.

1.2.3 Variational Method

The HF method, such as many others, makes use of the variational principle to generate approximate solutions of the energy equation (Eq. 1.12). The variational principle helps in this task providing an upper bound to the exact ground state energy. An approximate wave function, Φ, of the unknown exact solution, Ψ, can give a first estimate of the energy, which can then be minimized with respect to a variational parameter. Further, this can be systematically improved by introducing more variational parameters, with the certainty that every other solution will always be greater than or equal to the exact result E_{exact}. The variational principle is demonstrated in the Appendix B.

Let us now consider the energy associated with a single SD in the Hartree-Fock approach when $|\Psi\rangle$ represents a closed-shell molecule. The latter is a molecule where N electrons doubly occupy N/2 orbitals. Under this assumption the energy expression in Eq. 1.12 can be written as:

$$E_{HF} = 2\sum_{i}^{N/2}\langle\phi_i|\hat{h}_1|\phi_i\rangle + \sum_{i,j}^{N/2}\Big[2\langle\phi_i\phi_j|\hat{h}_2|\phi_i\phi_j\rangle - \langle\phi_i\phi_j|\hat{h}_2|\phi_j\phi_i\rangle\Big] + E_{nuc}. \tag{1.13}$$

The goal of the HF method is to use $\{\phi\}$ as a parameter to vary in order to minimize the energy according to the variational principle. This minimization can be done with the Lagrange function, L,

$$L = E_{HF} - 2\sum_{ij}\lambda_{ij}(\langle\phi_i|\phi_j\rangle - \delta_{ij}) \tag{1.14}$$

where the variation of the energy E_{HF} is given under the constraint of orbital orthonormality. Further, λ_{ij} are the Lagrange multipliers and are found to be symmetric ($\lambda_{ij} = \lambda_{ji}$). However, the energy minimization is reached with the values of λ_{ij} for which $\delta L = 0$. In that respect, the Fock operator can be defined as $\hat{F}_i = \hat{h}_i + \sum_j^{N/2}(2\hat{J}_{ij} - \hat{K}_{ij})$ and the Lagrange variation can be written through the well known canonical Hartree-Fock equation for orbital $|\phi_i\rangle$,

$$\hat{F}_i|\phi_i\rangle = \epsilon_i|\phi_i\rangle, \tag{1.15}$$

where the usage of canonical MOs makes the Lagrange multipliers be interpreted as orbital energies ϵ_i.

1.2.4 Basis Set Expansion

The solutions of the HF equations are given by the optimal form of the set of MOs $\{\phi\}$. However, the Fock operator depends on the MOs themselves through $\hat{J}_{ij}$ and $\hat{K}_{ij}$. So, the solution depends on itself and must be found self-consistently by iteration. This is accomplished introducing a set of spatial basis functions. In 1951, Roothaan [87] and Hall [88] proved independently that the HF equations can be written as a set of algebraic equations through a basis set expansion. The latter guarantees a solution guided by matrix techniques.

Nowadays, the basis set expansion is a well known route to solve many chemical problems and it is widely used in the QC community. In this way, each MO is expanded as a combination of known basis functions. The typical choice is to approximate these functions as a linear combination of atomic orbitals (LCAO). Although they must not represent the true atomic orbital, they are historically taken to resemble the solution of the 1-electron Schrödinger equation of the hydrogen atom. The combination of these non-orthogonal basis functions located on the nuclei follows as

$$\phi_i(\mathbf{r}) = \sum_{\mu=1}^{M} c_{i\mu}\chi_\mu(\mathbf{r}). \tag{1.16}$$

M represents the number of basis functions χ_μ given by the chosen basis set. Further, the $c_{i\mu}$ are the mixing (or MOs) coefficients which are variationally optimized in HF in order to minimize the energy. However, inserting Eq. 1.16 into Eq. 1.15, multiplying by a basis function and integrating provides a set of matrix equations for the MOs coefficients,

$$\mathbf{FC} = \mathbf{SC}\epsilon, \tag{1.17}$$

where $\mathbf{F}$ represents the Fock matrix and $\mathbf{S}$ the overlap matrix of the basis functions. These are the HF Roothaan-Hall equations for the closed-shell system in the atomic orbital basis. Such a matrix eigenvalue problem can be solved by iterative diagonalization, starting from a first guess of the coefficients in order to obtain an initial Fock matrix. The idea to reach a solution self-consistently gives an additional name to the HF approach, i.e. self consistent field (SCF) method.

The situation considered so far is the so called restricted HF (RHF) theory, where each spatial orbital is occupied by one spin-up and one spin-down electron. However, for open-shell systems the unrestricted HF (UHF) or restricted open HF (ROHF) methods are used. The former takes into account different spatial orbitals for different spin functions, which results in UHF solutions that break the total spin symmetry of the system. The latter still includes the same spatial orbital for different spins, but it offers solutions that are still an eigenfunction of the total spin operator $\hat{S}^2$. However, they both attempt to describe a qualitatively correct wave function upon expansion of orthonormal MOs.

In principle, any set of basis functions $\{\chi\}$ can be provided to construct the MOs, as long as it ensures the physics of the problem. In practice, two very common type of orbitals used in molecular electronic structure calculations are Slater type orbitals (STOs) and Gaussian type orbitals (GTOs). On the one hand, an exponential function ($\phi \propto e^{-\alpha r}$) that would mirror the exact solution of the hydrogen atom would be the best match. The latter are the STOs and can be very accurate but they are computationally inefficient. On the other hand, GTOs ($\phi \propto e^{-\alpha r^2}$), which are widely used in QC, provide a poorer description near the nucleus and at the tail of its radial function. Figure 1.1

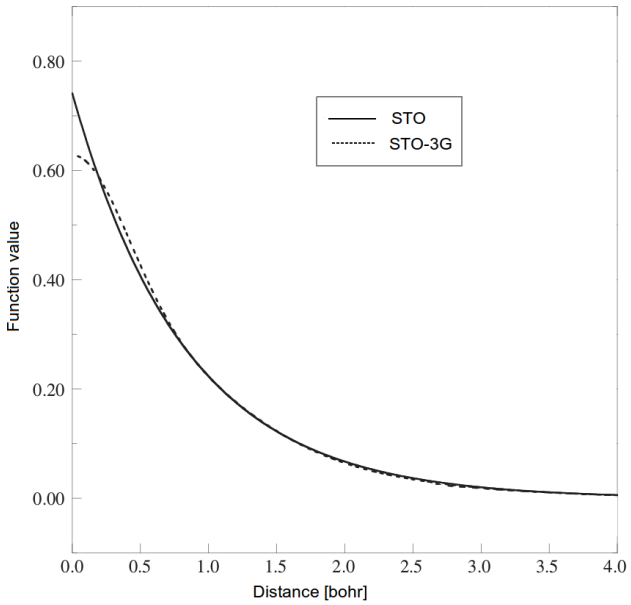

FIGURE 1.1: 1s STO approximated by three GTOs.

shows the representation of the radial function of a 1s H atomic orbital by a single STO and by the combination of three contracted GTOs. Indeed, as a rule of thumb, three times the number of STOs are necessary to achieve the same level of accuracy with Gaussian orbitals. However, the computational advantages with GTOs are so much

more beneficial that is preferred to use larger sets of GTOs rather than of more compact STOs. The basis sets used in the present work are constructed by contracted GTOs.

In a given basis set, the number of occupied orbitals are typically much smaller than that of the unoccupied orbitals. Although the virtual orbitals do not contribute to the energy in the HF method, they guarantee a certain flexibility to describe the wave function. In this way, excitations of spin orbitals from the single SD can generate a number of different other determinants. The space of all the possible SDs that can be generated in a system by a given basis set represents the so called Hilbert space. An increase in the number of orbitals would enlarge the size of this space and would represent a systematic approximation of the full Hilbert space.

Further, the number of basis functions can be infinitely enlarged up to the limit of the complete basis set (CBS) and, thus, the exact wave function obtained. However, in this case the number of SDs generated would be intractable. Hence, it is clear how the restricted number of basis functions and the finite SDs determine the limits of the computed many-electron wave function. On the one hand, every basis set with its finite size restricts the description of the spin orbitals. On the other hand, the many electron basis with its finite number of SDs restricts the description of electron correlation.

1.3 Electron Correlation

The HF method defines the energetically best single SD (in the given basis set) and describes a qualitatively correct electronic structure for a variety of systems. It is commonly recognized that the HF wave function is able to account for ∼99% of the total energy of a molecular system. However, the remaining ∼1% is usually the crucial part to properly define chemical phenomena. For that reason, quantitative results are of interest and many different methods have been devised to go beyond HF, i.e. the post-HF methods. All of these methods define a wave function which contains more than one SD and attempt to capture most of the correlation which is not accounted for at the HF level. The conventional definition of such an electron correlation is given by the difference between the exact energy (i.e. the lowest possible energy in a given basis set) and the HF energy:

$$E_{corr} = E_{exact} - E_{HF}. \tag{1.18}$$

This definition might be at moments misleading and bring to the wrong assumption that HF does not take any kind of electron correlation into account. As shown in the

Appendix A, the Fermi correlation, given by the repulsion of electrons with parallel spin, is already fully accounted in the HF method. Further, the Coulomb repulsion between electrons of opposite spin is ameliorated in the post-HF methods, in comparison to the mean-field level is accounted for in the HF theory.

Two different types of electron correlations are commonly distinguished in QC. Even though there is not an exact way of separating these effects. They are the so called *static* and *dynamic* correlation. The *static* correlation is also referred to as *strong* or $non - dynamic$ correlation and is found when different states of a wave function are equally important to describe the system. When these quasi-degeneracies arise, a single SD does not provide any longer a qualitatively correct reference wave function. Hence, this is usually taken into account by adding more flexibility with multiple SDs, i.e. a multi-reference wave function. The *dynamic* correlation, also known as *weak* correlation, is the remaining energy lowering associated with the motion of the electrons. As already mentioned, these two types of correlation are not trivially separated. For example, adding the right SDs into the wave function accounts for the static correlation. However, adding SDs also recovers for more and more dynamic correlation until the exact correlation treatment is eventually reached (in the given basis set).

Chapter 2

Coupled Cluster Theory

Coupled Cluster was first introduced in QC in the late 1960s by Čížek and Paldus [25–28]. Although, the origins of the method were already presented years back in the field of nuclear physics, almost a decade passed until Čížek showed the first CC equations in the QC world. This was also stated by one of the inventors: "*Considering the fact that the CC method was well understood around the late fifties it looks strange that nothing happened with it until 1966, as Jiři Čížek published his first paper on a quantum chemistry problem. [25] He had looked into the 1957 and 1960 papers published in Nuclear Physics by Fritz and myself. [89, 90]. I always found it quite remarkable that a quantum chemist would open an issue of a nuclear physics journal. I myself at that time had almost given up the CC method as not tractable and, of course, I never looked into the quantum chemistry journals.* " [91] As it emerges from the text of the physicist H. Kümmel, the gap between the two fields was such, to make the work done by Čížek quite remarkable. Nevertheless, the diagrammatic formalism used at first by Čížek made the acceptance of this theory slow in the QC community. Only by the end of the 1970s new derivations of CC equations [92–94] and their computer implementations started to be used and more accessible to a wider audience. That defined a turning point in the CC successful application to chemical problems.

Nowadays, CC represents one of the most popular techniques to solve the Schrödinger equation. After more than forty years of active development, CC results in a variety of methods able to provide accurate predictions in a wide range of chemical systems. The distinctive feature of CC is given by its exponential *ansatz* to approximate the many-electron wave function,

$$|\Psi_{\mathrm{CC}}\rangle = e^{\hat{T}}|\Phi_0\rangle, \tag{2.1}$$

where the exponential operator can be expanded as a Taylor series:

$$e^{\hat{T}} = \sum_{n=0}^{\infty} \frac{\hat{T}^n}{n!} = 1 + \hat{T} + \frac{\hat{T}^2}{2} + \frac{\hat{T}^3}{3!} + \dots \tag{2.2}$$

$\hat{T}$ represents the cluster operator which acts on the reference wave function Φ_0 (typically HF) in order to generate all the excited SDs.

The exponential *ansatz* guarantees the correct scaling of the correlation energy with the number of electrons present in the system. Indeed, already at the lowest level of approximation, $\hat{T} = \hat{T}_2$, CC equations show disconnected products of excitations , such as quadruples, hextuples and so on, which ensure the so called size-extensivity property of the method. In other words, the energy calculated by CC is proportional to the number of electrons. The latter is an advantage in comparison with Configuration Interaction theory.

Eq. 2.1 represents the central equation for CC theory. However, $\hat{T}$ includes all the excitations that can be generated in a system. This means that for N-electrons $\hat{T} = \hat{T}_1 + \hat{T}_2 + \dots + \hat{T}_N$ and the exact wave function is then produced for the given basis set. The first approximation that is usually introduced in the CC methods is the order of the excitation level to include in the calculation, i.e. the truncation of the cluster operator. The first workable equations introduced in 1966 were for the simplest model $\hat{T} = \hat{T}_2$. In the following, the CC working equations for energy and amplitudes will be derived considering CCD in sake of simplicity. Even though the more commonly used CC with singles and doubles (CCSD) [95] will be adopted throughout this work.

2.1 Second quantization

The task of deriving the CC equations can be more convenient to accomplish with the mathematical formalism known as second quantization. The basic blocks of second quantization are the creation, $a_p^\dagger$, and annihilation, a_p, operators, respectively defined by their action on a SD:

$$a_p^\dagger |\phi_q \dots \phi_s\rangle = |\phi_p \phi_q \dots \phi_s\rangle, \tag{2.3}$$

$$a_p |\phi_p \phi_q \dots \phi_s\rangle = |\phi_q \dots \phi_s\rangle. \tag{2.4}$$

The first operator adds the p spin orbital to the determinant, while the second removes it. The anticommutation relations that are followed by these two operators build the

SD antisymmetric property directly into its formalism:

$$a_p^\dagger a_q^\dagger + a_q^\dagger a_p^\dagger = 0, \tag{2.5}$$

$$a_p a_q + a_q a_p = 0, \tag{2.6}$$

$$a_p^\dagger a_q + a_q a_p^\dagger = \delta_{pq}. \tag{2.7}$$

The first equation is immediately derived knowing that $a_p^\dagger a_q^\dagger|\rangle = |\phi_p\phi_q\rangle = -|\phi_q\phi_p\rangle = -a_q^\dagger a_p^\dagger|\rangle$. In the same way the other two can be obtained.

The technique used in the previous chapter to represent the Hamiltonian and the wave function is sometimes referred to as first quantization. The latter can be very tedious to derive the CC equations. However, second quantization can be extremely useful to deal with many-body problems of identical particles. Following these basic rules it is possible to treat operators and wave functions in a unified way. Indeed, any SD can be written as a string of creation operators acting on the vacuum state

$$a_p^\dagger a_q^\dagger \dots a_r^\dagger|\rangle = |\psi_p\psi_q \dots \psi_r\rangle. \tag{2.8}$$

Instead, an annihilation operator acting on the vacuum state would be zero:

$$a_p|\rangle = 0, \tag{2.9}$$

because no orbital is possible to be removed. However, any operator can be defined in this second quantized form. For example, the one-particle cluster operator can be written as,

$$\hat{T}_1 = \sum_{ai} t_i^a a_a^\dagger a_i, \tag{2.10}$$

where an excitation from the occupied orbial ϕ_i to the unoccupied orbital ϕ_a takes place and t_i^a represents the cluster amplitude. Its action on the reference determinant generates the linear combination of singly excited determinants:

$$\hat{T}_1|\Phi_0\rangle = \sum_{ai} t_i^a|\Phi_i^a\rangle. \tag{2.11}$$

Further, also the electronic Hamiltonian from Eq. 1.11 can be defined by a combination of creation and annihilation operators:

$$\hat{H} = \sum_{pq} \langle p|\hat{h}|q\rangle a_p^\dagger a_q + \frac{1}{4}\sum_{pqrs} \langle pq||rs\rangle a_p^\dagger a_q^\dagger a_s a_r. \tag{2.12}$$

The latter equation is the second quantized form of $\hat{H}$ in a spin-orbital basis. Indeed, it does not depend on the number of electrons any longer, but it is defined by the general indices p, q, r, s which represent the spin-orbitals in a given basis.

A convenient way to calculate the matrix elements in second quantization is through the normal ordered operators (see Appendix C for further details and Wick's theorem). The electronic Hamiltonian as depicted in Eq. 2.12 can be cast into a normal ordered form making use of the Wick's theorem and the result is

$$\hat{H}_N = \hat{H} - \langle\Phi_0|\hat{H}|\Phi_0\rangle = \sum_{pq} f_{pq}\{a_p^\dagger a_q\} + \frac{1}{4}\sum_{pqrs}\langle pq||rs\rangle\{a_p^\dagger a_q^\dagger a_s a_r\} = \hat{F}_N + \hat{V}_N, \quad (2.13)$$

where f_{pq} represents the spin orbital Fock operator. The latter version of the Hamiltonian will be more practical to derive the CCD working equations in the next section.

Finally, a general definition of the cluster operator is here given,

$$\hat{T}_n = \left(\frac{1}{n!}\right)^2 \sum_{ij...ab...} t_{ij...}^{ab...}\{a_a^\dagger a_b^\dagger ... a_j a_i\}, \quad (2.14)$$

where the n-th excitation is considered and $t_{ij...}^{ab...}$ is the cluster amplitude. It is worth to underline that the cluster operator is already normal ordered in the particle-hole formalism.

2.2 Coupled Cluster energy expression

Once the CC *ansatz* (Eq. 2.1) is inserted into the Schrödinger equation the CC energy can be calculated by a projective technique, i.e. left multiplying the Schrödinger equation by the reference wave function $|\Phi_0\rangle$:

$$E = \frac{\langle\Phi_0|\hat{H}e^{\hat{T}}|\Phi_0\rangle}{\langle\Phi_0|\Psi_{CC}\rangle} = \langle\Phi_0|\hat{H}e^{\hat{T}}|\Phi_0\rangle \quad (2.15)$$

where intermediate normalization is assumed, $\langle\Phi_0|\Psi_{CC}\rangle = 1$. Inserting the power series expansion from Eq. 2.2 into Eq. 2.15 gives rise to the CC energy equation:

$$E = \langle\Phi_0|\hat{H}|\Phi_0\rangle + \langle\Phi_0|\hat{H}\hat{T}|\Phi_0\rangle + \langle\Phi_0|\hat{H}\frac{\hat{T}^2}{2}|\Phi_0\rangle, \quad (2.16)$$

where the higher order terms of $\hat{T}$ vanish. This natural truncation is due to the Slater-Condon rules [96, 97], which allow to write the Hamiltonian matrix in a very sparse way. Indeed, $\hat{H}$ is at most a two-particle operator whereas $\hat{T}$ is at least a one-particle excitation operator. The Slater-Condon rules state that matrix elements involving determinants which differ by more than two spin orbitals are zero. Hence, the matrix elements involving triple or higher excited determinants vanish in the CC energy expression. The main feature of Eq. 2.16 is that the equation is correct for every possible truncation of $\hat{T}$.

The same projective technique can be used to produce the cluster amplitudes equations:

$$\begin{aligned} \langle \Phi_i^a | \hat{H} e^{\hat{T}} | \Phi_0 \rangle &= E \langle \Phi_i^a | e^{\hat{T}} | \Phi_0 \rangle \\ \langle \Phi_{ij}^{ab} | \hat{H} e^{\hat{T}} | \Phi_0 \rangle &= E \langle \Phi_{ij}^{ab} | e^{\hat{T}} | \Phi_0 \rangle \\ &\vdots \end{aligned} \tag{2.17}$$

where the first line represents the equation for the single excitation amplitudes and $\langle \Phi_i^a |$ is the singly excited reference determinant. The second line represents the equation for the double excitation amplitudes and $\langle \Phi_{ij}^{ab} |$ is the doubly excited reference determinant. In the same way, one can generate the equations for all the order of excitation amplitudes. However, these equations are not linear since $e^{\hat{T}}$ is present. Further, they also depend on the energy.

The set of CC equations given in Eq. 2.16 and 2.17 represent already a set of working equations. However, a more practical version for computer implementation is usually adopted. This is done making use of the similarity transformed Hamiltonian, which is obtained left-multiplying by the inverse of the exponential operator, i.e. $e^{-\hat{T}} \hat{H}_N e^{\hat{T}}$, where the normal ordered $\hat{H}$ is considered. The projective technique is maintained and the new set of equations can be written as:

$$\langle \Phi_0 | e^{-\hat{T}} \hat{H} e^{\hat{T}} | \Phi_0 \rangle = E \tag{2.18}$$

$$\begin{aligned} \langle \Phi_i^a | e^{-\hat{T}} \hat{H} e^{\hat{T}} | \Phi_0 \rangle &= 0 \\ \langle \Phi_{ij}^{ab} | e^{-\hat{T}} \hat{H} e^{\hat{T}} | \Phi_0 \rangle &= 0 \\ &\vdots \end{aligned} \tag{2.19}$$

From now on, we simply define the similarity transformed normal ordered Hamiltonian as $\overline{H} = e^{-\hat{T}} \hat{H}_N e^{\hat{T}}$. Now, this set of equations present two advantages. First, they are decoupled from the energy equation. Second, $\overline{H}$ is possible to be simplified via the

Campbell-Baker-Hausdorff (CBH) expansion, which makes it feasible to reach an energy expression with a natural truncation as in Eq. 2.16. However, it must be noted that the operator $\overline{H}$ is not anymore Hermitian.

Before the further derivation of the CC equations, it is worth to underline that also a variational approach is possible to be defined for CC. For this reason, an expectation value equation can be generated by the symmetric formula:

$$E = \frac{\langle \Phi_0 | (e^{\hat{T}})^\dagger \hat{H} e^{\hat{T}} | \Phi_0 \rangle}{\langle \Phi_0 | (e^{\hat{T}})^\dagger e^{\hat{T}} | \Phi_0 \rangle} \leq E_{exact}, \tag{2.20}$$

where the variational parameters to minimize the energy are given by the CC amplitudes. Here, the high order terms of the cluster operator do not vanish as in Eq. 2.16 and this makes the expression impractical. Nevertheless, the energy in Eq. 2.20 is an expectation value of an Hermitian operator, while this is not valid any longer for $\overline{H}$ in Eq. 2.18. Finally, the CC methods are often implemented with the similarity transformed formulation, at the cost of variationality for truncated $\hat{T}$. However, the size-extensivity is still ensured by the exponential ansatz.

2.2.1 Derivation of the CC energy equation

In the present section, the energy equation in 2.18 will be further simplified and expressed for the CCD method which includes only double excitations. First, it is convenient to write the similarity transformed normal ordered Hamiltonian, $\overline{H}$, via the Hausdorff expansion for the truncation of the cluster operator $\hat{T} = \hat{T}_2$.

$$\overline{H} = \hat{H}_N + [\hat{H}_N, \hat{T}_2] + \frac{1}{2}\left[[\hat{H}_N, \hat{T}_2], \hat{T}_2\right] + \frac{1}{3!}\left[\left[[\hat{H}_N, \hat{T}_2], \hat{T}_2\right], \hat{T}_2\right] + \dots \tag{2.21}$$

where $[\hat{H}_N, \hat{T}_2] = \hat{H}_N\hat{T}_2 - \hat{T}_2\hat{H}_N$. It is possible to evaluate each term of the latter expansion in second quantized form using Wick's theorem. The latter allows an important generalization to be made upon the CBH expansion. That is, the only non-zero terms in Eq. 2.21 are those where the annihilation/creation operators in $\hat{H}_N$ have at least one contraction with those in the cluster operator $\hat{T}_2$, which is written as:

$$\hat{T}_2 = \frac{1}{4}\sum_{ijab} t_{ij}^{ab} \{a_a^\dagger a_b^\dagger a_j a_i\}. \tag{2.22}$$

Since the normal ordered Hamiltonian (Eq. 2.13) includes at most four annihilation/creation operators in $\hat{V}_N$, the contractions can be maximum with four different

cluster operators $\hat{T}_2$. This means that the CBH expansion truncates naturally at the quartic term. The latter is valid regardless the truncation of the cluster operator $\hat{T}$,

$$\overline{H} = \left(\hat{H}_N + \hat{H}_N\hat{T} + \frac{1}{2}\hat{H}_N\hat{T}^2 + \frac{1}{6}\hat{H}_N\hat{T}^3 + \frac{1}{24}\hat{H}_N\hat{T}^4\right)_c . \tag{2.23}$$

The subscript c indicates the connected cluster form of $\overline{H}$, where $\hat{H}_N$ must at least contract once to every cluster operator on its right.

In the present expression the truncation $\hat{T} = \hat{T}_2$ is considered. Thus, the correlation CCD energy can now be written as the expectation value in Eq. 2.18 with the introduction of the connected cluster form of the similarity transformed normal ordered Hamiltonian,

$$E_{CCD} = \langle\Phi_0|\left(\hat{H}_N + \hat{H}_N\hat{T}_2 + \frac{1}{2}\hat{H}_N\hat{T}_2^2 + \ldots\right)_c|\Phi_0\rangle. \tag{2.24}$$

This equation can then be calculated through the Wick's theorem once $\hat{H}_N$, Eq. (2.13), is introduced into $\overline{H}$. The first term is quickly evaluated based on the knowledge that the expectation value of a normal ordered operator in the particle-hole formalism is zero by construction,

$$\langle\Phi_0|\hat{H}_N|\Phi_0\rangle = 0. \tag{2.25}$$

Next, the second term can be evaluated:

$$\langle\Phi_0|\left(\hat{H}_N\hat{T}_2\right)_c|\Phi_0\rangle = \langle\Phi_0|\left[(\hat{F}_N\hat{T}_2)_c + (\hat{V}_N\hat{T}_2)_c\right]|\Phi_0\rangle. \tag{2.26}$$

It can be shown that the first term on the right hand side of Eq. 2.26 cannot give any fully contracted component. As it is evident in Eq. 2.27, the two second quantization operators in $\hat{F}_N$ cannot contract with all the four operators coming from $\hat{T}_2$.

$$\langle\Phi_0|\left(\hat{F}_N\hat{T}_2\right)_c|\Phi_0\rangle = \frac{1}{4}\sum_{pq}\sum_{abij} f_{pq}t_{ij}^{ab}\langle\Phi_0|\{a_p^\dagger a_q\}\{a_a^\dagger a_b^\dagger a_j a_i\}|\Phi_0\rangle \tag{2.27}$$

Thus, it results in a zero contribution. Whereas the second term can be as well evaluated with the Wick's theorem and give rise to four equivalent fully contracted components (all the remaining terms arising from Wick's theorem are not explicitly shown since

they would only result in null contributions),

$$\langle\Phi_0|\left(\hat{V}_N\hat{T}_2\right)_c|\Phi_0\rangle = \frac{1}{16}\sum_{pqrs}\sum_{abij}\langle pq||rs\rangle t_{ij}^{ab}\langle\Phi_0|\{a_p^\dagger a_q^\dagger a_s a_r\}\{a_a^\dagger a_b^\dagger a_j a_i\}|\Phi_0\rangle$$

$$= \frac{1}{16}\sum_{pqrs}\sum_{abij}\langle pq||rs\rangle t_{ij}^{ab}\Bigg(\{\overbrace{a_p^\dagger a_q^\dagger a_s a_r a_a^\dagger a_b^\dagger a_j a_i}\} + \{\overbrace{a_p^\dagger a_q^\dagger a_s a_r a_a^\dagger a_b^\dagger a_j a_i}\} +$$

$$\{\overbrace{a_p^\dagger a_q^\dagger a_s a_r a_a^\dagger a_b^\dagger a_j a_i}\} + \{\overbrace{a_p^\dagger a_q^\dagger a_s a_r a_a^\dagger a_b^\dagger a_j a_i}\}\Bigg)$$

$$= \frac{1}{16}\sum_{pqrs}\sum_{abij}\langle pq||rs\rangle t_{ij}^{ab}\Big(\delta_{pi}\delta_{qj}\delta_{ra}\delta_{sb} + \delta_{pj}\delta_{qi}\delta_{rb}\delta_{sa} - \delta_{pj}\delta_{qi}\delta_{ra}\delta_{sb} - \delta_{pi}\delta_{qj}\delta_{rb}\delta_{sa}\Big)$$

$$= \frac{1}{4}\sum_{abij}\langle ij||ab\rangle t_{ij}^{ab}. \quad (2.28)$$

All the subsequent terms of Eq. 2.24 involving quadratic cluster operator or higher exponents have all annihilation/creation operators that are more than those that can be paired by $\hat{H}_N$. Hence, no fully contracted terms would arise from them. In such a way, the CCD correlation energy has been derived and is represented by the only term:

$$E_{CCD} = \frac{1}{4}\sum_{abij}\langle ij||ab\rangle t_{ij}^{ab}. \quad (2.29)$$

In the same way, the expression for the CC energy can be found when also single excitations are considered, i.e. $\hat{T} = \hat{T}_1 + \hat{T}_2$:

$$E_{CCSD} = \sum_{ai} f_{ai}t_i^a + \frac{1}{4}\sum_{abij}\langle ij||ab\rangle t_{ij}^{ab} + \frac{1}{2}\sum_{abij}\langle ij||ab\rangle t_i^a t_j^b. \quad (2.30)$$

The latter equation is a general expression of CC energy which is not dependent on the higher order terms of the cluster operator $\hat{T}$. Although Eq. 2.30 is derived with $\hat{T} = \hat{T}_1 + \hat{T}_2$, the higher terms, such as $\hat{T}_3$, $\hat{T}_4$, and so on would not contribute to the final equation because they would not provide fully contracted terms with the Hamiltonian. Thus, they would not appear explicitly in the equation. However, such a convenient way to represent the energy in CC does not imply that the higher order cluster operators do not play a role in the method. Instead, they can contribute through the amplitude equations (2.19), where the excited determinants allow to reach full contraction also from such terms.

A close similarity can be seen between the last derived energy equation (2.30) and

Eq. 2.16. However, a rationalization of Eq. 2.30 in terms of Slater-Condon rules is inadequate, because there are terms in the amplitude equations which would still appear according to such rules. But, they would be missing in the actual equation because no full contraction would be possible. For example, the quintuply excited term in the $\hat{T}_3$ amplitude equations for the CCSD with triples (CCSDT) method, $\langle \Phi_{ijk}^{abc} | \frac{1}{5!} (\hat{V}_N \hat{T}_1^5)_c | \Phi_0 \rangle$. The determinants involved here differ only by two spin orbitals, since the first in the bra is triply excited and the second in the ket is quintuply excited by $\hat{T}_1^5$. According to the Slater-Condon rules such a matrix element would be non-zero. However, it is evident how the four annihilation/creation operators in $\hat{V}_N$ cannot connect to more than four cluster operators. The latter would violate the connected cluster properties of the CBH expansion of $\overline{H}$.

2.3 Diagrammatic representation of CC

The practice of deriving all the terms involved in the CC equations can quickly become quite a tedious task even with the Wick's theorem. Although the least laborious CC method, i.e. for $\hat{T} = \hat{T}_2$, has been here considered, the derivation of the amplitude equation, $\langle \Phi_{ij}^{ab} | \overline{H} | \Phi_0 \rangle = 0$, is already prone to possible errors from the multiple algebraic manipulations. For that reason, a diagrammatic formalism is introduced in order to make the derivation of these equations a lot quicker. The advantage of such an approach is that the Wick's contractions can be done in a visual way, and this results in the only non-zero contributions. In the following, it is shown how to represent each operator involved in the CC set of equations and the basic features which characterize these diagrams in the particle-hole formalism.

The approach exposed in the following makes use of the Brandow diagrams [98], which have been known in the CC field particularly by the works of Čížek [25, 26], Paldus [28] and Bartlett [99, 100], to name a few, and are usually referred to as "Feynman-like diagrams" or "antisymmetrized Goldstone diagrams". The reason for such names is that the historical relevant works using these diagrams were first accomplished by Feynman in his efforts to calculate matrix elements in quantum electrodynamics and then by Goldstone in his first applications to the electronic correlation problem [101]. In the following, the Brandow diagrams are first explained in their basic rules and then used for deriving the spin orbital formulation of the CC equations. A good introduction to this diagrammatic approach is also given by Crawford and Schaefer [102].

2.3.1 Fundamentals of diagrammatic formalism

The diagrams are built by basic components of the particle-hole formalism. For example, a hole is represented by a downward line and a particle by a upward line. That is, these lines give the focus on those orbitals which differ from those in the reference determinant, Φ_0. The combination of a hole and a particle line gives rise to an excited determinant. Fig. 2.1 represents Φ_i^a, i.e. the excitation of the orbital i to the orbital a

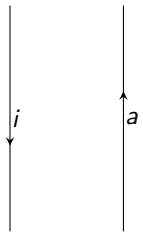

FIGURE 2.1: Excited determinant Φ_i^a in diagrammatic expression.

in the reference determinant Φ_0, which is simply the empty space in this representation.

The operators in this diagrammatic approach are represented by horizontal interaction lines, such as a dotted line for the electronic Hamiltonian and a solid line for the cluster operators. Every operator representation is connected to exactly two lines each vertex, which depicts the action of an operator on an electron. For example, in Fig. 2.2 the Fock operator is shown as a dotted line with only one vertex (the other vertex to the right is signed by an X to specifiy that is not an actual vertex) because $\hat{F}_N$ is a one-electron operator.

In order to convert the algebraic expressions of the CC equations into diagrams a set of basic rules must be followed:

1. q-creation/q-annihilation operators are located above/below the interaction line
2. upward/downward lines represent particles/holes
3. each vertex must have exactly two lines, one outgoing and one incoming
4. any pairwise interchange of two equal lines (incoming or outgoing) reproduce equivalent diagrams as long as the exchange happens on the vertices of the same operator
5. the excitation level is calculated in every diagram counting the number of lines from above the interaction line minus the number from below and then divided by 2

Following these rules one can reproduce the similarity transformed normal ordered Hamiltonian $\overline{H}$ in diagrams. For example, the one electron operator $\hat{F}_N$ (Eq. 2.13) can be divided into four components arising from the description in occupied/unoccupied spin orbitals and then transformed into diagrams:

$$\hat{F}_N = \sum_{ab} f_{ab}\{a_a^\dagger a_b\} \quad + \quad \sum_{ij} f_{ij}\{a_i^\dagger a_j\} \quad + \quad \sum_{ai} f_{ia}\{a_i^\dagger a_a\} \quad + \quad \sum_{ai} f_{ai}\{a_a^\dagger a_i\}.$$

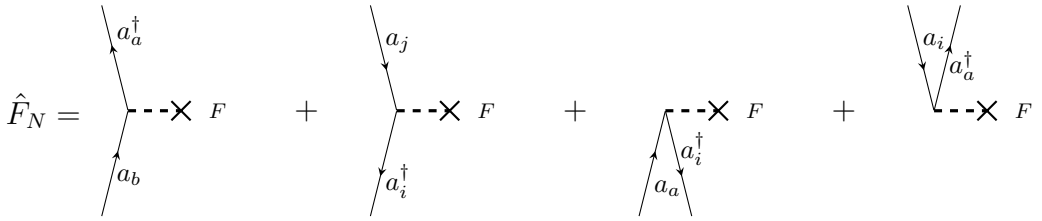

FIGURE 2.2: Diagrams of the one-electron part of the normal ordered Hamiltonian.

The diagrams in Fig. 2.2 represent the four components in the same order as shown in the above equation. The first two diagrams of $\hat{F}_N$ have an excitation level equal to 0, while the third is -1 and the last is +1. For clarity also the second quantization operators have been written in the diagrams of Fig. 2.2. However, from now on only the indices will be reported next to every line and only when necessary.

Next, the two electron operator $\hat{V}_N$ (Eq. 2.13) is considered and turned into its nine different components characterizing the description in occupied/unoccupied orbitals: Thus, the corresponding diagrams are shown in Fig. 2.3 where one can see again the same order of components in the relative equation above. The first line of diagrams is characterized by 0 excitation level. Indeed, one can see how the lines above and below the interaction one are the same number. That is different in the next six diagrams, where the first two account for an excitation level of -1, the next two +1 and the last two diagrams of Fig. 2.3 represent a +2 and -2 excitation.

Now, the cluster operators are the only missing components to allow a diagrammatic representation of the CC equations. In Fig. 2.4, the diagrams of the $\hat{T}_1$ and $\hat{T}_2$ cluster operators are shown. As already mentioned, the cluster operator is represented by a solid line. It is evident to notice that only q-creation operators are shown in Fig. 2.4. This is expected since the cluster operators are used to generate excited determinants from the reference wave function. Consequently, also the excitation level is positive because no lines are present below the interaction bar. $\hat{T}_1$ and $\hat{T}_2$ give respectively an excitation level of +1 and +2.

$$\hat{V}_N = \frac{1}{4}\sum_{abcd}\langle ab||cd\rangle\{a_a^\dagger a_b^\dagger a_d a_c\} + \frac{1}{4}\sum_{ijkl}\langle ij||kl\rangle\{a_i^\dagger a_j^\dagger a_l a_k\} + \sum_{iabj}\langle ia||bj\rangle\{a_i^\dagger a_a^\dagger a_j a_b\} +$$
$$\frac{1}{2}\sum_{aibc}\langle ai||bc\rangle\{a_a^\dagger a_i^\dagger a_c a_b\} + \frac{1}{2}\sum_{ijka}\langle ij||ka\rangle\{a_i^\dagger a_j^\dagger a_a a_k\} + \frac{1}{2}\sum_{abci}\langle ab||ci\rangle\{a_a^\dagger a_b^\dagger a_i a_c\} +$$
$$\frac{1}{2}\sum_{iajk}\langle ia||jk\rangle\{a_i^\dagger a_a^\dagger a_k a_j\} + \frac{1}{4}\sum_{abij}\langle ab||ij\rangle\{a_a^\dagger a_b^\dagger a_j a_i\} + \frac{1}{4}\sum_{ijab}\langle ij||ab\rangle\{a_i^\dagger a_j^\dagger a_b a_a\}$$

$\hat{V}_N =$

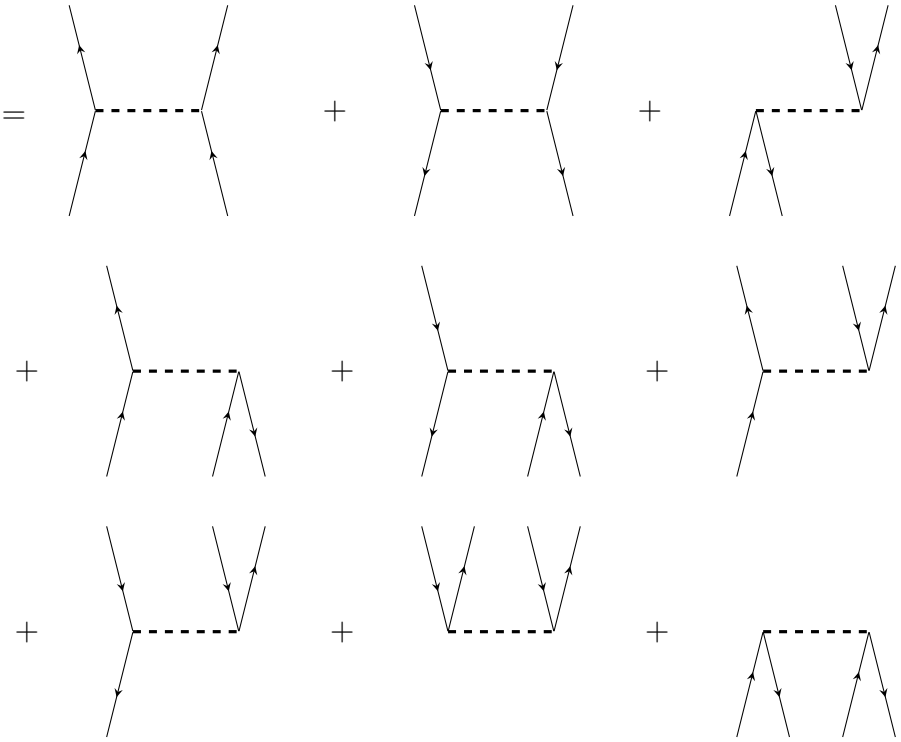

FIGURE 2.3: Diagrams of the two-electron part of the normal ordered Hamiltonian.

$$\hat{T}_1 = \sum_{ai} t_i^a\{a_a^\dagger a_i\} \quad ; \quad \hat{T}_2 = \sum_{abij} t_{ij}^{ab}\{a_a^\dagger a_b^\dagger a_j a_i\}$$

$\hat{T}_1 =$ 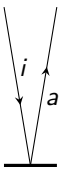 ; $\hat{T}_2 =$ 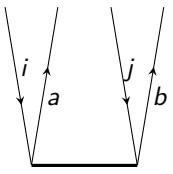

FIGURE 2.4: Diagrams of the cluster operators $\hat{T}_1$ and $\hat{T}_2$.

Finally, the contraction between two different operators is still to be determined in the diagrammatic approach. This is shown by two horizontal bars representing each

operator connected by a line, the so called *internal* line. In this way, two type of lines can be defined, *internal* and *external*. The *internal* lines are those connecting two different operators, i.e. the contraction, and the *external* lines are those connected to only one operator. Wick's theorem states that only the fully contracted terms have non-zero contributions in the expectation value of the reference determinant. This means that in the diagrammatic approach the representation of the CC energy equation cannot have external lines. In other words, all lines must be connected and therefore the excitation rank of each final diagram is 0.

For example, let us consider the only term contributing to the CCD energy equation, $\langle\Phi_0|\left(\hat{V}_N\hat{T}_2\right)_c|\Phi_0\rangle$. Such a term imposes a contraction between the $\hat{V}_N$ and the $\hat{T}_2$ operators. Since the $\hat{T}_2$ term provides a +2 excitation, the only $\hat{V}_N$ diagram that can equilibrate such an excitation is given by the last diagram in Fig. 2.3, which is -2. The union of the latter with the $\hat{T}_2$ diagram in Fig. 2.4 results in the final diagram of Fig. 2.5. In a diagrammatic contraction, the rightmost operator of the matrix element must lie at the bottom of the final diagram. For that reason, the $\hat{T}_2$ solid line in Fig. 2.5 is presented below the Hamiltonian operator and connected with $\hat{V}_N$ through the only two vertices available. It is evident in Fig. 2.5 that no external lines are present and

$\langle\Phi_0|\left(\hat{V}_N\hat{T}_2\right)_c|\Phi_0\rangle \quad =$

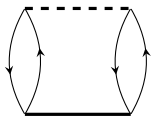

FIGURE 2.5: Example of contraction in the only final diagram of the CCD energy equation.

this represents a fully contracted term which obeys Wick's theorem.

The final diagram can now be translated into an algebraic expression following a set of rules:

1. assign indices to all the directed lines in the diagrams. The convention of $i, j, k, l, ...$ for holes and $a, b, c, d, ...$ for particles is here used [a].

2. summation over indices of the internal lines.

[a] Special attention must be given to assign indices for external lines (which will be found in the final diagrams of CC amplitude equations), because they must be named according to the indices of the excited reference determinant in the bra side.

3. $\hat{F}_N$ and $\hat{V}_N$ interaction lines provide respectively a Fock matrix element $f_{out,in} = \langle out|f|in\rangle$ and an anti-symmetrized two electron integral $\langle out_1 out_2||in_1 in_2\rangle$. Here, *out* and *in* indicate the indices of the outgoing and the incoming line, respectively, and 1 and 2 represent the two different vertices in the two electron operator. The cluster amplitudes are defined in a similar way with: t_{in}^{out}, $t_{in_1,in_2}^{out_1,out_2}$, and so on.

4. factor: equivalent pairs of internal lines give each a factor of 1/2 (where equivalent means internal lines between the same two operators and a pair is given by two hole or two particle lines) and m equivalent operators connected in the same manner add another $1/m!$ factor (e.g. Fig. 2.5).

5. sign (-1)$^{h+l}$ is considered, where h is the number of hole lines and l is the number of loops (which is the path of a series of directed lines that either returns to the same vertex where it starts or begins at an external line and ends at another).

6. each pair of unique external lines, such as two particle or hole lines p and q at two different operators, brings in a permutation P(pq): $P(pq)f(p,q) = f(p,q) - f(q,p)$.

These six rules allow to convert diagrams into algebraic expressions. For example, let us consider the CCD final diagram in Fig. 2.5. The latter diagram shows the operators $\hat{T}_2$ and $\hat{V}_N$ connected by two equivalent pairs of internal lines. This accounts for a factor of $\frac{1}{4}$ according to rule 4. Further, the summation over a, b, i, j is due to the four internal lines and the two electron integral and the double cluster amplitude are easily derived according to rule 3, giving the equation shown in Fig. 2.6. The sign is not changed,

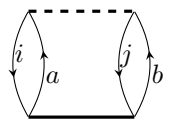

$$= \quad \tfrac{1}{4}\sum_{abij} \langle ij||ab\rangle t_{ij}^{ab}$$

FIGURE 2.6: Example of translation of a diagram into algebraic expression.

because the number of internal hole lines is 2 and the number of loops is also 2. Thus, $(-1)^4$ gives simply a plus sign.

It is worth to remember that a permutation of a pair of hole or particle lines give antisymmetric relations between the $\hat{T}_2$ and $\hat{V}_N$ operator diagrams. For example, the latter CCD energy diagram can also be represented as in Figure 2.7,

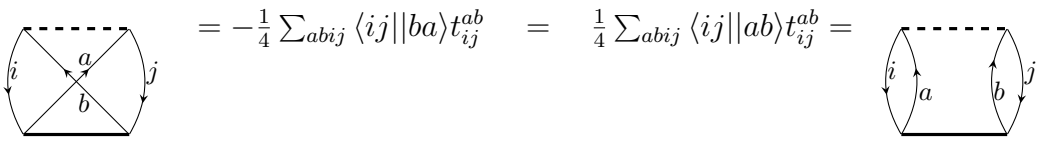

FIGURE 2.7: Antisymmetric property of the Brandow diagrams.

where the two particle lines a and b are exchanged at the Hamiltonian vertices. The algebraic expressions make use of the antisymmetry of the two electron integrals in the Dirac notation: $\langle ij||ab\rangle = -\langle ij||ba\rangle = -\langle ji||ab\rangle = \langle ji||ba\rangle$.

2.3.2 Diagrammatic CC energy equation

In the previous section, all the operators which take part into the CC equations have been described in diagrammatic representation, giving all the necessary tools to derive these equations with diagrams. Further, the basic rules supporting this diagrammatic formalism have driven to a simpler derivation of the CCD energy equation, in comparison to the tedious application of Wick's theorem as in Eq. 2.28.

$$E_{CCD} = \frac{1}{4}\sum_{abij}\langle ij||ab\rangle t_{ij}^{ab}. \tag{2.31}$$

In the same way, the further application of diagrammatic approach to the $\hat{T} = \hat{T}_1 + \hat{T}_2$ truncation can be shown in the following.

Let us consider the general expression of the CC energy equation for the truncation of the cluster operator which includes singles and doubles:

$$E_{CCSD} = \langle\Phi_0|\left(\hat{H}_N + \hat{H}_N\hat{T}_1 + \hat{H}_N\hat{T}_2 + \frac{1}{2}\hat{H}_N\hat{T}_1^2 + \frac{1}{2}\hat{H}_N\hat{T}_2^2 + \hat{H}_N\hat{T}_1\hat{T}_2 + \ldots\right)_c|\Phi_0\rangle. \tag{2.32}$$

The first term on the right hand side, $\langle\Phi_0|\hat{H}_N|\Phi_0\rangle$, is immediately evaluated. Indeed, since the reference determinants are depicted by an empty space and no further contraction with another operator is present, such a matrix element is already represented by the diagrams in Fig. 2.2 and 2.3. It is evident to notice that such diagrams do not satisfy the full contraction condition. Thus, none of them can bring any contribution to the energy equation as such. However, this is expected since the reference expectation value of a normal ordered operator is zero by construction.

In the next terms of Eq. 2.32, contractions between the Hamiltonian and $\hat{T}_1$, $\hat{T}_2$ occur with different order of exponents for the cluster operators, giving various possibilities to reach final diagrams without any external line. Let us consider the second term $\langle\Phi_0|\left(\hat{H}_N\hat{T}_1\right)_c|\Phi_0\rangle$. Here, only the one-electron part of $\hat{H}_N$ can give rise to a fully contracted term. That is, the third diagram in Fig. 2.2, which is the only one with -1 excitation rank, connects with $\hat{T}_1$ giving a final diagram with no external lines and therefore 0 excitation level:

$\langle\Phi_0|\left(\hat{F}_N\hat{T}_1\right)_c|\Phi_0\rangle \quad =$ 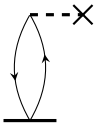

FIGURE 2.8: Contraction of the second term in CCSD energy equation (2.32).

There are also two diagrams from $\hat{V}_N$, fourth and fifth in Fig. 2.3, which give a -1 excitation level. However, their connection with the $\hat{T}_1$ diagram would leave two external lines. Thus, no fully contracted term would be obtained.

Next, the term $\langle\Phi_0|\left(\hat{H}_N\hat{T}_2\right)_c|\Phi_0\rangle$ has already been evaluated in the previous section. So, the subsequent term is evaluated, $\frac{1}{2}\langle\Phi_0|\left(\hat{H}_N\hat{T}_1^2\right)_c|\Phi_0\rangle$. The $\hat{T}_1^2$ term provides a +2 excitation. Hence, the only Hamiltonian diagram that can equilibrate such an excitation is the $\hat{V}_N$ diagram, whose deexcitation -2 can give a fully contracted term (see last diagram in Fig. 2.3). The two $\hat{T}_1$ solid lines in Fig. 2.9 are connected with the two-electron Hamiltonian operator through the only vertices available. and a final

$\frac{1}{2}\langle\Phi_0|\hat{V}_N\hat{T}_1^2|\Phi_0\rangle \quad =$ 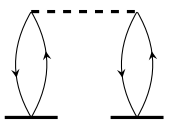

FIGURE 2.9: Example of contraction in one diagram of the CCSD energy equation.

diagram with no external lines is obtained.

Finally, the only terms which are demonstrated to contribute to the CCSD energy equation are given by:

$$E_{CCSD} = \langle \Phi_0 | \left(\hat{F}_N \hat{T}_1 + \hat{V}_N \hat{T}_2 + \frac{1}{2} \hat{V}_N \hat{T}_1^2 \right)_c | \Phi_0 \rangle. \tag{2.33}$$

All the following terms of Eq. 2.32 add higher order contributions of $\hat{T}_1$ and $\hat{T}_2$, which introduce excitation levels higher than +2. The latter would not be possible to be equilibrated by any Hamiltonian diagrams, whose maximum deexcitation level is -2 by $\hat{V}_N$. Thus, *no fully contracted terms can be obtained by higher order contributions than $\hat{T}_2$ in the CCSD energy equation.*

An overview of the three final diagrams giving rise to the CCSD energy equation is given in Fig. 2.10. These diagrams can now be quickly translated into algebraic

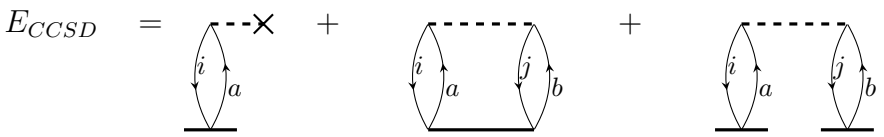

FIGURE 2.10: Diagrammatic representation of the CCSD energy equation with Brandow diagrams.

expressions following the set of rules listed in the previous section. For example, the first diagram in Fig. 2.10 shows two internal lines, which account for a summation over a and i. Further, the Fock matrix element is given by f_{ia}, as expected from rule 3. The single cluster amplitude is also easily derived according to the outgoing and incoming lines, giving the first term in Eq. 2.34. The sign is not changed, because the number of internal hole lines is 1 and the number of loops is also 1. Thus, $(-1)^2$ gives simply a plus sign.

Next, the second diagram of Fig. 2.10 has already been converted into a mathematical expression in the previous section, giving rise to the CCD energy term.

Finally, the third diagram in Fig. 2.10 shows the operators $\hat{T}_1$ and $\hat{V}_N$ connected exactly in the same way for two times. This accounts for a factor of $\frac{1}{2}$ according to rule 4. Further, the four internal lines account for a summation over a, b, i, j and the two electron integral and the two single cluster amplitudes are easily derived from it, resulting in the last term of Eq. 2.34. The sign is also here unchanged, since the number of internal hole lines is 2 and the number of loops is 2.

$$E_{CCSD} = \sum_{ia} f_{ia} t_i^a + \frac{1}{4} \sum_{abij} \langle ij||ab\rangle t_{ij}^{ab} + \frac{1}{2} \sum_{abij} \langle ij||ab\rangle t_i^a t_j^b. \tag{2.34}$$

The latter is the CCSD energy equation. It is worth to underline once again that this equation is not dependent on the higher order terms of the cluster operator, such as $\hat{T}_3$, $\hat{T}_4$, ... The latter would produce diagrams with +3, +4, ... excitation level. However, no diagrams with excitation rank lower than -2 can be generated by the Hamiltonian. Thus, $\hat{H}_N$ can not produce a full contraction with such terms. This means that all the possible further truncation of $\hat{T}$, such as CCSDT or CCSDTQ methods, would still have the energy correctly computed by Eq. 2.34. However, they would affect the calculation of the single and double amplitudes.

2.3.3 Diagrammatic CCD amplitude equation

A derivation of the expression for the CCD amplitude equation is here given in diagrams (the same approach can be generally applied to the CCSD case). Inserting the connected cluster form of $\overline{H}$ (2.23) for $\hat{T} = \hat{T}_2$ into Eq. 2.19 gives the following expression of the amplitude equation:

$$\langle \Phi_{ij}^{ab}|\overline{H}|\Phi_0\rangle = \langle \Phi_{ij}^{ab}| \left(\hat{H}_N + \hat{H}_N \hat{T}_2 + \frac{1}{2} \hat{H}_N \hat{T}_2^2 + \dots \right)_c |\Phi_0\rangle = 0. \tag{2.35}$$

In order to apply the same diagrammatic formalism used in the previous section, some precaution must be used. Indeed, the bra side of the CC amplitude equation contains a doubly excited determinant, $\langle \Phi_{ij}^{ab}|$, which can be also written as $\langle \Phi_0|\{a_i^\dagger a_j^\dagger a_b a_a\}$. The latter can be expressed in a diagram with excitation level -2 with four lines below the operator line. However, this is not shown in the final diagrams, but taken into account keeping a double pair of external lines above the interaction line of the Hamiltonian. This allows to maintain the consistency with the doubly excited determinant $\langle \Phi_{ij}^{ab}|$.

A first consideration can be done once again about the order of the exponents in the components of Eq. 2.35. The terms higher than $\hat{T}_2^2$ introduce more second quantization operators than the ones that can be fully contracted by $\langle \Phi_{ij}^{ab}|$ and $\hat{H}_N$. For that reason, only the first three terms of $\overline{H}$ shown in Eq. 2.35 will give non-zero contributions. In the following, all the possible final diagrams coming from the CCD amplitude equation are derived based on the rules exposed in section 2.3.1 and presented in Fig. 2.11. These diagrams compose the ten terms of the algebraic expression of such equation. Their translation is again based on the rules of section 2.3.1. In comparison to the

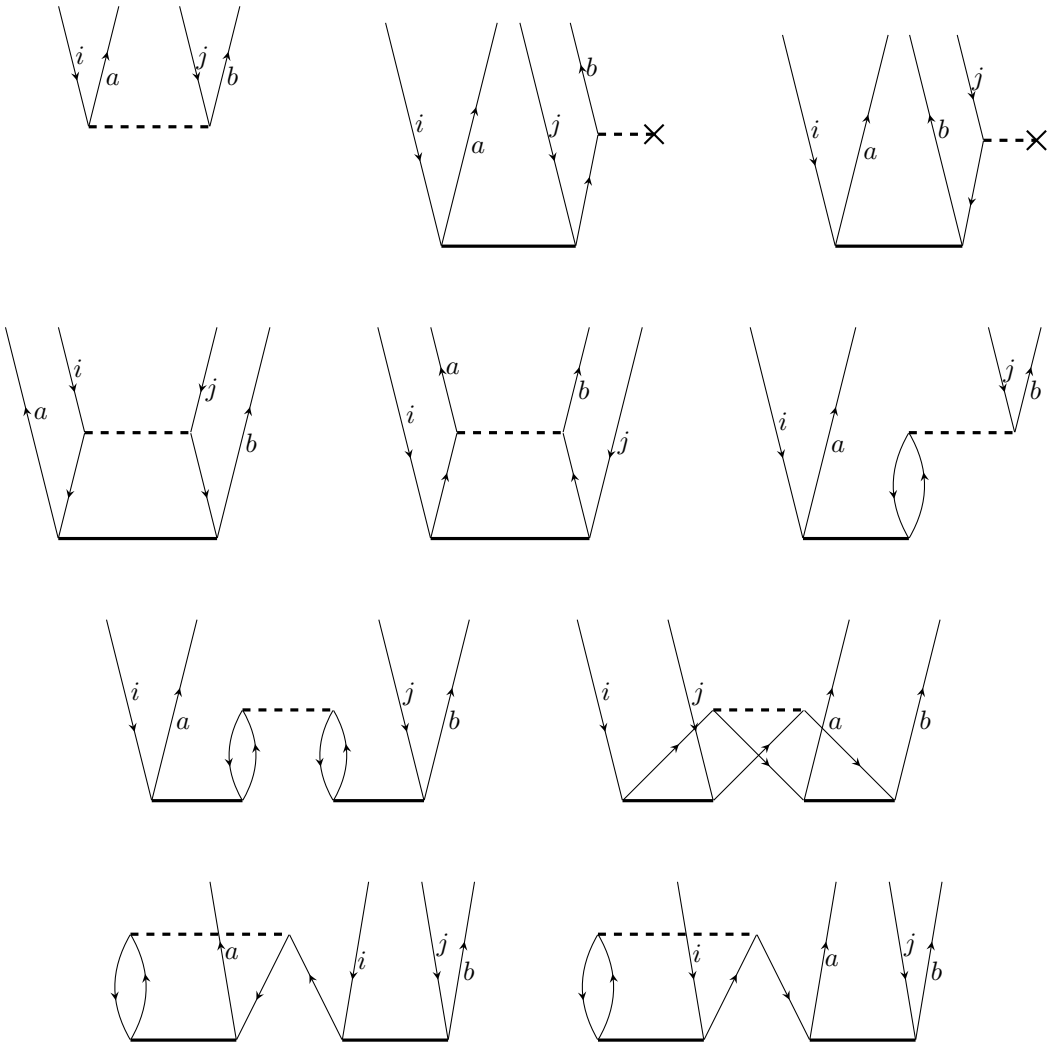

FIGURE 2.11: Diagrammatic representation of the CCD amplitude equation with Brandow diagrams.

energy equation, one must pay attention in the translation step to assign the indices of the external lines from Fig. 2.11. The latter must be consistent with the indices of the doubly excited determinant. While the indices of the internal lines are only dummy indices that can be freely chosen (but still in accordance with the convention for hole and particle lines). Thus, the final CCD amplitude equation can be written as:

$$\begin{aligned}\langle ab||ij\rangle + P(ab)\sum_{c} f_{bc}t_{ij}^{ac} - P(ij)\sum_{k} f_{kj}t_{ik}^{ab} + \frac{1}{2}\sum_{kl}\langle kl||ij\rangle t_{kl}^{ab} + \frac{1}{2}\sum_{cd}\langle ab||cd\rangle t_{ij}^{cd} \\ + P(ab)P(ij)\sum_{kc}\langle kb||cj\rangle t_{ik}^{ac} + \frac{1}{2}P(ab)P(ij)\sum_{klcd}\langle kl||cd\rangle t_{ik}^{ac}t_{lj}^{db} + \frac{1}{4}\sum_{klcd}\langle kl||cd\rangle t_{ij}^{cd}t_{kl}^{ab} \\ - \frac{1}{2}P(ab)\sum_{klcd}\langle kl||cd\rangle t_{kl}^{ca}t_{ij}^{db} - \frac{1}{2}P(ij)\sum_{klcd}\langle kl||cd\rangle t_{ki}^{cd}t_{lj}^{ab} = 0, \quad (2.36)\end{aligned}$$

where the order of the terms reflects the order of the diagrams in Fig. 2.11.

2.4 Distinguishable Cluster Theory

The distinguishable cluster (DC) theory was first introduced in 2013 by Kats and Manby [61] as a slight modification of the double cluster amplitude equation in the CCD method. The DC approach falls into the category of those methods, such as ACP [52, 103], 2CC [58] or pCCSD [59] to name a few, whose derivation is obtained modifying the quadratic portion of the amplitude equation. Such a portion has been derived with diagrams in the previous section as part of the CCD amplitude equation and it can be expressed by four different terms,

$$\langle \Phi_{ij}^{ab} | (\frac{1}{2} \hat{H}_N \hat{T}_2^2)_c | \Phi_0 \rangle = A + B + C + D, \tag{2.37}$$

i.e. the last four terms shown in Eq. 2.3.3 (or the last four diagrams in Fig. 2.11):

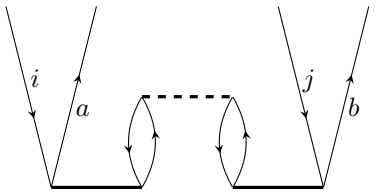

$$A = \frac{1}{2} P(ab) P(ij) \sum_{klcd} \langle kl||cd\rangle t_{ik}^{ac} t_{lj}^{db}$$

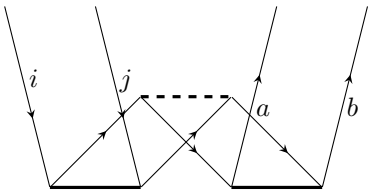

$$B = \frac{1}{4} \sum_{klcd} \langle kl||cd\rangle t_{ij}^{cd} t_{kl}^{ab}$$

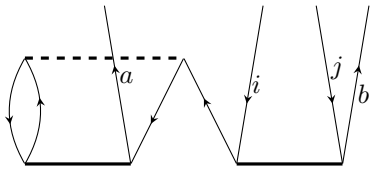

$$C = -\frac{1}{2} P(ab) \sum_{klcd} \langle kl||cd\rangle t_{kl}^{ca} t_{ij}^{db}$$

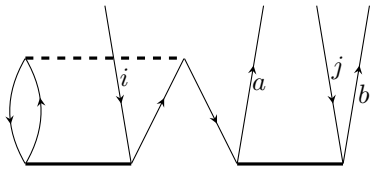

$$D = -\frac{1}{2} P(ij) \sum_{klcd} \langle kl||cd\rangle t_{ki}^{cd} t_{lj}^{ab}$$

FIGURE 2.12: Brandow diagrams of the quadratic portion of the CCD amplitude equation.

The main concept behind the DC approach is the removal or modification of intercluster exchange diagrams, which would play a special role when quasi-degeneracy

arises. The inclusion of such terms in the conventional truncated CC is believed to be one of the sources of the poor behavior encountered in strongly correlated systems.

In the DC theory the attention is given to the ring diagram, i.e. the A term in Fig. 2.12. Such a diagram can be divided into its two components, the Coulomb (A^c) and the exchange (A^{ex}) part. It is relevant to note that such a decomposition of a single Brandow diagram generates two nonantisymmetrized Goldstone diagrams, such as those shown in Fig. 2.13. Thus, contrary to the convention used so far, the Hamiltonian interaction line does not represent an antisymmetrized two electrons integral (e.g. this difference is visible in the algebraic expressions of the antisymmetrized integrals as shown in Fig. 2.12, $\langle kl||cd\rangle$, while in Fig. 2.13 the same Hamiltonian interaction line denotes only $\langle kl|cd\rangle$). However, a further consideration is possible upon these two components of the ring diagram. While the A^c diagram shows the Hamiltonian which

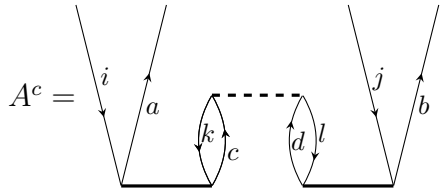

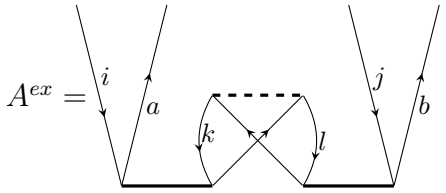

$$A^c = \frac{1}{2}P(ab)P(ij)\sum_{klcd}\langle kl|cd\rangle t_{ik}^{ac}t_{jl}^{bd} \qquad A^{ex} = -\frac{1}{2}P(ab)P(ij)\sum_{klcd}\langle kl|dc\rangle t_{ik}^{ac}t_{jl}^{bd}$$

FIGURE 2.13: Nonantisymmetrized components of the ring diagram from CCD amplitude equation.

interacts with two separate double excitation processes, its exchange counterpart shows the two particles that are exchanged from different double excitations. In a physically exact treatment of a separated system, the contribution arising from the particles exchange of two independent fragments would be expected to be zero, i.e. canceled from higher order terms contributions. For that reason, DC neglects the exchange term arising from the ring diagram. Such a violation of the indistinguishability of electrons in a many-electron system gives the name to the method.

The removal of the exchange term in the ring diagram makes the necessity to rescale also the other three terms, i.e. B, C and D, in order to restore the exactness for two electrons and the particle-hole symmetry of the equation. This factorization of the quadratic term can be written as, $\langle\Phi_{ij}^{ab}|(\frac{1}{2}\hat{H}_N\hat{T}_2^2)_c|\Phi_0\rangle = A^c + A^{ex} + B + C + D + \alpha(2A^{ex} + C) + \beta(2B + D)$, where by setting $\alpha{=}\beta{=}-\frac{1}{2}$, the DC amplitude equation is obtained. Namely the other intercluster exchange diagram is neglected, i.e. the ladder

diagram represented by the B term in Fig. 2.12. The final quadratic portion of the cluster amplitude equation in the DC approach can be written as:

$$\langle \Phi_{ij}^{ab} | (\frac{1}{2} \hat{H}_N \hat{T}_2^2)_c | \Phi_0 \rangle_{DC} = A^c + \frac{C}{2} + \frac{D}{2}. \tag{2.38}$$

The resulting DC approach is invariant to orbital rotations within the occupied or unoccupied orbitals, size extensive, and particle-hole symmetric in the equations. Once a partial orbital relaxation is introduced by the single excitations $e^{-\hat{T}_1} \hat{H}_N e^{\hat{T}_1}$, the corresponding DC with singles and doubles (DCSD) method [62] is also exact for a two electrons system.

In the last decade, a number of different works have demonstrated DCSD to outperform CCSD in strongly and weakly correlated systems [64–70]. Indeed, a qualitatively good result is observed where typically CCSD breaks down in a strongly correlated regime. Even a surprising improvement at the equilibrium geometries is noticed in comparison to CCSD. This is a remarkable performance for DCSD in comparison with other *ic*CC methods. On the one hand, while ACPQ [54–57] and 2CC [58] (which is equivalent to pCCSD(1,0) [59]) are superior to the CCSD method in strongly correlated systems, they show a reduced accuracy in the weakly correlated regime. On the other hand, when an higher accuracy is obtained in the weakly correlated systems, such as pCCSD(μ,1) (where μ is chosen between -1 and -1.5 [104]), the performance for static correlation is not any better than CCSD. In that respect, the DC approach combines both of the advantages introduced separately by these *ic*CC methods and benefits in both strongly and weakly correlated systems.

The particle-hole (*ph*) symmetry is believed to provide the additional property which might partly explain the surprising accuracy of the DC method [105]. Indeed, while the other *ic*CC methods mentioned above all share the properties of exactness for a two electrons system, size-extensivity and orbital invariance, DCSD satisfies also the further criterion of particle-hole symmetry, such as CCSD. The latter property is normally guaranteed in the derivation of approximate wave function methods in terms of second quantized operators or diagrams (this is obviously not true whenever any kind of approximation that destroys the *ph* symmetry is introduced). By definition, a *ph* symmetric formalism is one where the particle and the holes can be interchanged not changing the final set of diagrams: *a set of diagrams is ph symmetric when the replacement of particles by holes and vice versa does not change the set of diagrams.* At the same time, derivation of such methods in terms of second quantization carries even a more restrictive property, i.e. an individual *ph* symmetry for every loop in the

diagrams, the so called local particle-hole (*lph*) symmetry. The latter is defined in the diagrammatic representation of the equation where *the interchange of the particles and holes in each loop of every diagram produces another diagram that already appears in the equation.*

The *ph* and *lph* symmetries do not necessarily provide a more accurate method. However, they are desired properties based on the knowledge that also the exact treatment carry them and their loss can have consequences for the accuracy of the resulting method. Although the *ic*CC methods lack an explicit form of the wave function, it is still possible to evaluate properties and density matrices via Lagrange technique (in the same way as in the traditional CC methods). However, *ic*CC methods that do not properly retain the *ph* and *lph* symmetries in the residual equations might get affected through the one- and two-electron density matrices in the particle-number conservation property. Indeed, such methods do not show the correct null traces [b] and, thus, directly affect the calculation of the correlation energies [105].

[b] In some cases one can still devise *ic*CC approaches that do not satisfy the *lph* symmetry and nevertheless produce the correct traces. However, they might still carry other defects not easily measurable. pCCSD is an example of such methods.

Chapter 3

Further Theoretical Concepts

In this chapter, different theoretical concepts related to the scope of this thesis are introduced. First, the CI method is briefly addressed and, next, an approach in the category of Quantum Monte Carlo methods is presented, namely the Full Configuration Interaction Quantum Monte Carlo. The latter is introduced as a stochastic interpretation of the well known FCI method and the working principles of the NECI algorithm are outlined. Finally, CASSCF is also shortly presented in its basic concepts and the Lagrangian formalism is explained in the calculation of reduced density matrices.

3.1 Configuration Interaction theory

The Configuration Interaction method is introduced as the first natural evolution upon HF and is defined by a wave function of a linear expansion of SDs generated as excitations of the reference determinant Φ_0 (typically HF):

$$|\Psi_{CI}\rangle = \sum_I C_I|\Phi_I\rangle = c_0|\Phi_0\rangle + \sum_{ai} c_i^a|\Phi_i^a\rangle + \sum_{abij} c_{ij}^{ab}|\Phi_{ij}^{ab}\rangle + \dots \tag{3.1}$$

Such a wave function is determined by variational optimization of the expansion coefficients, also called CI coefficients. Whereas the molecular orbitals building each SD are fixed and given by the previous calculation (such as HF). A Lagrange multiplier can be introduced, analogous to the HF method, where the energy is minimized under the constraint of a normalized total CI wave function, i.e. $\langle\Psi_{CI}|\Psi_{CI}\rangle = 1$. In turn, this brings to the CI secular matrix equations $\mathbf{Ha} = E\mathbf{a}$, where the diagonalization of such a matrix leads to the lowest energy in the given basis set (i.e. an upper bound to the true lowest energy of the system). Such an eigenvalue solution provides the corresponding eigenvector with the CI coefficients relative to Ψ_{CI}.

The full CI method is obtained in case no truncation of the excitations in Eq. 3.1 is considered. On the one hand, this makes the resulting method exact in the given basis set. On the other hand, the computational expense becomes intractable very quickly. Indeed, the N-electrons wave functions basis would comprise all the possible determinants constructable from a given basis set. Such a number increases factorially according to the number of electrons and basis functions:

$$N_{det} = \binom{N_\alpha}{M}\binom{N_\beta}{M} = \frac{M}{N_\alpha!(M-N_\alpha)!}\frac{M}{N_\beta!(M-N_\beta)!}, \tag{3.2}$$

where N_α and N_β are respectively the number of α and β electrons and M is the number of spatial orbitals in the given basis set. Although the dimension of the FCI determinants can be also decreased in a number of ways, such as considerations about symmetry and freezing core orbitals, it is evident how the number of SDs raises pretty quickly. For example, for a system of 10 electrons in 10 orbitals a number of 63.5×10^3 determinants is generated, while for a system of 10 electrons in 30 orbitals the amount goes up to 20.3×10^9 . Consequently, such an exact method would result in a memory bottleneck in the actual relative algorithm (due to the storage of more than one vector, each containing the CI coefficients of the entire Hilbert space). In that respect, FCIQMC is introduced as a stochastic method in the context of the FCI approach that allows the calculation of ground state energies of exceptionally large Hamiltonians, well beyond the possibilities of deterministic FCI.

3.2 Full Configuration Interaction Quantum Monte Carlo

The complexity related to exact electronic structure calculations has been naturally driven to approximated methods still able to provide satisfying solutions. One example is given by the truncated CC approach, explained in the previous chapter. However, there is a family of methods that makes use of the classical Monte Carlo scheme [106] to solve the Schrödinger equation. The MC method exploits the principles of inferential statistics to estimate values of an unknown quantity, based on the random sampling of the universe of all the possibilities. Such a method is nowadays used in a variety of different applications [107]. The approach which is focused on the solution of the Schrödinger equation is characterized by the name of Quantum Monte Carlo (QMC).

A variety of different methods has been based on the QMC approach along the years. However, only the review of the FCIQMC method is within the scope of this thesis.

FCIQMC has been proposed in 2009 by Booth et al. [42] as a new variation of the QMC methods able to perform a stochastic diagonalization of large fermionic systems without any additional *a priori* restriction to face the Fermion sign problem. Such a method has been continuously implemented and developed in the NECI program [108] since then. FCIQMC is based on the time integration of the imaginary-time Schrödinger equation,

$$-\frac{\partial \Psi}{\partial \tau} = \hat{H}\Psi, \tag{3.3}$$

where τ=it is the imaginary time. The formal solution of Eq. 3.3 can be written as,

$$|\Psi(\tau)\rangle = e^{-\tau \hat{H}}|\Psi(\tau = 0)\rangle, \tag{3.4}$$

where an arbitrary initial wave function $|\Psi(\tau = 0)\rangle$ is given. Let us assume an initial wave function $\Psi_0^{(0)}$ with a non-zero overlap with the true ground state wave function Ψ_0, i.e. $\langle\Psi_0^{(0)}|\Psi_0\rangle \neq 0$. Thus, $\Psi_0^{(0)}$ can be expanded in terms of the eigenstates of the Hamiltonian. In that way, the system will converge onto the ground state in the limit of a long time propagation,

$$|\Psi_0\rangle = \lim_{\tau\to\infty} e^{-\tau(\hat{H}-S)}|\Psi_0^{(0)}\rangle. \tag{3.5}$$

where an arbitrary shift S is subtracted to the diagonal elements of the Hamiltonian. In the long term limit, such a shift takes the value of the ground state energy and make Eq. 3.5 project out all higher energy states but the ground state. Shifting the Hamiltonian by a constant is possible since the eigenstates do not get changed and the eigenvalues are only shifted.

The advantage related to the FCIQMC approach in comparison with other QMC methods is the stochastic integration of Eq. 3.3 in a pure antisymmetric space. Such a space prevents the method to converge onto a Bosonic solution, but it does not make it circumvent the Fermion sign problem, typical of the QMC methods. The walker annihilation is the crucial step which allows to overcome such a problem. However, in order to work in an antisymmetric space the FCIQMC wave function Ψ is expanded in a basis of SDs, such as Eq. 3.1. The latter is then introduced into the imaginary-time

Schrödinger equation providing a set of linear first order differential equations,

$$-\frac{dC_i}{d\tau} = \underbrace{(K_{ii} - S)C_i}_{\substack{death \\ step}} + \underbrace{\sum_{j \neq i} K_{ij} C_j}_{\substack{spawning \\ step}}, \tag{3.6}$$

where a new matrix K is used, which is the difference between the matrix elements of the Hamiltonian and the HF energy, $K_{ij} = \langle \Phi_i | \hat{H} | \Phi_j \rangle - E_{HF}\delta_{ij}$. Eq. 3.6 is the working equation of the FCIQMC method and can also be solved deterministically. However, the memory bottleneck, which is related especially to the prohibitive costs of the storage of the CI coefficients, makes its stochastic integration much more practical. Indeed, such an integration is performed by a number of signed walkers which sample the SDs space. This sampling follow the population dynamics dictated by Eq. 3.6. Such an evolution algorithm can be performed in three steps (the *spawning*, *death* and *annihilation* steps) at each iteration, once a discrete time step $\Delta\tau$ is considered:

1. *Spawning step*: Each walker that lives on a determinant D_i is attempted to randomly spawn to a coupled determinant D_j [a] with probability: $p_s = \Delta\tau \frac{|K_{ij}|}{p_{gen}(i|j)}$, where p_{gen} is the probability given by the excitation generator algorithm taken into account[b]. Ideally, the excitation generator would provide a non-uniform p_{gen} proportional to the Hamiltonian matrix element, such that strongly coupled determinants are more likely to be proposed and $\frac{|K_{ij}|}{p_{gen}(i|j)} \approx const.$ Indeed, in such a case the spawning probability would be only determined by the time step.

2. *Death step*: All the walkers populating the current wave function are evaluated through the death probability $p_d = \Delta\tau(K_{ii} - S)$. The latter defines how likely a walker dies, thus not participating in the following *annihilation* step. In other words, p_d favors the low energy determinants to survive. In the rare case when a positive shift occurs (e.g. when a rapid increase of walker population is required), then $p_d < 0$ and the walker is instead cloned with probability $|p_d|$.

3. *Annihilation step*: This is the crucial step that allows to overcome the Fermion sign problem. All the new walkers arising in the previous two steps are evaluated with the remaining walkers populating the same determinant. Pairs of walkers of opposite sign are then annihilated. This is done for every populated determinant.

[a] The term coupled refers to two determinants whose matrix element is not zero, in our example $\langle D_i | \hat{H} | D_j \rangle \neq 0$. Since the Hamiltonian is at most a two-electron operator, the pairs of determinants that will give a non-zero matrix element can differ only by one or two spin orbitals.

[b] A variety of different algorithms for excitation generators are available in NECI [108]

At first, the shift is kept constant in order to allow the walker population to grow. Once the designated number of walkers, N_w, is reached (which is set in the input), S start to change, thus enhancing the death probability of walkers until a constant value of the target population is achieved.

Finally, the FCIQMC correlation energy can be calculated with the projective technique:

$$E_{corr} = \frac{\langle \Phi_0 | \hat{K} | \Psi \rangle}{\langle \Phi_0 | \Psi \rangle}, \tag{3.7}$$

where $|\Phi_0\rangle$ represents the reference determinant, i.e. typically the most populated SD. Such an energy should agree with the shift S in stationary condition, in order to confirm the proper convergence. Indeed, it is worth to note that the ground state wave function is achieved only if a sufficient number of walkers samples the Hilbert space, i.e. the space of all the possible configurations of the electronic wave function. If a number of walkers under this critical value is considered, a manifestation of the sign problem would be evident providing an unphysical dominant solution rather than the true ground state of the system under study [109].

An effective solution has been introduced in the *spawning* step by the initiator approximation, i-FCIQMC, [43] in order to achieve convergence at a lower number of walkers than this critical value. At first, only one initiator determinant is defined which corresponds to the reference SD. Then, the set of initiators can dynamically grow to include the important determinants. This set includes the only determinants that can spawn onto unoccupied determinants. In other words, i-FCIQMC introduces the neglect of certain matrix elements between non-initiator determinants and unoccupied determinants. However, one exception is given by two non-initiator determinants spawning walkers with same signs onto the same unoccupied determinant. In that case, the spawning is maintained. The set of initiators is controlled by a minimum threshold value n_{in}. This means that any non-initiator determinant whose number of walkers exceeds n_{in}, can in turn become an initiator and thus spawning onto other unoccupied determinants. Usually n_{in} is defaulted to 3 [43]. Such a threshold approach leaves then the flexibility to the set of initiator determinants to be dynamically enlarged, but without incurring into the sign-incoherence experienced in the original algorithm. In i-FCIQMC, the convergence on the ground state energy is not longer controlled by a minimum critical value, however, the N_w is required to grow until the population on the reference determinant achieves several thousands of walkers (50000 walkers as a rule of thumb) [110]. The initiator approximation is here used by default, thus the i-FCIQMC is always implied when talking about FCIQMC.

It is worth to note, that a certain bias is introduced together with the initiator approximation. Such an error can get substantial in large systems, where the number of walkers used is not sufficient, thus introducing a systematic undersampling of the non-initiator determinants. This bias has been recently corrected by the so called adaptive shift [84], which is used in some of the calculations in the present thesis.

Additionally, the semi-stochastic approach [111, 112] can be used in the FCIQMC calculations. Such a scheme considers a subset of the occupied determinants, typically the most populated ones, to be treated deterministically. The latter allows to reduce the stochastic noise, thus reaching a lower stochastic error for equal time integrations.

3.3 Complete Active Space Self-Consistent Field

Ab-initio electronic structure methods have always been challenged by systems where static correlation plays a crucial role. Indeed, a special focus is given in QC to cases where the electronic wave functions are characterized by multiple equally important configurations, which all significantly contribute to the final ground-state. This is obviously not possible to be described by HF with a single SD. The multi-configurational self consistent field (MCSCF) approach, for example, is a method which allows to properly describe such systems, and it was developed as a natural extension of the HF method. Here, compared to CI methods, not only the expansion coefficients of the SDs are optimized, but also the MOs. Such an optimization is performed by iterative technique such as SCF. Indeed, the method is equal to HF when a single configuration is considered. This means that such MCSCF methods take into account a further step in comparison to an FCI confined in a given orbital space. The latter is usually referred to as CAS-CI, where only the CI coefficients are optimized. It is worth to remember that an FCI wave function which is properly expanded in all possible configurations of a given basis set is invariant to orbital changes. The reason is that when all possible configurations are considered, the orbitals changes can only modify the expansion coefficients, but the total energy (or any density matrices) will stay the same.

The simultaneous variational optimization of CI and MOs coefficients ensures that the orbitals used do not introduce any bias towards a particular reference determinant from a previous SR calculation. Indeed, since the choice of a CAS is often done on SR orbitals, the MOs optimization gives the needed flexibility to provide the best orbitals associated to a MR wave function. However, such a double optimization represents a complicated computational problem for two reasons. The first regards the number

of possible SDs arising from all the excitations in a given orbital space, that becomes unbearable very quickly (as already mentioned in Sec. 3.1). The second regards the MCSCF wave functions, which are more prone to converge on local solutions. The former limits the applicability of such a method to small size active spaces. The latter is normally solved optimizing by a second order expansion of the energy in the variational parameters. This second-order SCF procedure can be performed by different optimization techniques [113], such as Newton-Raphson or Super-CI.

The static electron correlation normally recovered by MCSCF wave functions is pivotal when near-degenerate configurations are encountered. However, a challenging step involved in the MCSCF methods is the choice of the configurations which properly describe the properties of interest. Among the different MR strategies, the Complete Active Space Self-Consistent Field [30–34] represents the conventional first step to study these problems. In CASSCF, the selection of configurations is done at the orbital level, in the so called active and inactive orbitals. The active MOs are those where the double

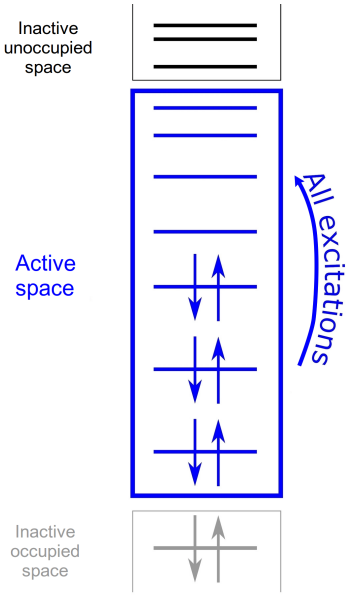

FIGURE 3.1: Schematic illustration of CAS orbitals division.

optimization is performed and usually consist of doubly or singly occupied orbitals together with the relative consistent virtuals. While the inactive space is characterized by doubly occupied and empty orbitals. Typically, the active space is supposed to contain most of the static correlation given by the important orbitals involved in the problem under study. For that reason, CASSCF is not a black-box method and the choice of the orbitals requires some chemical insights about the system at hand and must be done manually. The conventional notation in CASSCF is given by CAS(N_e,M),

where N_e represents the number of electrons considered in the active space and M is the number of orbitals in it. Thus, the notation CAS indicates an orbital space where all the configurations arising from the possible distributions of these N_e electrons in M orbitals are considered into the MR wave function (see Fig. 3.1).

The exponential computational cost related to the CASSCF method can be reduced by different strategies. For example, the Restricted active space SCF (RASSCF) [114] can be taken into account, where the active space is divided into three sections and restrictions are introduced in the number of excitations allowed. A similar approach is given by the Generalized active space SCF (GASSCF) [115], where the RASSCF method is further generalized considering multiple restricted active spaces. Further, the multiple studies in this field over the years made different flavors of CASSCF available. For example, the DMRG-CASSCF [47] or the Stochastic-CASSCF [50]. The latter exploits FCIQMC in a similar way to the external correction for tailored CC explained in this work. Indeed, in both methods the large CI eigensolver made available by the efficient NECI algorithm [108] is used to get CI coefficients of active space sizes well beyond deterministic limits. Naturally, the subsequent step characterizes each method, relaxing the amplitudes out of the active space with CC in the TCC approach and optimizing the MOs using an approximated form of the super-CI method in Stochastic-CASSCF.

The factorial increase in the configurations generated in an active space is the main limit of the CASSCF method. Such a limit makes the selection of the proper active orbitals important to target the right configurations in the problem at hand. A few guidelines can be used here, such as in the following, in order to choose a correct set of orbitals:

1. for every included occupied orbital the corresponding virtual can be taken (e.g. when an occupied $2p$ orbital is considered, the relative $3p$ is typically chosen in order to take into account the radial correlation)

2. a correct CASSCF wave function can be obtained once the active space consists of all the valence orbitals (obviously this is practical only in small molecules)

3. as a rule of thumb, the highest occupied and lowest unoccupied RHF orbitals can give a good insight into the selection of the important orbitals (however this can result in a vicious circle since CASSCF is generally adopted in cases where the MR character is significant and in those cases RHF is usually qualitatively wrong)

4. natural orbitals (NOs) are a noticeable help. Their occupation numbers can differ significantly from 0 or 2 (in a closed-shell system) and this is usually a sign of

important contribution into electron correlation given by the relative orbital. This path has been especially used in the present work and a further explanation of NOs can be found in Section 3.4.

Once the active space targets the right orbitals, the CASSCF method offers a qualitative good description of the system that can subsequently be used to recover additional electron correlation. Indeed, a MCSCF method does not typically recover a large fraction of the total correlation energy of the system. For that reason, the choice is usually driven onto further MR methods such as CASPT2 [116, 117], MRCI [118] or MC-PDFT [119], where an additional calculation is performed on top of the CASSCF wave function. Such methods represent a valid alternative in the dynamic correlation problem and in the present work they are used as a comparison to the novel tailored DC approach.

3.4 Natural Orbitals

The natural orbitals are obtained upon diagonalization of the one-electron density matrix. In this process, the resulting eigenfunctions would then be the natural orbitals and the eigenvalues the corresponding occupation numbers. The NOs were first introduced in 1955 by Löwdin [120] in his research for a simpler and more physically meaningful interpretation of the CI wave function. In the limit of the full CI method, the energy does not depend anymore on the specific set of molecular orbitals employed. However, a carefully chosen set of MOs would provide a compact CI expansion, i.e. a minimal number of orbitals with significant occupation. Whereas a poorly chosen set will give many orbitals with significant occupation. Löwdin showed that if the chosen orbitals are eigenfunctions of the one-electron density matrix the corresponding orbitals would give the most compact CI expansion. Further, the resulting natural orbitals would produce physically meaningful eigenvalues, i.e. the occupation numbers.

The one- and two-electron density matrices are commonly used in QC, since they allow an efficient evaluation of molecular properties of the system under study, such as the expectation values of one- and two-electron operators. The CC equations derived with a projection technique, as in the present work, provide a non-variational wave function. For that reason, the calculation of density matrices must undergo the construction of a Lagrangian that yields the same energy of the non-variational CC wave function, but which is variational in all parameters [121]. This variational Lagrange

functional [122] introduces the so called Lagrange multipliers, λ, which are determined variationally together with the cluster amplitudes.

The CC Lagrange functional can be formulated via the standard CC energy expression, Eq. (2.15), and its set of constraints given by the connected amplitude equations, Eq. (2.19). Thus, the resulting Lagrangian can be written as a function of the cluster amplitudes t and the Lagrange multipliers λ:

$$\mathcal{L}_{CC}(t,\lambda) = \langle\Phi_0|\hat{H}e^{\hat{T}}|\Phi_0\rangle + \sum_{\mu}\lambda_{\mu}\langle\mu|e^{-\hat{T}}\hat{H}e^{\hat{T}}|\Phi_0\rangle, \tag{3.8}$$

where μ represents the excited projection manifold and λ_μ the relative Lagrange multiplier. The variational conditions are then imposed onto all the Lagrangian variables, t_μ and λ_μ:

$$\frac{\partial\mathcal{L}_{CC}}{\partial\lambda_{\mu}} = 0 = \langle\mu|\overline{H}|\Phi_0\rangle \tag{3.9}$$

$$\frac{\partial\mathcal{L}_{CC}}{\partial t_{\mu}} = 0. \tag{3.10}$$

The first stationary condition for the multipliers, Eq. (3.9), provides the standard projected equations for the CC amplitudes. This ensures that the constraint is satisfied. At the same time, the stationary condition for the cluster amplitudes, Eq. (3.10), gives the equations to determine the multipliers. The Lagrange multipliers are then obtained iteratively by this set of equations and can be used to provide the one-electron density matrix.

Once the CC Lagrangian is stationary, it corresponds to a variational expression of the CC energy, $\mathcal{L}_{CC} = E_{CC,\mathcal{L}} = \langle\Lambda|\hat{H}|\Psi_{CC}\rangle$, where the bra state is defined as $\langle\Lambda| = \langle\Phi_0| + \sum_\mu \lambda_\mu\langle\mu|e^{-\hat{T}}$. Such an energy is less sensitive to numerical errors in the CC amplitudes in comparison to $E_{CC} = \langle\Phi_0|\hat{H}|\Psi_{CC}\rangle$. Inserting the Hamiltonian in spin orbital basis, Eq. (2.12), into $\mathcal{L}_{CC}$, Eq. (3.8), one can obtain:

$$E_{CC,\mathcal{L}} = \sum_{pq} f_{pq}\gamma^p_q + \frac{1}{4}\sum_{pqrs}\langle pq||rs\rangle\Gamma^{pq}_{rs}, \tag{3.11}$$

where the one- and two-electron CC Lagrangian density matrices are introduced, respectively γ_q^p and Γ_{rs}^{pq}. The latter can be written as:

$$\gamma_q^p = \langle \Lambda | a_p^\dagger a_q | \Psi_{CC} \rangle, \tag{3.12}$$

$$\Gamma_{qs}^{pr} = \langle \Lambda | a_p^\dagger a_r^\dagger a_s a_q | \Psi_{CC} \rangle, \tag{3.13}$$

where the matrices are non-Hermitian due to the similarity transformed Hamiltonian. Thus, the one-electron density matrix, for example, can be calculated as the derivative of the Lagrangian with respect to the Fock matrix elements:

$$\gamma_q^p = \frac{d\mathcal{L}_{CC}}{df_{pq}}. \tag{3.14}$$

If the energy expression and the amplitude equations in Eq. (3.8) are replaced by the corresponding DCSD ones, DCSD one-electron density matrices can be obtained and the relative NOs determined upon their diagonalization.

In the present work, DCSD NOs are often used to define the active space where the external correction will be applied. In cases when NOs are defined on a wave function different from FCI, the most compact CI expansion can not be assumed to be rigorously guaranteed. However, since the majority of the correlation energy is recovered by most practical methods, and, DCSD even provides good qualitative description in strongly correlated systems, the resulting occupation numbers are still considered to give a good guideline to select the important orbitals for the active space.

Chapter 4

Embedding schemes

The following embedding schemes have been implemented in the Molpro package [123–125] and the CI coefficients collection from FCIQMC in the NECI algorithm [45, 108].

4.1 Tailored Coupled Cluster or Distinguishable Cluster

The tailored Coupled Cluster approach was first proposed in 2005 by Kinoshita et al. [80]. However, the field of externally corrected CC methods had already started to move the first steps many years back. Although the first approaches were based on the idea of adding the three- and four-particle clusters in the CCSD amplitude equations from an external calculation, the idea used in TCC to properly choose an active space and exploit the relative CI-type function can be dated back to 1994 [126], followed by further similar works by Paldus and Planelles [73, 74] [a]. Bartlett and coworkers [80], however, proposed the TCC approach on a slightly different idea from the previous *ec*CC methods. Here, the external correction is given by the $\hat{T}_1$ and $\hat{T}_2$ cluster amplitudes, rather than higher excited clusters. This means that, unlike other *ec*CC methods, the tailored CC approach insists on the correct structure of the reference function.

The main concept these split-amplitudes strategies [127] is based on is the possibility to define two different cluster operators thanks to the exponential formalism of CC. In TCC, such cluster operators are defined as:

$$|\Psi_{\mathrm{TCC}}\rangle = e^{\hat{T}}|\Phi_0\rangle = e^{\hat{T}^{\mathrm{CC}}+\hat{T}^{\mathrm{CAS}}}|\Phi_0\rangle, \tag{4.1}$$

[a] An interesting overview of such methods is available from Paldus [51]

where $\hat{T}^{CAS}$ represents the cluster amplitudes which are extracted from an higher accuracy calculation such as CAS-CI, while $\hat{T}^{\mathrm{CC}}$ is the cluster operator which is relaxed at the CC level. In principle, this split-amplitude enforces a separation of the electron correlation into static and dynamic parts. Such a separation is done at the orbital level in an active space concept (for that reason the superscript CAS is used). In this way, $\hat{T}^{\mathrm{CAS}}$ is assumed to describe most of the static correlation and such information would be transferred in the amplitudes of the singles and doubles cluster operators, $\hat{T}_1^{\mathrm{CAS}}$ and $\hat{T}_2^{\mathrm{CAS}}$. $\hat{T}^{\mathrm{CC}}$ would then take care of the remaining dynamic part in a subsequent step handled by the CC equations. Obviously, accounting for the entire active space, i.e. the space of all the possible SDs arising from any excitation of the reference determinant, by only single and double amplitudes whose value is kept frozen is an approximation. However, since the projected energy expression contains only single and double amplitudes, the FCI energy is retained in the CAS.

In the tailored formalism, the externally corrected amplitudes, $\hat{T}^{\mathrm{CAS}}$, are frozen in the subsequent CC step for two reasons [80]. First, a remarkable difference is noted between the cluster amplitudes which are responsible for the static correlation of the system and the corresponding ones obtained from the CAS-CI coefficients. Then, freezing the CAS operator and thus neglecting the effects of the remaining CC operator, $\hat{T}^{\mathrm{CC}}$, onto it is chosen as a "reasonable compromise" to alleviate the deficiency of CC in strongly correlated regimes. Second, its implementation into an existing CCSD code is facilitated. Indeed, one needs to read in the external CAS amplitudes and zero out the relative residual vectors.

The $\hat{T}_1^{\mathrm{CAS}}$ and $\hat{T}_2^{\mathrm{CAS}}$ amplitudes are first extracted as CI coefficients from an external calculation, such as CAS-CI, and then converted into CC amplitudes according to the well-known relations:

$$\begin{aligned} \hat{C}_1 &= \hat{T}_1, \\ \hat{C}_2 &= \frac{1}{2}\hat{T}_1^2 + \hat{T}_2, \\ \hat{C}_3 &= \frac{1}{3!}\hat{T}_1^3 + \frac{1}{2}(\hat{T}_1\hat{T}_2 + \hat{T}_2\hat{T}_1) + \hat{T}_3. \end{aligned} \tag{4.2}$$

Indeed, the exact wave functions shown in Eq. 2.1 and Eq. 3.1 are equal, i.e. $\hat{C}|\Phi_0\rangle = e^{\hat{T}}|\Phi_0\rangle$, even though a different parametrization is in place. Thus, the excitations can be matched rank by rank providing the relations of Eq. 4.2 [b]. After the conversion, $\hat{T}^{\mathrm{CAS}}$ is inserted and frozen into the projective CCSD amplitude equations, where $\hat{T}^{\mathrm{CC}}$

[b] The final working relations can be found writing explicitly the second quantized form of them and projecting onto the relevant determinants. Resulting in $t_a^i = c_a^i$, $t_{ab}^{ij} = c_{ab}^{ij} - t_a^i t_b^j + t_b^i t_a^j$, ...

is optimized as usual:

$$\begin{aligned} \langle \Phi_i^a | e^{-\hat{T}^{\mathrm{CC}} - \hat{T}^{\mathrm{CAS}}} \hat{H} e^{\hat{T}^{\mathrm{CC}} + \hat{T}^{\mathrm{CAS}}} | \Phi_0 \rangle = 0 \qquad & \{i, a\} \not\subset \mathrm{CAS} \\ \langle \Phi_{ij}^{ab} | e^{-\hat{T}^{\mathrm{CC}} - \hat{T}^{\mathrm{CAS}}} \hat{H} e^{\hat{T}^{\mathrm{CC}} + \hat{T}^{\mathrm{CAS}}} | \Phi_0 \rangle = 0 \qquad & \{i, j, a, b\} \not\subset \mathrm{CAS} \end{aligned} \tag{4.3}$$

$i, j, ...$ and $a, b, ...$ represent respectively the occupied and unoccupied orbitals in the $|\Phi_0\rangle$ reference determinant. Cluster operators containing only active orbitals are excluded from $\hat{T}^{\mathrm{CC}}$ and the relative optimization.

It is worth remembering that the tailored approach is inherently a SR formalism. Therefore, an underlying CC method that can provide better results than the canonical CCSD can be beneficial. In the present work, the DCSD approach is considered since its qualitatively correct description of the strongly correlated systems and the enhanced accuracy of the weakly correlated ones [64], in comparison to CCSD, can be advantageous in the respective tailored formalism. Although the TCC method has been shown so far in terms of CC formalism, its application to the DC theory is not limited by the lack of the latter of a formal wave function. Indeed, it is simply possible to apply the same strategy explained above to the DCSD amplitude equations and the relative TDCSD method is obtained. Size-consistency is still a property of the final TCC as long as the external correction is provided by a size-consistent calculation [80]. The same is valid for TDC, since the underlying DC approach is also size-consistent.

The missing optimization of the $\hat{T}^{\mathrm{CAS}}$ operator represents of course an approximation within the tailored formalism. Such a lack has been investigated in further detail in the present work through the adoption of a simple intermediate region approach (see Section 5.2). That is, a buffer region is chosen in the CAS space, where the amplitudes are allowed to relax in both CAS-CI and subsequent CC/DC equations. Whereas the rest of the CAS amplitudes are frozen as usual after the CAS-CI step.

The definition of an active space where the external correction is applied represents a delicate step in order to obtain a physically meaningful result. For example, the potential energy curves analyzed in the present work (see Chapter 5) make near-degenerate configurations appear when a molecular dissociation is studied, e.g. in N_2. This gives a SR wave function, typical of the equilibrium geometry, a MR character in the stretched region. Normally, the CASSCF calculations are an obvious choice to define the active space. However, the expensive computational costs of such a method make it impractical to apply to large active spaces. An alternative to such an approach is proposed here, i.e. through the DCSD natural orbitals. The latter, obtained by diagonalization of the one-body density matrix, provide information about the most

correlated orbitals of the system through its occupation numbers (which significantly differ from zero or two). In such a way, one can make use of the ability of DC theory to qualitatively correctly describe strongly correlated systems.

FCIQMC is the external correction of choice for the resulting tailored CC/DC approach employed in the present work. Indeed, the tailored formalism is plagued by two main drawbacks, the bias toward a specific reference determinant and the missing relaxation of the CAS amplitudes. The choice of an external correction that can evaluate active spaces well beyond a deterministic FCI possibility is the key to alleviate such limits. In that respect, FCIQMC provides an efficient tailored approach that can be systematically improved as long as a stochastic CAS-CI is computationally possible. In the past few years, a combination of CC with FCIQMC had already been accomplished [128, 129]. However, in both previous studies the goal was different, i.e. improving the efficiency of both methods, high order CC and FCIQMC, to approach the exact FCI energy. In the first work [128], the objective is to exploit FCIQMC in order to select important high-order excitations for CC(P,Q) methods. In the second [129], the main idea is to speed up the CC convergence towards FCI energetics by means of three- and four-body cluster amplitudes from FCIQMC. In the present work, a different methodology is presented. That is, making use of FCIQMC as a powerful CI eigensolver, whose single and double amplitudes are then extracted for a specific active space in order to externally correct the CCSD/DCSD amplitude equations. On the one hand, the resulting tailored method would allow treating much larger problems than those possible by direct application of FCIQMC. On the other hand, the CC/DC description of the dynamic correlation out of the active space is likely to be very accurate. Thus, providing an attractive novel method whose performance is shown in the following, see Chapters 5, 6 and 7.

In the present work, the CI coefficients are often collected from the stochastic CI eigensolver provided by FCIQMC. This can be done by exploiting the direct relationship between the number of walkers, N_i, on each SD, D_i, and the relative CI coefficients: $\frac{C_i}{C_0} = \frac{N_i}{N_0}$, where N_0 refers to the number of walkers on the reference determinant. After the FCIQMC calculation reaches the preset number of walkers chosen to populate the Hilbert space, in principle the collection of CI coefficients can start. However, a certain number of iterations is usually required first to let the projected correlation energy converge and then the collection begins. At each iteration, the code loops over the list of all the populated determinants, which are stored using a hash table, and extract its excitation level. The latter is determined by a comparison of the bit representations of

the considered determinant with the reference. If the excitation matches the desired one, then the coefficient value is extracted and stored as well in a hash table. In the present implementation, only the coefficients related to single, double and triple excitations are considered. However, a lookup of the hash table is always executed first. In case the considered CI coefficient is already in the table, it is updated by simple summation. In case it is not present yet, a new hash table entry is created. The algorithm is required to store the coefficients over a certain number of iterations, i.e. a time integration at convergence that is long enough to reduce the stochastic error, and only at the end to average them and to normalize them with respect to the average number of walkers onto the reference determinant, N_0. Further, due to intermediate normalization, $\langle\Phi_0|\Psi_{CAS-CI}\rangle = 1$ (where $|\Psi_{CAS-CI}\rangle$ is characterized by an expansion as Eq. (3.1)), it is important to consider a reference determinant among the top-weighted ones in the CAS space [130, 131]. Finally, this extraction and average mechanism in NECI is ameliorated by the semi-stochastic approach, which greatly reduces the stochastic error.

One of the main advantages of the NECI algorithm is its efficient parallelization on large compute clusters [108]. This is possible due to the distribution of the walkers over many processors and a small general communication. The latter is mainly limited by the annihilation step. However, the CI coefficients collection is also extended to work in parallel. Indeed, the above mentioned loop over the populated determinants can be run on every processor and none of the determinants is evaluated twice in the same iteration, since every specific determinant is never handled by more than one processor. Indeed, one of the features of the NECI algorithm is to keep the number of walkers per processor constant and move some determinants to other processors in order to maintain a certain load balance.

Finally, a further extension of the TCC approach with perturbative triples has been evaluated in the present work, i.e. TCCSD(T). Such a perturbative correction was introduced in the tailored formalism in 2011 by Bartlett and coworkers [130]. The resulting method augmented with the (T) correction is introduced to partially alleviate the problem due to the missing relaxation of the active space at the CC level. However, TCCSD(T) follows the same implementation as standard CCSD(T), with the only difference that the latter involves all the CCSD amplitudes and the former only the $\hat{T}^{\mathrm{CC}}$ ones, i.e. those amplitudes with at least one inactive index. The main idea of CCSD(T) is to introduce triples in a non-iterative manner in order to evaluate the perturbative correction only once [29, 132–134]. Thus, such a treatment transforms a method correct through third order of perturbation theory, CCSD, into a method correct through

fourth order. The latter is already achieved by the previous CCSD+T(4) and CCSD[T] methods [135]. However, CCSD(T) includes also one fifth order singles-triples term into the energy correction. Such an addition was devised to balance the contribution of single and double excitations in order to prevent an overestimation arising from the connected triples [29]. The formula of the perturbative triples correction for CCSD(T) can be written as:

$$E_{(T)} = E_T^{[4]} + E_{ST}^{[5]} \tag{4.4}$$

where the first term on the right-hand side is the missing contribution to make the final energy correct through fourth order PT and the second term is the additional contribution arising from fifth order perturbation theory, which couples the single and triple excitations. These energy contributions can be expressed in terms of second order triple amplitudes, $\hat{T}_3^{(2)}$, which can be calculated with the corresponding second order CC amplitude equation for triples. In turn, the latter is characterized by first order $\hat{T}_2$ amplitudes that, in the CCSD(T) implementation, are replaced by the converged CCSD double amplitudes (see Ref. [132–134] for explicit expressions of the energy correction and the $\hat{T}_3^{(2)}$ equation). The final correlation energy is then calculated as $E_{corr} = E_{CCSD} + E_{(T)}$. The same is valid for TCCSD(T) if the amplitudes used for (T) are from $\hat{T}^{\mathrm{CC}}$. It is worth to notice that an additional term arises in Eq. (4.4), $E_{DT}^{[4]}$, in case non-HF orbitals are used [132], which is normally the case in the present thesis.

This non-iterative perturbation treatment introduces the energy correction a posteriori. This means that the CCSD amplitudes are relaxed as usual (with a computational cost that scales as $n_o^2 n_v^4$) and, only then the non-iterative perturbation treatment is applied to the system (scaling as $n_o^3 n_v^4$) [c]. Since non-HF orbitals are usually employed in the calculations of the present work, the occupied-occupied and virtual-virtual blocks of the Fock matrix are diagonalized and $\hat{T}_1$ and $\hat{T}_2$ are transformed into this pseudo-canonical basis before the (T) calculation. TCCSD(T) keeps the same computational cost as CCSD(T) and accounts for triples connected clusters, which make the excitation space more balanced and symmetrical. Additionally, it is used in Chapter 6 as a further comparison with the TDCSD method.

4.1.1 Triple excitations

An additional contribution of triple excitations from the external correction has been evaluated in the tailored approach. Indeed, in the CCSD method, the disconnected

[c] The n_o and n_v refer to the number of occupied and virtual orbitals, respectively.

contributions in the wave function account for all excitations through fourth order MBPT, except for the connected triples. However, the latter can also be important, since they contribute to the fourth order MBPT energy [100]. Further, the importance of connected triples has been studied in CC from the very first works [28, 95]. Since then, it has been known that the dominant contribution to $\hat{C}_3$ is represented by $\hat{T}_3$ when HF orbitals are used in a ground-state calculation of closed-shell systems. Although the application of different orbitals, such as the natural orbitals in the present work, in systems away from the equilibrium geometry makes the disconnected triples in $\hat{C}_3$ more and more important, the $\hat{T}_3$ correction included in the tailored formalism is studied and seen to accelerate the convergence with respect to the active space size.

In order to include the connected triples arising from the active space, the CC equations in 4.3 are modified such that $\hat{T}_3^{\mathrm{CAS}}$ is now included:

$$\begin{aligned}
&\langle \Phi_i^a | e^{-(\hat{T}_1+\hat{T}_2)} \hat{H}_N e^{\hat{T}_1+\hat{T}_2} + \hat{H}_N \hat{T}_3^{\mathrm{CAS}} | \Phi_0 \rangle = 0 \\
&\langle \Phi_{ij}^{ab} | e^{-(\hat{T}_1+\hat{T}_2)} \hat{H}_N e^{\hat{T}_1+\hat{T}_2} + (\hat{H}_N \hat{T}_3^{\mathrm{CAS}} + \hat{H}_N \hat{T}_1 \hat{T}_3^{\mathrm{CAS}})_c | \Phi_0 \rangle = 0.
\end{aligned} \tag{4.5}$$

These new equations give rise to seven additional contributions in the resulting single and double amplitude equations. The latter are shown by diagrams in Fig. 4.1 for the single amplitudes equation and in Fig. 4.2 for the double amplitudes equation.

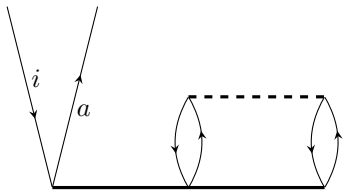

FIGURE 4.1: Additional $\hat{T}_3^{\mathrm{CAS}}$ contribution in the CC amplitude equation for singles.

It is important to notice that only the two diagrams arising from $\langle \Phi_{ij}^{ab} | \hat{V}_N \hat{T}_3^{\mathrm{CAS}} | \Phi_0 \rangle$, i.e. the first two diagrams in Figure 4.2, have an actual influence on the final energy of the total system [d]. Indeed, all the other terms would contribute only to the double residual with indices acting only in the active space. However, even their implementation has been useful, since a countercheck of the corresponding residual equal to zero is possible to guarantee a proper functioning of the extraction, conversion and addition of

[d] The final energy of the active space is completely determined by the single and double CAS amplitudes.

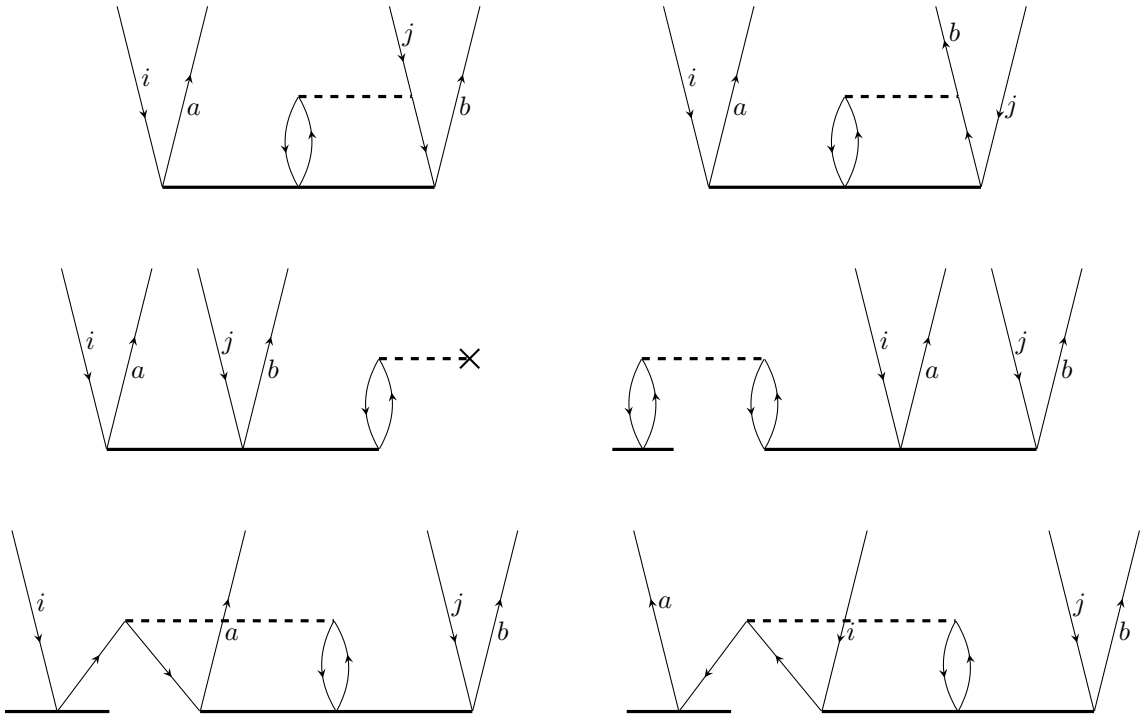

FIGURE 4.2: Additional $\hat{T}_3^{\mathrm{CAS}}$ contributions in the CC amplitude equation for doubles.

triples [e].

Finally, a simple addition of the first two terms from Figure 4.2 into the double amplitude equations of TDCSD or TCCSD results in a method with the final energy further corrected also from the triple CAS amplitudes. The latter are kept frozen as the other CAS amplitudes during the iterative solutions of the DCSD or CCSD amplitude equations. The resulting method is denoted in the present work TDCSD@T and TCCSD@T.

4.2 Screened Coulomb formalism

A further embedding is here presented based on the screened Coulomb formalism. The main concept is to absorb the long range nature of the Coulomb interaction into the collective behavior of the system. That is, an effective screened interaction that accounts for the screening of the charge of an electron by the other electrons. Here, such an interaction is taken into account by a screened fluctuation density inspired by the direct

[e] In the Molpro implementation, the one- and two-electron integrals are dressed with the single amplitudes. This means that the last three diagrams in Figure 4.2 coming from the quadruple excitation $\hat{T}_1\hat{T}_3^{\mathrm{CAS}}$ are already accounted for once the other contributions from $\hat{T}_3^{\mathrm{CAS}}$ are implemented.

random phase approximation (dRPA). The RPA method was first devised in 1953 by the physicists Bohm and Pines [136] in their attempt to study metals through the model system of the uniform electron gas by a physically motivated approximation. RPA applications have seen a revival in the quantum chemistry community [137], especially for the intimate relationship with CC [138].

In the present approach, the embedding is obtained at the orbital level. The system is divided into embedding and embedded fragments. Then, the screened integrals are generated for the embedded region and saved into the FCIDUMP [139], which is by now a standard file format to write one- and two-electron integrals. Such embedding at the mean-field level corresponds to the frozen core (and frozen virtuals) approximation. However, in this case the information about the embedding is introduced into the fragment only at the one-body level. Additional information can be provided by using screened integrals.

The screened integrals are obtained by introducing a screened fluctuation density in a dRPA manner [63]:

$$\tilde{\rho}_{ai} = \rho_{ai} + \tilde{T}^{ik}_{ac}\rho_{kc}, \tag{4.6}$$

Then, the corresponding screened Coulomb interaction can be written as

$$(\widetilde{pq}|\widetilde{rs}) = \int d\mathbf{r}_1 \int d\mathbf{r}_2 \tilde{\rho}_{pq}(\mathbf{r}_1)|\mathbf{r}_1 - \mathbf{r}_2|^{-1}\tilde{\rho}_{rs}(\mathbf{r}_2), \tag{4.7}$$

where

$$\tilde{\rho}_{pq} = \begin{cases} \tilde{\rho}_{ai} & p \in \text{virt}, q \in \text{occ} \\ \rho_{pq} = \phi^*_p\phi_q & \text{otherwise}, \end{cases} \tag{4.8}$$

and $\tilde{T}^{ij}_{ab}$ are the contravariant doubles amplitudes $\tilde{T}^{ij}_{ab} = 2T^{ij}_{ab} - T^{ij}_{ba}$. For example, one-external screened integrals $(\widetilde{ki}|\widetilde{ai})$ correspond to $(ki|bj) + (ki|ld)\tilde{T}^{il}_{ad}$. Here, the indices $i, j, k, \ldots$, $a, b, c, \ldots$, and $p, q, r, \ldots$ denote occupied, virtual, and general spatial orbitals, respectively, and the summation over repeated indices is assumed.

The screened effective one-electron part of the Hamiltonian can be obtained by screening integrals of the Fock matrix in a local particle-hole symmetric representation,

$$\tilde{f}_{pq} = \tilde{h}_{pq} + (\widetilde{pq}|\widetilde{kk}) - \frac{1}{2}(\widetilde{pk}|\widetilde{kq}) - (\widetilde{pq}|\widetilde{aa}) + \frac{1}{2}(\widetilde{pa}|\widetilde{aq}) + (\widetilde{pq}|rr) - \frac{1}{2}(pr|rq) \tag{4.9}$$

$$= \begin{cases} f_{ji} + \frac{1}{2}\tilde{T}^{il}_{bd}(ld|jb) & p,q \in \text{occ} \\ f_{ab} - \frac{1}{2}\tilde{T}^{kl}_{ad}(ld|kb) & p,q \in \text{virt} \\ f_{pq} & \text{otherwise.} \end{cases} \tag{4.10}$$

The $\tilde{f}_{ai}$ block of the screened Fock matrix is left unscreened, since this block is used only in the singles amplitude equations, which correspond to orbital relaxation and are thus not modified. Using the screened integrals the distinguishable cluster amplitude equations can be derived.

The screened Coulomb formalism can be employed to fold an additional bath information into the Hamiltonian of the embedded system. The integrals of the subsystem are replaced by screened integrals $(\widetilde{pq}|\widetilde{rs})$ and $\tilde{f}_{pq}$. The double-counting is avoided by ensuring that at least one of the indices of the double amplitudes utilized in the screening corresponds to the orbital space outside of the embedded region. Additionally, the single and double residual contributions coming from the singles and doubles with at least one bath index are added to the effective one-, $\tilde{h}_{ai}$, and two-, $\widetilde{(ai|bj)}$, body part. The RPA embedding does not increase the effective particle manifold of the operator. Thus the resulting embedded Hamiltonian still contains only one- and two-body terms, however, the hermiticity is lost. With this definition, DCSD embedded in the DCSD produces the total DCSD energy.

Two different procedures have been devised to apply the screened embedding approach to a certain system. One adopts the DCSD calculation as a starting point to generate the embedded space and the subsequent dressed FCIDUMP. Whereas the other relies on the TDCSD calculation. Then, the FCIQMC calculation is performed starting from the dressed FCIDUMP, which is now non-Hermitian as a consequence of the dressing. Both of the procedures are presented in the corresponding results given in Chapter 7.

4.3 Perturbative Basis Set Correction

The introduction of a finite Gaussian basis set allowed to reduce the electronic structure problem into a large matrix eigenvalue problem. However, the inherent error of these finite basis sets has to be considered when solving the Schrödinger equation. Indeed, the *ab-initio* results depend on the quality of the basis set and it is known from the Kato's cusp condition [140] that the Gaussian functions fail to properly describe the exact wave function for the electron-nucleus and for the electron-electron coalescence points. Such an error is usually taken care of by basis set corrections. In the present work, a perturbative F12 correction is considered [141, 142]. Such a correction is calculated with the DCSD/CCSD F12 Lagrangian removing the contribution of the DCSD/CCSD active-space residual,

$$L[\mathbf{T_1}, \mathbf{T_2}, \mathbf{C}] = E[\mathbf{T_1}, \mathbf{T_2}, \mathbf{C}] + \sum_{i=1}^{2} \tilde{\mathbf{T}}_i \boldsymbol{\Omega}_i[\mathbf{T_1}, \mathbf{T_2}, \mathbf{C}] - \tilde{\mathbf{T}}_i \boldsymbol{\Omega}_i^{\mathrm{AS}}[\mathbf{T_1}, \mathbf{T_2}] + \tilde{\mathbf{C}} \boldsymbol{\Omega}^{\mathrm{F12}}[\mathbf{T_1}, \mathbf{T_2}, \mathbf{C}], \quad (4.11)$$

where $\mathbf{T_1}$, $\mathbf{T_2}$, represent the usual single and double TDCSD/TCCSD amplitudes, $\mathbf{C}$ denotes the F12 amplitudes satisfying the first order coalescence conditions and the tilde shows the corresponding contravariant quantities, which replace the Lagrange multipliers. Finally, the DCSD-F12/CCSD-F12 amplitude equations and the DCSD/CCSD residuals in the active space are given by $\boldsymbol{\Omega}_i$, $\boldsymbol{\Omega}_i^{\mathrm{AS}}$, while the F12 amplitude equations are represented by $\boldsymbol{\Omega}^{\mathrm{F12}}$.

In the following results part of this thesis (see Chapters 5-7), the F12a and F12b approaches [64, 143, 144] are employed. Further, in the closed-shell systems (Chapter 5), a further F12 correction is introduced to the FCIQMC method, FCIQMC$_{\mathrm{F12}}$, as an alternative to the previous established F12 approaches [145, 146]. This is obtained once the active space spans the complete orbital space. That is, the CI coefficients are collected in a FCIQMC calculation which considers the entire basis set. After the extraction, they are inserted in Molpro [123–125], converted into CC amplitudes and frozen as in the tailored approach, yielding the same energy as FCIQMC, since no orbitals are left for the CC amplitudes relaxation to take place. Finally, the perturbative basis set correction is applied, giving the FCIQMC$_{\mathrm{F12}}$ method.

Part III

Results

Chapter 5

Closed-shell molecular systems

The novel tailored DCSD method is applied to a few closed-shell molecules, from the dissociation of the diatomic nitrogen molecule to the evaluation of the ozone isomers. The goal is to assess the validity of TDCSD in the strongly correlated regime and recover the quantitatively correct results in comparison to conventional DCSD. In this chapter, the study is guided by the different possibilities of choosing an active space. In addition to the more common CASSCF route, an alternative based on natural orbitals given by a DCSD calculation is presented. In this way, large active spaces can be defined and subsequently studied by FCIQMC calculations.

In the present chapter, potential energy curves of three different molecules and additional various case studies are considered [147]. *Ab-initio* methods that aim to generate precise and reliable PECs must account for an accurate dynamic and static electron correlation description. Conventional SR methods break down when applied to bond breaking regimes, due to the degeneracy arising in the reference state. In the following, the accuracy and reliability of the newly implemented FCIQMC-TDC method are assessed through these non-trivial problems, in comparison with accurate reference values.

5.1 Computational Details

The evaluation of the TDCSD method has taken place through a number of test systems, such as the diatomic molecules of nitrogen and fluorine and the water molecule. Further, ethylene and cyclobutadiene have also been studied in order to assess TDCSD in geometries whose small structural variations cause immediate changes in the wave function. Finally, the study of closed-shell systems have been extended to the ozone molecule. Such a system represents an interesting problem in QC, since a strong

interaction of static and dynamic electron correlation is at work in O_3, even when no bond breaking is considered [148–151].

All the systems considered in this chapter are closed-shell, i.e. the reference determinant of the ground state electronic structure presents only doubly occupied orbitals. The results from every molecule are presented in graphs with the TDCSD values together with the corresponding TCCSD ones as comparison. Furthermore, the new external correction in the context of tailored methods given by FCIQMC, i.e. FCIQMC-TDC/TCC, has been benchmarked versus calculations where a deterministic FCI would provide the external CAS amplitudes whenever computationally affordable, denoted in the following as FCI-TDC/TCC.

Internally contracted multi-reference CI (MRCI) with Davidson correction (MRCI+Q) [118], has been calculated and used as accurate reference value throughout the present chapter. Such reference is obtained from the Molpro package [123–125] and explicit correlation can also be included [152].

Every tailored calculation has been performed on top of natural orbitals. The DCSD NOs have been obtained from the orbital-relaxed density matrices provided by the closed-shell implementation in Molpro. A perturbative basis set correction is applied upon TCC/TDC methods based on the Valeev's perturbative F12 approach [141]. The cc-pVTZ basis set has been used, while the core electrons have been maintained frozen in the correlated computations. In the basis set corrections the cc-pVTZ/mp2fit and cc-pVTZ/jkfit basis sets have been employed respectively for the density fitting and the complementary auxiliary basis (CABS).

A subtractive embedding scheme has been used in the strongly correlated systems, in a similar manner as defined by the embedded MRCC methods [153]. The space of the most active DCSD NOs determines the embedded space where the FCI calculation is accomplished. The difference in energy between the embedded FCI and the embedded DCSD gives the correction, which is then applied to the total DCSD energy: $E = E^{\mathrm{tot}}_{\mathrm{DCSD}} + (E^{\mathrm{CAS}}_{\mathrm{FCI}} - E^{\mathrm{CAS}}_{\mathrm{DCSD}})$.

The FCIQMC calculations have been performed sampling the Hilbert space with different number of walkers, according to the system under study. This brought to consider a minimum of 10^5 walkers, for example, in the CAS(10,8) of the N_2 molecule up to a maximum of 10^8 walkers employed in the ozone case. Furthermore, the semi-stochastic method has also been used with deterministic space defined by the 1000 most populated SDs. The adaptive-shift method has been applied only in the ozone case and the trial space which determines the new shift [84] was defined by 1000 determinants.

Finally, the CI coefficients have been collected over a fixed number of iterations which was set to 5000 for the following closed-shell systems.

5.2 Nitrogen (N_2)

The first dissociation presented with the novel tailored approach regards the N_2 molecule. Its characteristic triple-bond breaking has been studied since decades and the relative difficulties encountered in a SR framework are especially long known [154–156]. Multiple solutions have been proposed and successfully applied along the years in order to overcome such shortcomings, some of them represented by the multi reference approaches. The latter have shown to provide reliable results, which are here included as comparison in the form of MRCI+Q. The TDCSD is applied on the N_2 diatomic molecule and the results are presented in Figure 5.1.

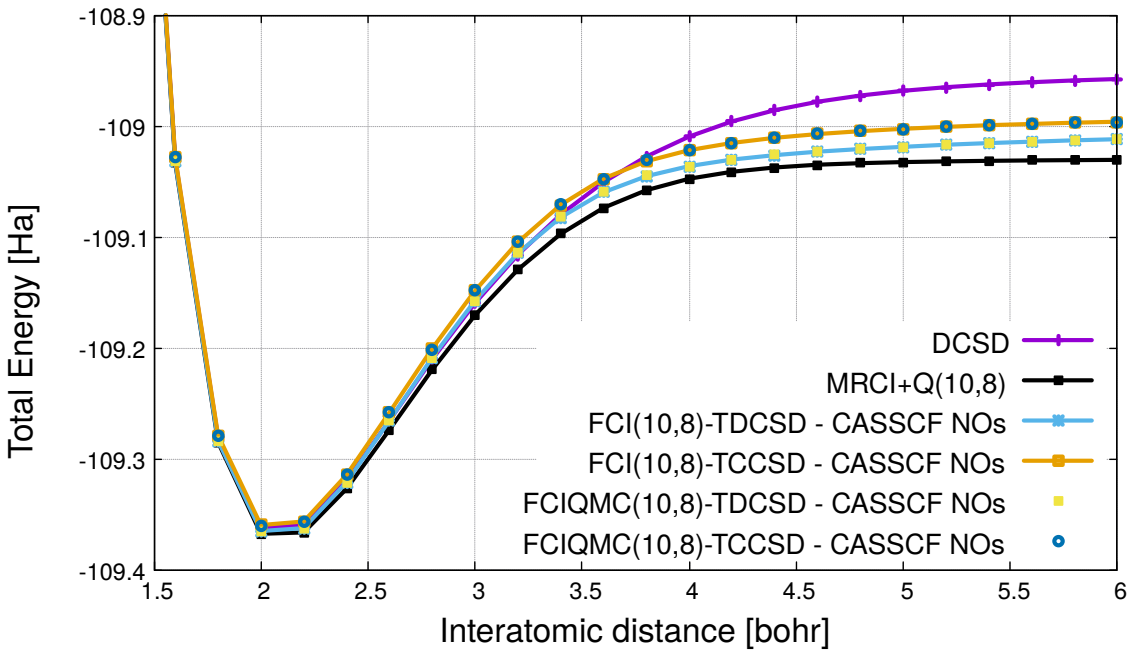

FIGURE 5.1: Potential energy curves for N_2 with (10,8) active space

The tailored DCSD/CCSD results are shown for both external corrections, from deterministic and stochastic FCI. The amplitudes extraction is performed in an active space consisting of 10 electrons in 8 orbitals. Such CAS(10,8) is determined by CASSCF NOs and composed of the complete valence space, i.e. two σ and two π orbitals with the corresponding antibonding orbitals, which originate from the $2s$ and $2p$ orbitals of both atoms.

It is evident from Figure 5.1 that the tailored DCSD/CCSD calculations corrected by FCIQMC are on top of FCI based results, as expected. Further, the TDCSD dissociation shows a closer curve to the reference MRCI+Q than the TCCSD, especially from the stretched region on. The DCSD curve shows a qualitatively good dissociation that is remarkable if compared to conventional CCSD, which breaks down. Specifically, DCSD is on top of the TDCSD results up to 3.4 bohr and after that the error increases.

Figure 5.2 shows the tailored calculations with a larger active space considered for the external correction. Here, 10 electrons in 16 orbitals constitute a new CAS where the DCSD NOs and the CASSCF NOs are both evaluated. In the CASSCF calculation, the CAS(10,16) corresponds to the $3s$ and $3p$ orbitals from both atoms added onto the CAS(10,8). These additional virtuals gradually acquire a $3d$ character along the larger

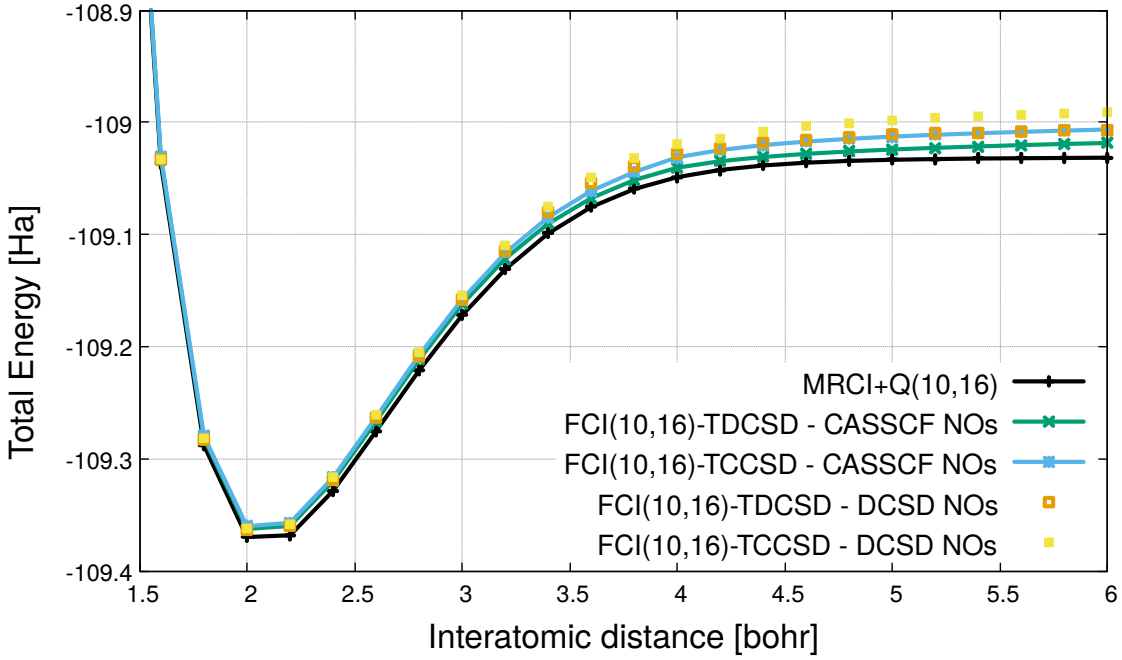

FIGURE 5.2: Potential energy curves for N_2 with (10,16) active space

distances of the dissociation. In the DCSD NOs, the CAS(10,16) also consists of s, p, and d atomic orbitals.

It is possible to see from Figure 5.2 that the CASSCF NOs definition of the active space provides more accurate tailored results than the DCSD NOs ones. The TDCSD based on DCSD NOs is even shown to accidentally overlap with the TCCSD curve based on CASSCF NOs. This confirms that the quality of the active space and the accuracy of the correlated method are here comparably important. As shown in the CAS(10,8), the TDCSD approach performs better than TCCSD also in this larger active space.

Further, the TDCSD-CASSCF NOs curve is even more parallel than the other methods to the reference curve. Indeed, the non-parallelity errors (NPEs) amount to 15 mHa for TCCSD-CASSCF NOs in the region between 1.4 and 5 bohr, while only to 5 mHa for TDCSD-CASSCF NOs.

Figure 5.3 presents various TDCSD results based on DCSD NOs that differ in the active space choice. For example, a larger active space is considered, CAS(10,26), and also a subtractive embedding scheme. The largest CAS is taken with the size of the double-zeta basis set in order to make the subsequent TDCSD act as a basis set correction. Indeed, such a CAS would already include a large portion of the dynamic correlation. The

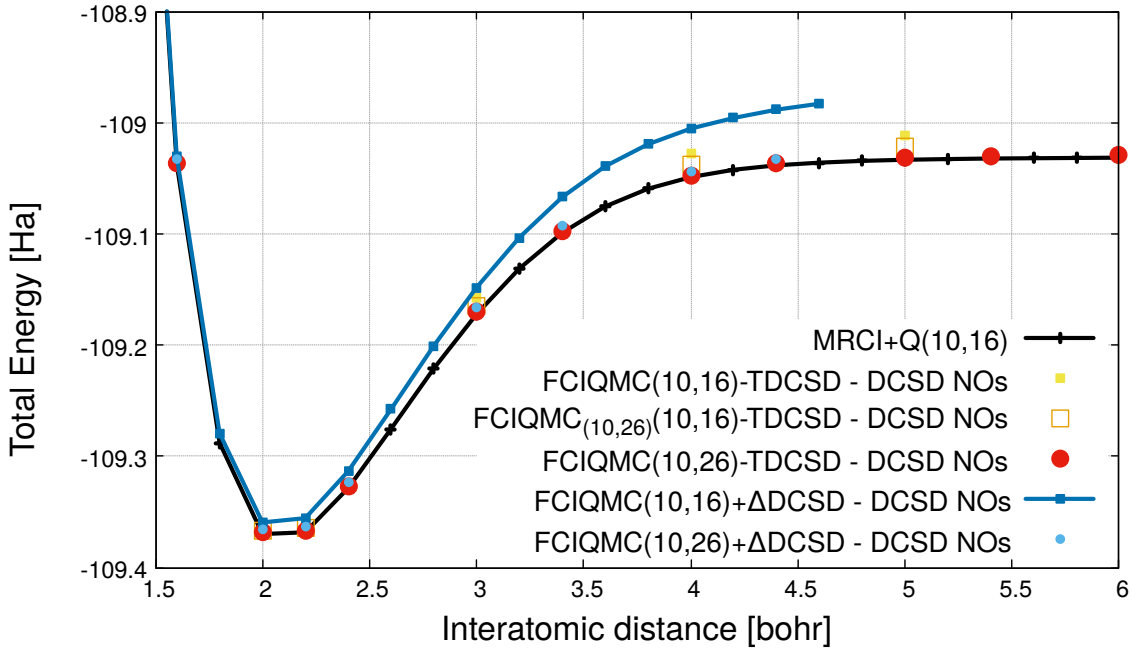

FIGURE 5.3: Comparison of N_2 PECs from various TDCSD methods with MRCI+Q and the subtractive embedding scheme

high accuracy provided by TDCSD(10,26) is evident in Figure 5.3, since the results lie on the MRCI+Q(10,16) curve. Additionally, a subtractive embedding scheme is presented on the two largest active spaces considered in N_2, FCIQMC(10,16)+ΔDCSD and FCIQMC(10,26)+ΔDCSD. Evidently, the curve shown by FCIQMC(10,16)+ΔDCSD is less accurate than the TDCSD based on the same CAS. This confirms that the coupling between the active space and the remaining region is important. However, when the subtractive embedding is applied to the larger CAS(10,26), the resulting curve is much closer to the corresponding TDCSD values.

An intermediate region approach is also introduced in Figure 5.3, denoted as $\text{FCIQMC}_{(10,26)}$(10,16)-TDCSD. The latter notation indicates that the CI coefficients extracted from the FCIQMC(10,26) calculation are used in the smaller CAS(10,16). This means that the buffer region provides amplitudes for a partial relaxation. Thus, they can still influence the CI coefficients, even though they are relaxed in the subsequent DCSD step. The resulting dissociation in Figure 5.3 shows a PEC which lies between the TDCSD(10,16) and TDCSD(10,26) curves. It is evident that in this case the accuracy of the method in the region is more relevant than the relaxation of the amplitudes in the buffer.

The next graph shown for N_2 dissociation, Figure 5.4, regards the basis set correction of the methods seen so far. This perturbative F12 is applied to TDCSD calculations as well as to the FCIQMC in the full cc-pVTZ basis set. The $\text{TDCSD}_{\text{F12b}}$ and $\text{FCIQMC}_{\text{F12b}}$

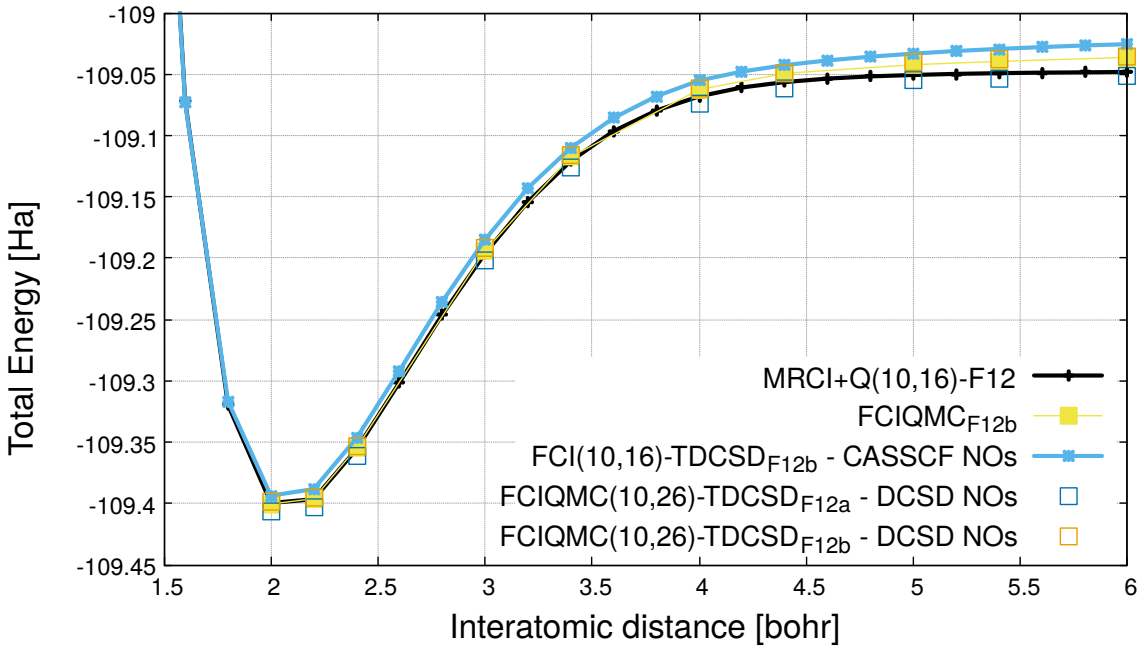

FIGURE 5.4: Potential energy curves for N_2 with the F12 correction

calculations overlap with the MRCI+Q-F12 results around the equilibrium geometry. However, for stretched geometries deviations from the reference curve are visible. This can be due to the usage of contravariant amplitudes instead of Lagrange multipliers in Eq. (4.11). Such a problem in a previous study of the N_2 dissociation [142] brought to errors of ∼10 mHa. Additionally, the F12 approximation itself carries a potential error, as seen in Figure 5.4 with the $\text{TDCSD}_{\text{F12a}}$ and $\text{TDCSD}_{\text{F12b}}$ curves. Indeed, the former is much closer to the reference PEC than the latter.

Finally, the $\hat{T}_3^{\mathrm{CAS}}$ corrected tailored methods are also evaluated for the triple bond breaking of N_2. This further correction is applied to the TDCSD and TCCSD methods on the CAS(10,16), where there is still room for improvement towards the reference MRCI+Q curve.

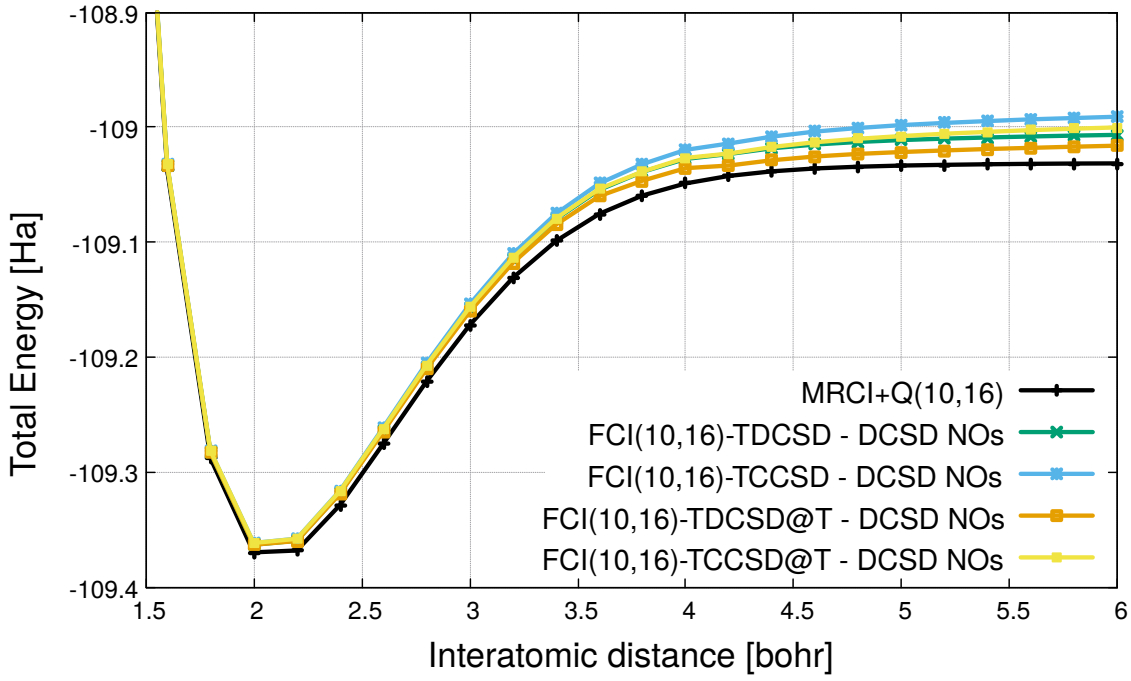

FIGURE 5.5: N_2 PECs of TDCSD/TCCSD with additional $\hat{T}_3^{\mathrm{CAS}}$ correction

In Figure 5.5, the $\hat{T}_3^{\mathrm{CAS}}$ corrected methods show a similar effect on both TDCSD and TCCSD approaches. Indeed, all the PECs mostly overlap at the equilibrium region. They start to deviate from r=3 bohr on, showing the TDCSD@T and TCCSD@T results closer to the MRCI+Q(10,16) for the stretched geometries, in comparison with the TDCSD and TCCSD curves, respectively. Interestingly, the TDCSD@T results approach the reference PEC in the dissociated region, showing values almost halfway between the TDSCD and MRCI+Q curves.

In case CASSCF NOs are considered, the same effect of Figure 5.5 is found. However, a reduced energy lowering towards the reference PEC is shown. Indeed, the largest $\hat{T}_3^{\mathrm{CAS}}$ correction is seen in the intermediate stretched region (for r=3-4 bohr) with differences between the conventional tailored methods and the corresponding @T up to 2 mHa closer to MRCI+Q(10,16). Whereas, such differences take values up to 10 mHa in the DCSD NOs case. Such a variation between the different NOs can be seen as a

consequence of the more accurate description given by the CASSCF NOs already at the TDCSD/TCCSD level, see Figure 5.2.

5.2.1 Comparison with analytic potential function

In the present section, a further study of the N_2 dissociation is accomplished in the cc-pVQZ basis set. The analysis of the resulting PECs is evaluated in comparison with a similar work performed with another *ec*CC method, the RMR-CCSD approach and its (T) corrected variant, RMR-CCSD(T) [157]. The RMR method has been introduced in 1997 by Paldus and coworkers [75, 76] in order to study quasi-degenerate systems with a less prohibitive computational cost than full MR treatments. It has proven to be very accurate and reliable in strongly correlated systems [158–160]. As in the tailored approach, RMR involves the selection of a proper reference space and relies on an external correction, that is MR-CISD. However, the latter is used to extract approximated $\hat{T}_3$ and $\hat{T}_4$ cluster amplitudes, which are then added to the standard CCSD equations to obtain new $\hat{T}_1$ and $\hat{T}_2$ amplitudes and the relative RMR energy.

The N_2 PECs provided by Ref. [157] are supported by an accurate analytic potential function based on a thorough experimental data analysis from another work [161]. In the following, the focus is given to the critical region represented by interatomic

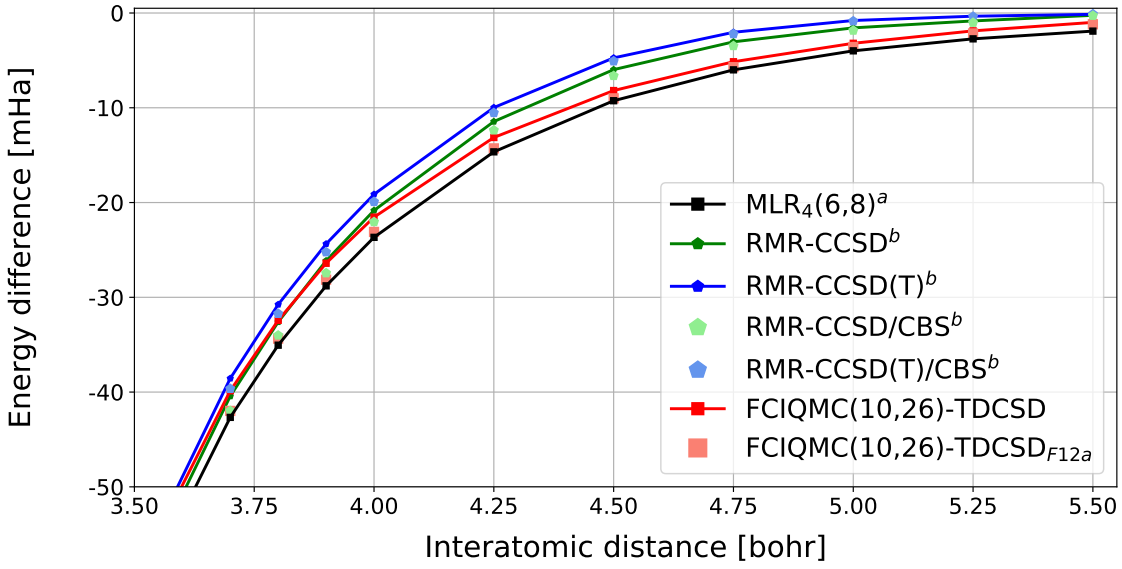

FIGURE 5.6: N_2 PECs in the critical region of highly stretched geometries, plotted as E(r)-$E_{equilibrium}$-D_e. [a] direct potential fit of experimental data from Ref. [161]. [b] RMR values from Ref. [157]

distances between 3.5 and 5.5 bohr, in order to reproduce Fig. 2 of Ref [157]. In their

work, Paldus and coworkers plot all the curves with respect to a dissociation limit, D_e, taken as the origin, whereas the analytic function uses an experimentally obtained dissociation energy. In the present work, as in Ref. [157], the D_e value is extrapolated with a least-squares fit to a Morse-type potential based on the last 8 computed values of the PEC. Further, the only potential shown from Le Roy et al. [161] is the $MLR_4(6,8)$, which is defined as the best possible choice by the authors.

It is evident from Figure 5.6 that all the curves show a general good agreement with the $MLR_4(6,8)$ potential. However, a remarkable trend is shown for the explicitly correlated TDCSD method, which almost overlaps with the analytic potential. Further, the non-parallelity errors of the values in Figure 5.6 amount to ∼1.9 mHa for the RMR-CCSD/CBS method and to only ∼0.5 mHa for $TDCSD_{F12a}$, highlighting the consistency of the results between $TDCSD_{F12a}$ and $MLR_4(6,8)$. Interestingly, the RMR-CCSD(T) curve seems to give lower accuracy if compared to its RMR-CCSD counterpart. The latter is further confirmed by the NPE which amounts to ∼2.4 mHa in the RMR-CCSD(T)/CBS case.

5.3 Fluorine (F_2)

In this section, the accuracy of tailored methods is evaluated through PECs of F_2 molecule. The first CAS under study consists of the full valence active space, as in the N_2 case. The resulting active space is composed by the $2s$ and $2p$ atomic orbitals with their 14 electrons, CAS(14,8), thus containing only one single virtual spatial orbital. Such an active space does not allow any excitation but singles and doubles. Indeed, the FCI is equivalent to CCSD and DCSD in such a CAS. Consequently, the tailored methods suffer from such a limited external correction lowering their accuracy, as shown in Figure 5.7. The PEC given by MRCI+Q on top of a CASSCF(14,8) does not provide either an accurate curve, in comparison to the CCSDTQ reference, even though a performance better than the tailored methods must be acknowledged. The TCCSD PEC is on top of the MRCI+Q around the equilibrium, but it diverges for larger distances, while the TDCSD PEC shows too low values at the equilibrium. The comparison with the DCSD curve makes it clear that the addition of some relaxation to the active space would improve the PEC.

In Figure 5.8 the PECs are definitely better, thanks to a larger considered active space. The latter consists of eight additional virtual orbitals on top of the CAS(14,8). Such virtuals are composed by the $3s$ and $3p$ atomic orbitals in the CASSCF calculation,

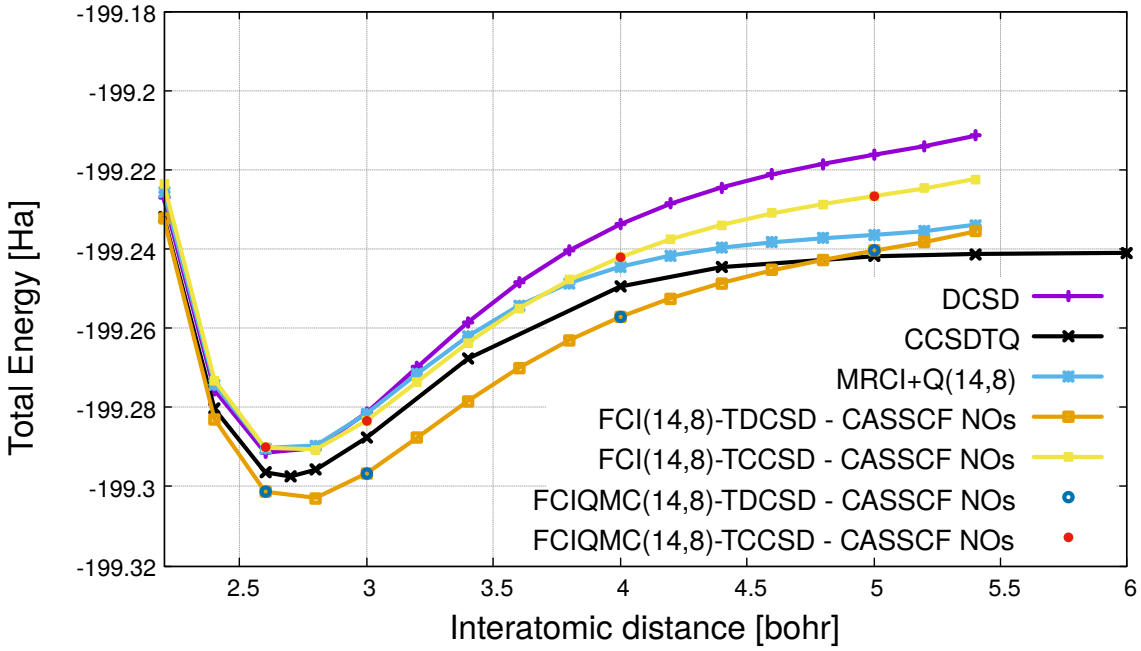

FIGURE 5.7: Potential energy curves for F_2 with (14,8) active space

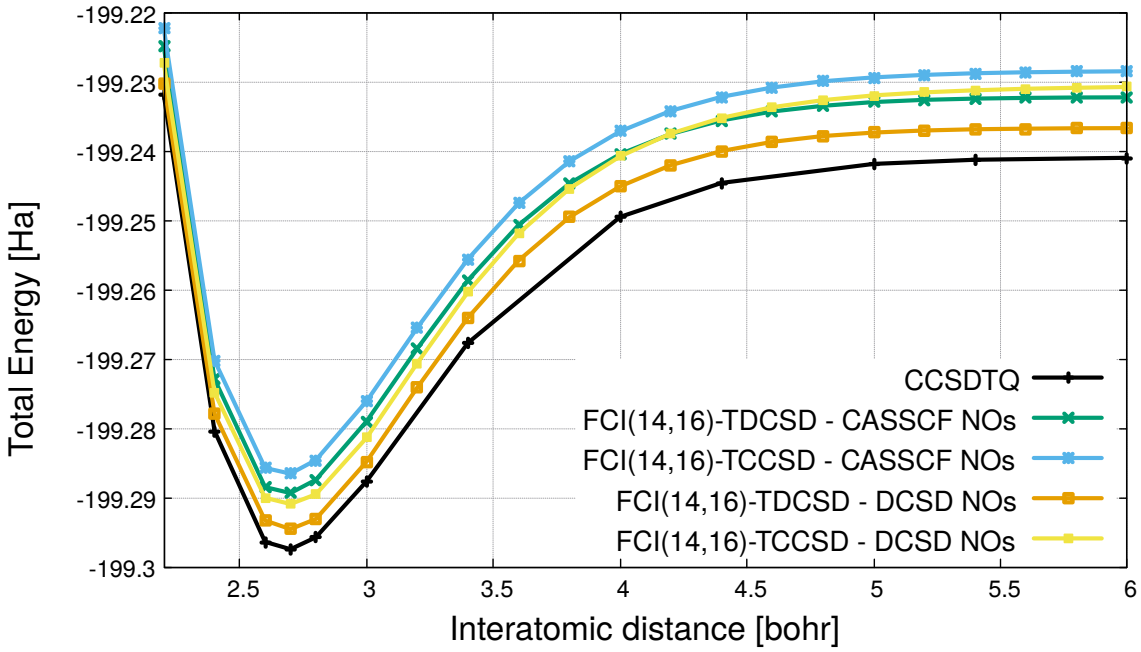

FIGURE 5.8: PECs of F_2 with (14,16) active space

while the DCSD NOs contain somewhat larger $3d$ character. Differently from the N_2 case, the tailored DCSD/CCSD methods provide results closer to the reference PEC for DCSD NOs rather than for CASSCF NOs. However, the TDCSD approach performs again better than TCCSD.

Next, an even larger active space is considered with the same size of the double-zeta basis set. The resulting CAS(14,26) provides a more accurate TDCSD PEC. Although

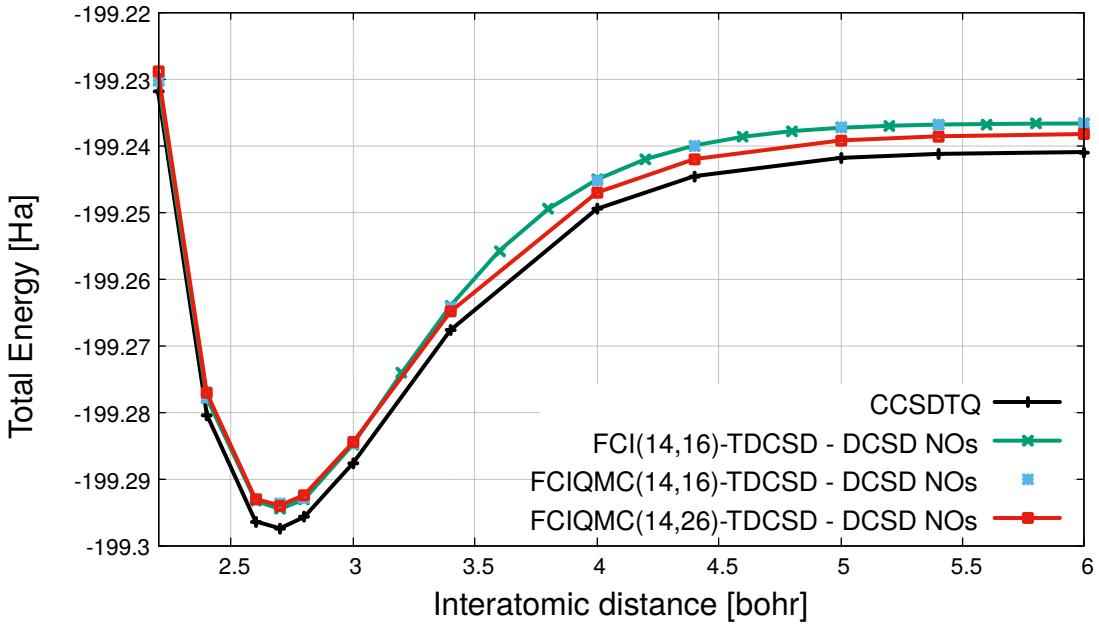

FIGURE 5.9: PECs of F_2 from various TDCSD methods

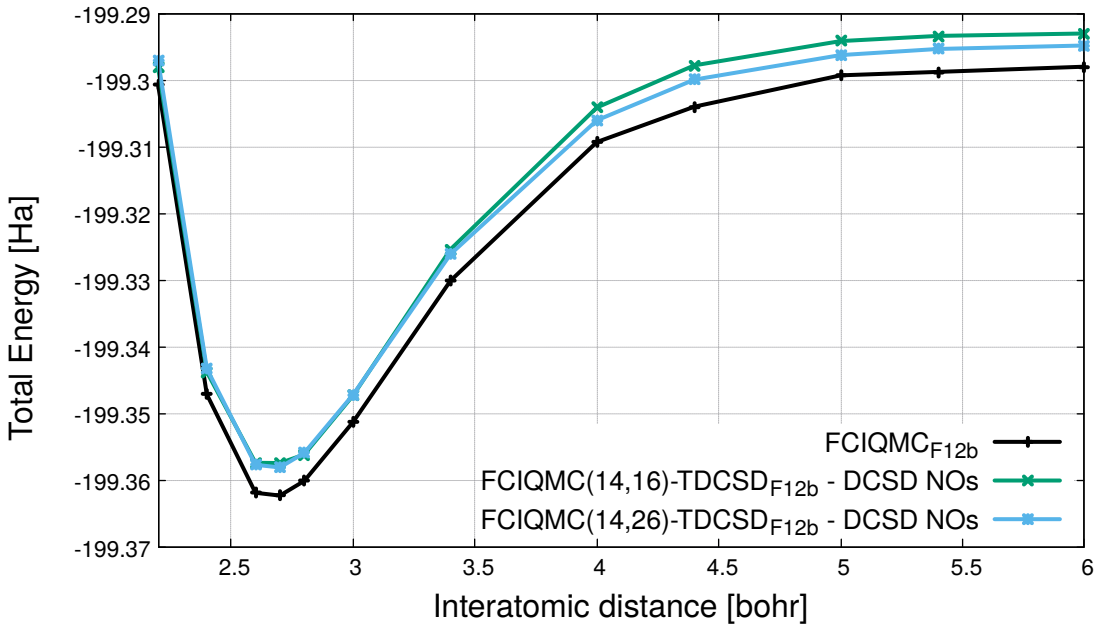

FIGURE 5.10: PECs of F_2 with basis set correction

the latter is still shifted in comparison to CCSDTQ, the curve is much more parallel to the reference than the TDCSD(14,16). The two TDCSD curves for different CASs

overlap at the equilibrium geometry and get further apart along the stretched region. Again, the FCIQMC and FCI corrected tailored methods are essentially equal.

The explicitly correlated methods are presented in Figure 5.10. This does not change the picture. Indeed, the TDCSD(14,26) is consistent with the reference curve provided by $\text{FCIQMC}_{\text{F12b}}$, but shifted by a constant.

Finally, the tailored methods with the additional external correction given by $\hat{T}_3^{\text{CAS}}$ are here presented in Figure 5.11 for DCSD NOs. It is evident to notice that the @T

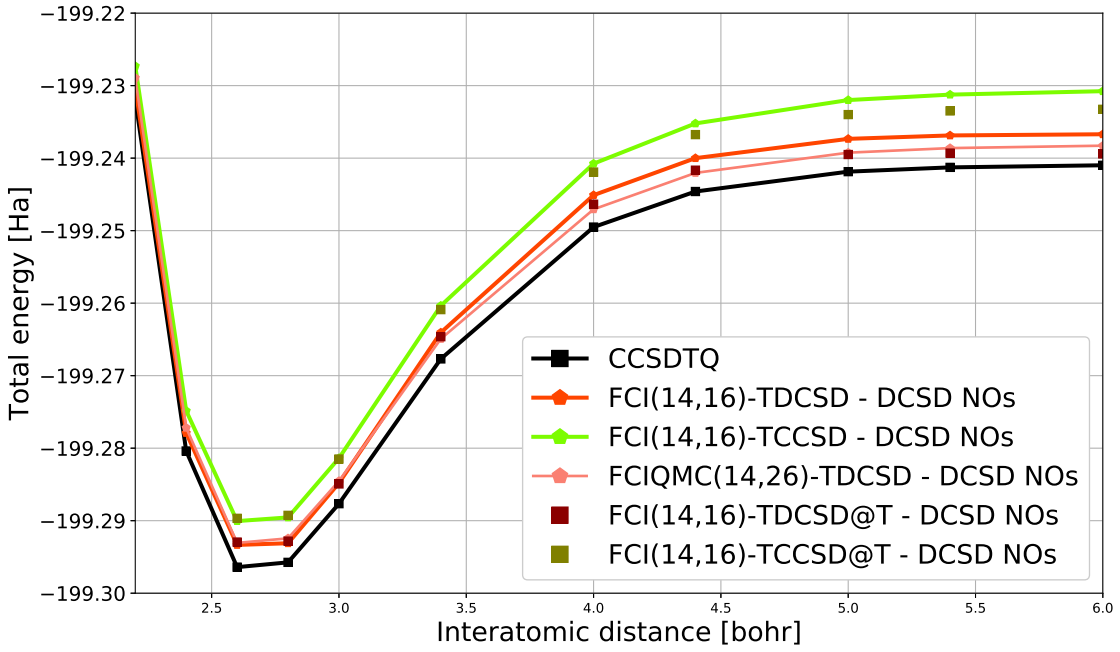

FIGURE 5.11: F_2 PECs of TDCSD/TCCSD with additional $\hat{T}_3^{\text{CAS}}$ correction

methods show a difference with the conventional ones only in the stretched region. This confirms the beneficial effects that can arise from the addition of connected triples in the active space amplitudes in systems away from the equilibrium geometry and studied with natural orbitals. Further, the convergence with respect to the active space size is further improved since the results shown by the largest CAS(14,26) and the $\hat{T}_3^{\text{CAS}}$ corrected in the smaller CASs provide very similar PECs. Again, as in the N_2 case, the triples correction shown in Figure 5.11 has an almost negligible effect in case CASSCF NOs are considered.

5.4 Water molecule (H_2O)

Next, the double bond breaking process of the water molecule dissociation is evaluated. The simultaneous stretching of the two O-H σ bonds is studied while a fixed bond-angle is kept to 107.6 degree. As previously done, a full valence active space is considered, where the $1s$ hydrogen orbitals and $2s$ and $2p$ oxygen orbitals form the CAS(8,6). Figure 5.12 shows the PECs where a general overlap is evident in the equilibrium region.

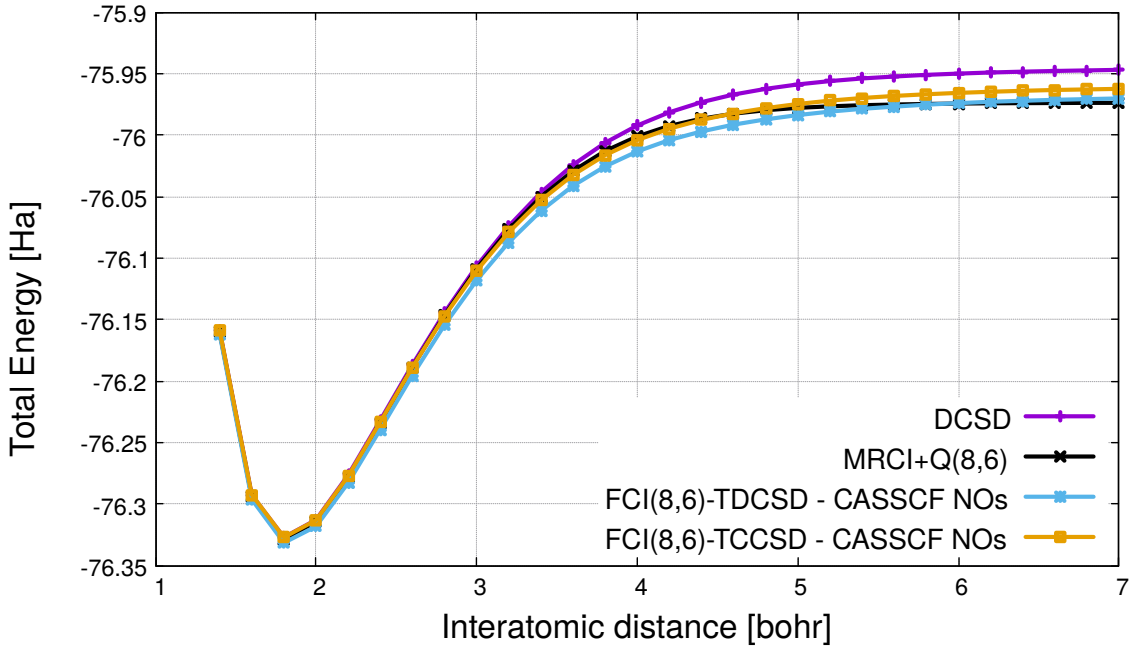

FIGURE 5.12: PECs for H_2O with (8,6) active space

However, the TCCSD curve diverges to high values in the stretched region if compared to the MRCI+Q results, while the TDCSD curve is too low in the intermediate region. Hence, a larger active space is necessary to be considered in order to obtain accurate results over the whole dissociation curve.

A new active space is introduced, CAS(8,18), where twelve additional virtuals are given by the $2s$ and $2p$ orbitals of the hydrogen and the $3s$ and $3p$ orbitals of the oxygen atoms. Figure 5.13 shows that tailored results are indistinguishable from the MRCI+Q curve on this scale. The inclusion of explicit correlation does not change the picture, see Figure 5.14, since the $\text{TDCSD}_{\text{F12b}}$ essentially overlaps the MRCI+Q-F12 curve. Finally, the consideration of $\hat{T}_3^{\text{CAS}}$ corrected tailored methods did not show any noticeable improvement in this case.

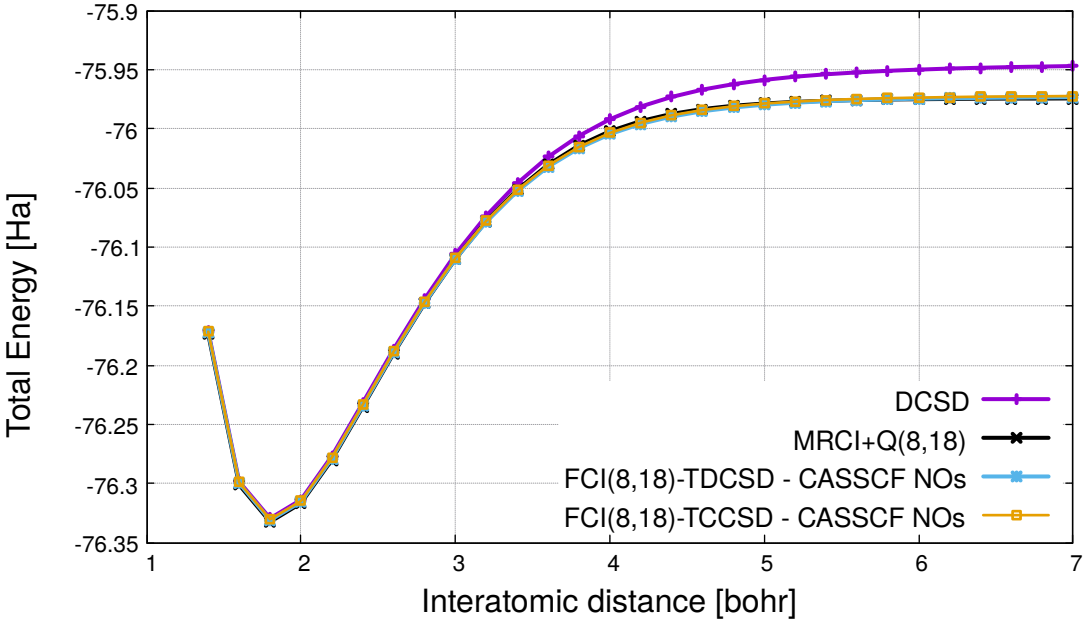

FIGURE 5.13: PECs for H_2O with (8,18) active space

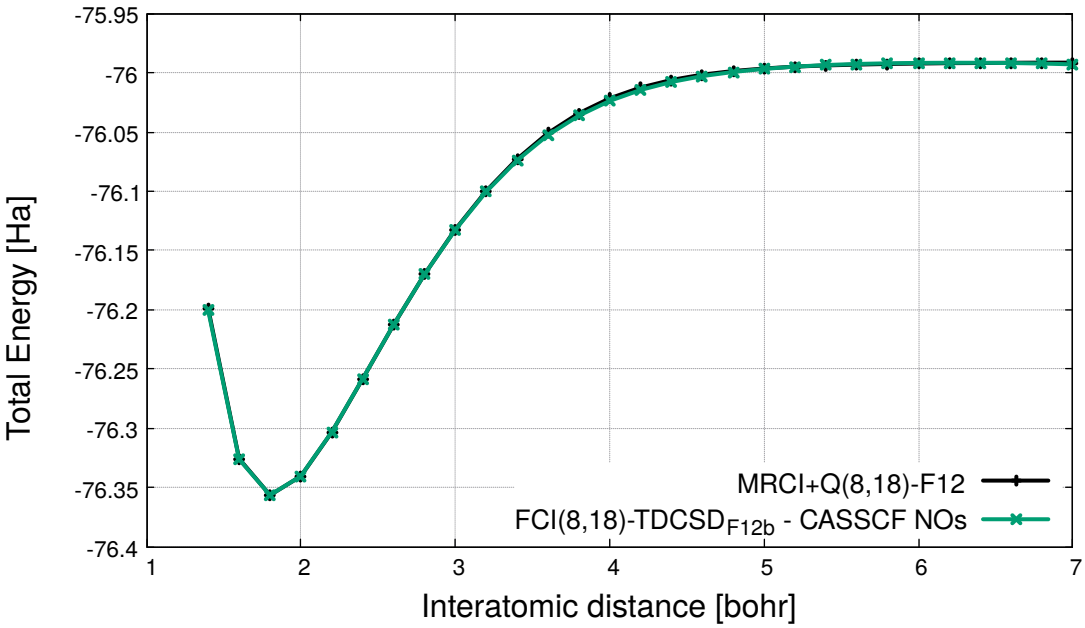

FIGURE 5.14: PECs for H_2O with the F12 correction

5.5 Ethylene (C_2H_4)

The torsion of the ethylene molecule is another typical process which is dominated by static electron correlation. Although its equilibrium geometry has only a SR character, at the transition state the wave function of this molecule shows two equally-weighted

determinants. This is due to the bonding π and anti-bonding π^* orbitals that get degenerate. The rotation along the C-C axis is presented in the PECs of Figure 5.15.

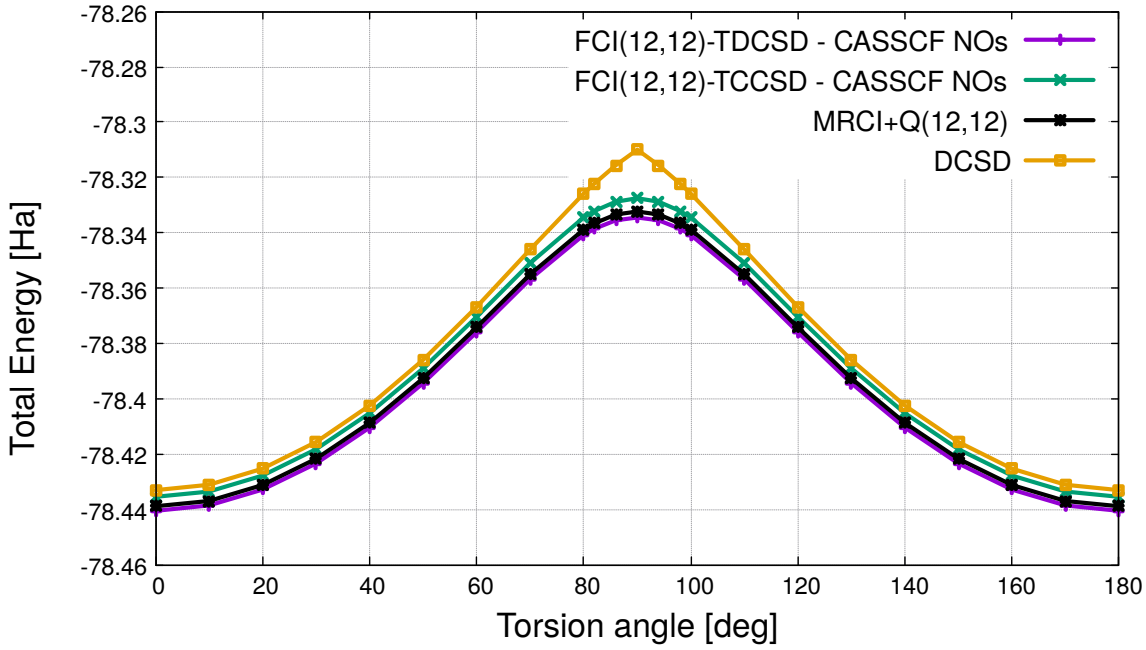

FIGURE 5.15: PECs of C_2H_4 with (12,12) active space

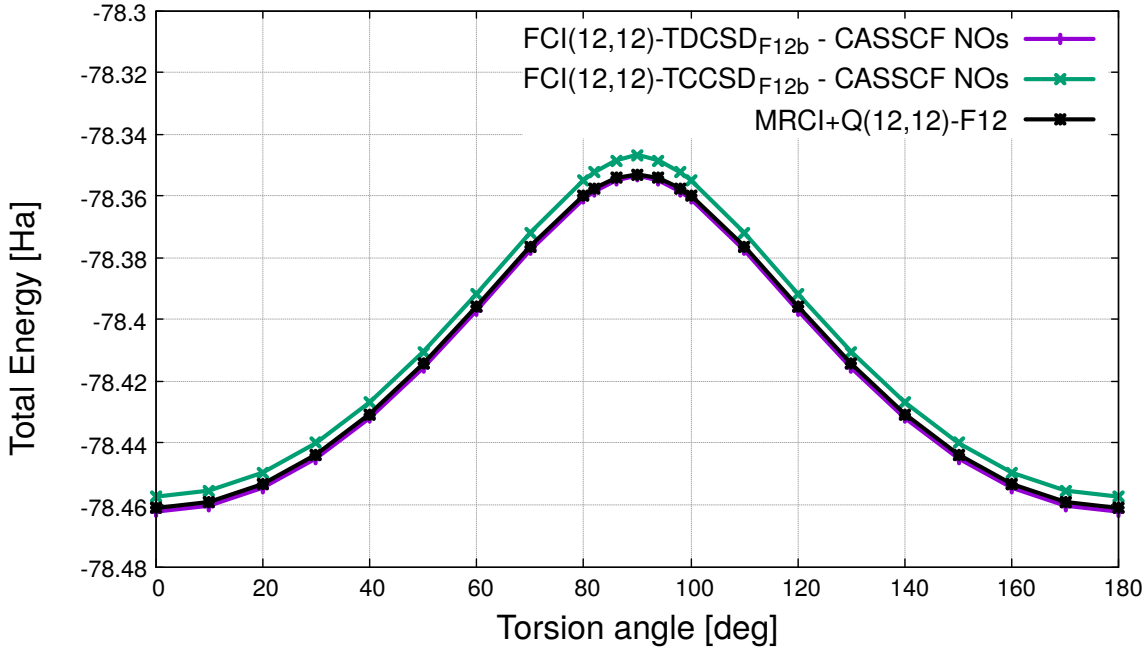

FIGURE 5.16: PECs of C_2H_4 with the F12 correction

The active space is defined by the full valence space, i.e. CAS(12,12), and the geometry is relaxed at every fixed torsion angle by DCSD, as in previous works [64, 162].

The TDCSD and TCCSD curves are both in good agreement with the MRCI+Q(12,12) PEC and quite parallel to it. The non-parallelity error is calculated to be equal to 0.5 mHa for TDCSD and to 1.4 mHa in the TCCSD case.

The explicitly correlated versions of the tailored methods is presented in Figure 5.16. As previously noticed with the water molecule, the performance of TDCSD/TCCSD remain the same in the basis set corrected results. Indeed, the parallelity does not change and the $\text{TDCSD}_{\text{F12b}}$ curve is shown on top of the MRCI+Q-F12.

5.6 Cyclobutadiene (C_4H_4)

Cyclobutadiene (CBD) has been the focus of different studies for many decades [163–170]. In the early works, it was already clear that the CBD ground state is represented by a closed shell singlet in a planar rectangular geometry [163–165]. In this section, the focus is given on the automerization reaction, which manifests a pronounced MR wave function in its transition state at the square geometry [130, 168, 171, 172].

Such a reaction is obtained by the double bond flipping of the two equivalent rectangular singlets and is presented in Figure 5.17. The structural parameters are determined by a linear interpolation of the optimized geometries, which are taken from Ref. [170]. Figure 5.17 is plotted against the λ value, which is a variable used to define the internal coordinates l_i, i.e. $l_i(\lambda) = (1-\lambda)l_i(\text{rt}) + \lambda l_i(\text{sq})$. Here, λ takes the values from 0 to 1 in steps of 0.2. Further, the $l_i(\text{rt})$ and $l_i(\text{sq})$ reproduce the optimized parameters, respectively, in the rectangle and square geometry. In other words, they represent the C-C bond distances and correspond to $l_1(\text{rt}) = 1.349$ Å and $l_2(\text{rt}) = 1.562$ Å for the rectangle and to $l_1(\text{sq}) = l_2(\text{sq}) = 1.447$ Å for the square. The remaining coordinates which are necessary to completely determine the geometry are kept frozen with the following values: 135.0° for the H-C-C angle, 1.076 Å for the H-C distance and 90.0° for the C-C-C angle.

A CAS(12,12) is employed here, where the corresponding CASSCF calculations includes MOs related to the C-C bonds. In Figure 5.17 it is clear that CCSD, DCSD and CCSD(T) produce qualitatively wrong curves. However, DCSD is still a noticeable improvement upon CCSD, if the absolute energies and the relative barrier heights are considered, see Table 5.1. The trend shown by the tailored methods is similar to

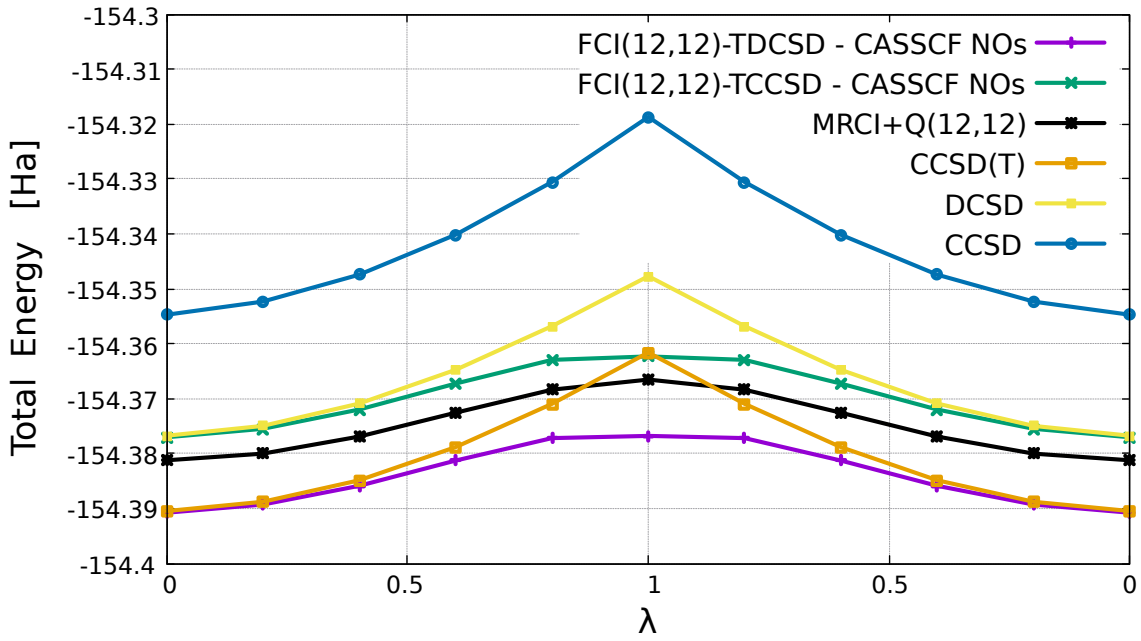

FIGURE 5.17: Potential energy curves for C_4H_4 with (12,12) active space in cc-pVTZ basis

the reference MRCI+Q curve. Interestingly, at the equilibrium geometry the absolute energy of TDCSD matches with CCSD(T).

Table 5.1 reports all the energy barrier heights calculated in this work, together with some energy values from literature of the same double bond shift. Even an experimental range is available, which goes from 1.6 to 10 kcal/mol [173, 174]. The tailored methods seem to provide quite accurate results. Indeed, the TCCSD barrier height coincides with the MRCI+Q value. Further, one of the best estimates given by the MR average-quadratic CC (MR-AQCC) accounts for an energy barrier of 8.9 kcal/mol [170], which is the same for the MR Mukherjee's CCSD(T) (MR-MkCCSD(T)) method [175]. The latter values are in between the TDCSD and TCCSD@T results. The $\hat{T}_3^{\mathrm{CAS}}$ correction shows a further reduction on the energy barrier heights in comparison with the corresponding tailored DCSD and CCSD methods. Finally, the tailored approaches based on the CAS(12,12) shown in the present work clearly improve upon the TCCSD calculation which employs RHF orbitals in a (2,2) active space [130].

Method	ΔE (kcal/mol)
DCSD	18.2
CCSD	22.6
CCSD(T)	18.1
TDCSD - CASSCF NOs	8.8
TCCSD - CASSCF NOs	9.2
TDCSD@T - CASSCF NOs	8.5
TCCSD@T - CASSCF NOs	9.0
MRCI+Q	9.2
TCCSD - (2,2) RHF orbitals[130]	12.9
TCCSD(T) - (2,2) RHF orbitals[130]	7.0
RMR-CCSD(T)[171]	7.5
MR-MkCCSD(T)[175]	8.9
MR-AQCC[170]	8.9
Experimental range [173, 174]	1.6-10

TABLE 5.1: Energy barrier heights (ΔE) of the automerization reaction.

5.7 Ozone (O_3)

The pioneering studies of Hay et al. [148, 149] date back to 1975 and shed light on the electronic structure of O_3, whose description is well known to be challenging without high-order excitations or true MR methods. Many different studies have been accomplished on this molecule along the years, with special focus on structural optimizations and vibrational frequencies [150, 151, 176–184], where Ref. [180] represents the first application of the tailored CC on such a molecule.

Two ground state minima are found on the potential energy curve of ozone, the local ring minimum and the global open minimum [148, 185, 186]. The local ring was demonstrated to exist only by theoretical computations, while experimental evidences are not available. Additionally, it was shown in previous works on the analysis of a CI wave function [148, 186] that both of the mentioned isomers present a large MR character. Thus, this represents a non-trivial problem to undergo for SR methods. Furthermore, another strongly correlated isomer is known to exist as a transition state between these two minima. Therefore, a balanced description of these different geometrical structures is very difficult to reach, in case no MR treatment is considered or no high order excitations are included. In this section, the three different geometries represented by the open minimum (OM), the ring minimum (RM) and the transition state (TS) are taken from Ref. [187] and evaluated in the calculation of the relative energy differences. The ground state of the transition state geometry and its first

excited state are found to be almost degenerate in previous works [183, 187], with a corresponding excitation energy of $0.01 - 0.1$ eV. Here, both of the states are calculated and reported in Table 5.2, where the notation of TS and TS2 indicates respectively the ground state and the first excited state of the transition geometry, as ordered in Ref. [183].

The full valence space is first considered in the active space for the ozone molecule. The resulting CAS(18,12) is defined by both DCSD and CASSCF NOs. Table 5.2 lists all the absolute energies of the OM geometry and the relative energies with respect to TS, TS2 and RM. The tailored calculations based on the CASSCF NOs provide

Method	OM Ha	TS-OM eV	TS2-OM eV	RM-OM eV
DCSD	-225.1204	2.33	2.75	1.11
CCSD	-225.0838	2.42	3.13	0.95
FCI(18,12) using CASSCF NOs				
TDCSD	-225.1440	2.44	2.38	1.28
TCCSD	-225.1258	2.47	2.46	1.26
TDCSD@T	-225.1404	2.35	2.40	1.18
TCCSD@T	-225.1225	2.38	2.47	1.17
FCI(18,12) using DCSD NOs				
TDCSD	-225.1413	2.39	2.59	1.20
TCCSD	-225.1233	2.42	2.66	1.19
TDCSD@T	-225.1374	2.28	2.59	1.09
TCCSD@T	-225.1198	2.33	2.66	1.10
FCIQMC(18,39) using DCSD NOs				
TDCSD	-225.1347	2.43	2.44	1.29
TCCSD	-225.1337	2.43	2.44	1.29
SHCI[187]	-	2.41	2.42	1.30

TABLE 5.2: Absolute energies of the CCSD/DCSD tailored and non-methods for the ozone in the OM geometry and the relative energies of the transition states (TS and TS2) and the RM with respect to OM. The SHCI values are taken from Ref. [187].

already good results in such a confined active space. Indeed, deviations below 0.1 eV are shown if compared to the reference values given in Table 5.2 from the Semistochastic Heath-Bath CI (SHCI) method of Chien et al. [187]. Specifically, the TS-OM gap is found to differ by 0.03 eV for TDCSD and 0.06 eV for TCCSD from the SHCI values. The difference gets to 0.04 eV for both tailored methods in the first excited state, TS2. In the RM-OM relative energy, the deviations are only of 0.02 eV and 0.04 eV in the TDCSD and TCCSD case, respectively. It is worth to notice that the energetic order of

the TS and TS2 states is exchanged in both tailored results. Interestingly, the latter order is recovered once the $\hat{T}_3^{\mathrm{CAS}}$ correction is included in the tailored methods, as shown in Table 5.2. A CAS defined by DCSD NOs increases the differences from SHCI values in some of the relative energies. However, the errors are mostly much smaller than from conventional DCSD and CCSD methods and also the energetic order is kept correct.

A better accuracy can be reached by increasing the active space. For that reason, the DCSD NOs have been used to select the CAS(18,39), i.e. the size of the double-zeta basis set. This represents once more the basis set correction type approach that was used also in the previous sections. The absolute energies of TDCSD and TCCSD corrected from the FCIQMC(18,39) are in good agreement with high level CC results. For example, the TDCSD(18,39) total energy in the OM geometry is found to be in the middle of the CCSDT (-225.1317 Ha) and CCSDTQ (-225.1378 Ha) energies. The relative energies resulting from TDCSD and TCCSD in the largest CAS agree with each other and show discrepancies from SHCI values of only $0.01 - 0.02$ eV.

5.8 Conclusions

In this chapter, the novel tailored distinguishable cluster method has been benchmarked with six representative case studies. In all of them, the TDCSD approach shows an evident improvement in comparison to the standard DCSD. The tailored DCSD is also more accurate than a simple subtractive embedding scheme and this is especially proven in smaller active spaces. In the ozone molecule, the TDCSD and TCCSD results provide very accurate isomerization energies for the CAS(18,39). This is confirmed by the small deviations of only $0.01 - 0.02$ eV from the reference values.

The tailored distinguishable cluster shows to be remarkably more accurate than TCC in most of the cases. Such a difference in the results is less pronounced when larger active spaces are considered. However, the demonstrated higher accuracy of DCSD over CCSD will be particularly relevant in bigger systems with large inactive spaces.

The accuracy of the TDC approach is also investigated with a different selection of active spaces than the conventional CASSCF. The CAS choice guided by the most correlated DCSD NOs has shown comparable accuracy to CASSCF-defined active spaces, even though this depends on the system and the size of CAS under study. This confirms that the tailored methods are sensitive to the orbital choice and the active

space used. DCSD NOs facilitate the selection of active spaces also when large CASs are involved.

The H_2O double-dissociation and the C_2H_4 torsion curves have yielded noticeably accurate results in the explicitly correlated tailored approaches, overlapping with the MRCI+Q-F12 results. Furthermore, the $FCIQMC_{F12}$ method has been introduced as a new type of explicit correlation correction and used as a reference.

The additional external correction provided by the $\hat{T}_3^{CAS}$ cluster operator yields more accurate tailored results in some of the case studies, especially noticeable in case DCSD NOs are used. Specifically, the accelerated convergence with respect to the active space size is evident in the F_2 case, where the TDCSD@T(14,16) shows almost overlapping results with the larger externally corrected TDCSD(14,26), both with DCSD NOs.

The intermediate region approach has confirmed the importance of the amplitudes relaxation in the active space. However, many different strategies can be applied to alleviate such a problem, as demonstrated in previous works [188–190].

The present chapter has been focused only on closed-shell systems and their dissociation/torsion curves and isomerization energies in the ozone case. In the next chapter, the accuracy of the tailored distinguishable cluster approach is also evaluated for the open-shell systems.

Chapter 6

Open-shell molecular systems

Accurate spin gap estimations of transition metal (TM) complexes represent a challenge for both experimental and theoretical chemistry. On the one hand, experimental measurements in TM compounds require the adoption of multiple techniques in order to determine the spin state unambiguously [191]. On the other hand, QC studies have shown that obtaining reliable qualitative spin state orderings can be a difficult task [192]. Indeed, the correct identification of the ground state among different near degenerate spin states is not trivial [193]. However, spin gap predictions are not only important to find the relatively most stable system, but are crucial to evaluate their influence on the reactivity patterns of enzymatic and catalytic processes. Indeed, different electronic properties, such as magnetism and reactivity, are determined by different spin states.

The majority of TM complexes have various low lying spin states, due to their partially occupied d orbitals. Indeed, the latter can give rise to different stability of spin states depending on the ligands that form the complex, the metal oxidation state and the coordination geometry. Such a spin multiplicity is particularly common in octahedral complexes of the first row of TMs with d^4-d^7 electrons. This phenomenon is explained by the ligand field theory that justifies different spin states according to the ligand field strength, which proportionally affects the orbital splitting. However, these spin state changes have mostly consequences on the metal-ligand bond distances and the resulting magnetic properties of the compound. For that reason, magnetic measurements are typically adopted to establish the electronic spin state of TM complexes.

In QC, DFT has been widely used to study such systems [194–197], due to the size of the molecules which are usually involved in the most interesting biochemical processes. However, the results strongly depend on the choice of the functional which makes its application very problematic [195, 196, 198–201]. The latter causes differences in the spin gaps up to 20 kcal/mol and makes the DFT method questionable if the

energies of different spin states themselves are a few kcal/mol apart. Instead, wave function based methods usually have higher accuracy and systematic improvability, but at the cost of computationally more expensive calculations.

In the following, the TDCSD approach is applied to open-shell molecular systems and used to evaluate spin state splittings of various single-center Fe(II) complexes [202]. Although such systems are not defined by a strong MR character, accurate estimations of their spin gaps are not straightforward. Dynamic correlation effects play a key role. The corresponding amounts characterizing each spin state make a systematic error cancellation not reliable in the final energy difference between high and low spin states. Tailored DC has been shown to properly describe closed-shell systems with a large amount of static correlation, such as seen in the previous Chapter 5. However, TDC can also be useful to accurately recover dynamic correlation in systems where an accurate description is typically retrieved by high level SR methods, such as the single-center transition-metal complexes [203–218]. Thus, they provide a further interesting assessment of the proposed FCIQMC-TDCSD method.

6.1 Computational Details

Five Fe(II) complexes have been studied with the TDCSD method by computation of their electronic spin states. These five systems consist of four Fe(II) octahedral complexes, $[Fe(H_2O)_6]^{2+}$, $[Fe(NH_3)_6]^{2+}$, $[Fe(NCH)_6]^{2+}$ and $[Fe(CO)_6]^{2+}$, which have already been the focus of many different studies [203–215], and the four-coordinated ferrous porphyrin (FeP) model [216, 217, 219–222]. The spin gap estimates show values of tens of kcal/mol for the former systems and only a few kcal/mol for FeP.

The geometries of the octahedral complexes are taken from a work of Song et al. [211], while the FeP geometry from the works of Li Manni et al. [220, 221]. The active space is defined either through (Stochastic-)CASSCF or DCSD NOs, as demonstrated in the previous Chapter 5. Thus, all the tailored calculations are performed on the reference specified by these NOs. The semi-core orbitals of the Fe atom ($3s3p$ shell) have been always included at the CC level [216, 217]. Further, the basis set employed in the Fe(II)-porphyrin is the generally contracted atomic natural orbitals, ANO-RCC-VTZP, while in the other four complexes cc-pVTZ was used.

The semi-stochastic approach has been used by default in all the FCIQMC calculations with a deterministic space of up to 10^6 SDs. The adaptive shift has been also considered with a trial space determining the new shift composed by 1000 determinants.

Further, the number of walkers populating the SDs space has been taking values up to 2×10^8, adopted according to the size of the CAS under study. Finally, the number of iterations set to average the CI coefficients has been chosen equal to 20000.

Additionally, a comparison of the tailored results with the conventional DCSD, CCSD and CCSD(T) calculations, based on the ROHF orbitals, is presented. Further, the CASPT2 and MC-PDFT values, based on the CASSCF wave function, are considered [202]. A perturbative basis set correction has not been evaluated for the DCSD and CCSD results, since its application would act similarly to the correction obtained with CCSD(T) and the tailored methods. The results of the calculations on the open-shell molecular systems reported can be found in the Supporting Information (SI) of Ref. [202], together with the visualization of the selected DCSD NOs in the largest studied CASs.

6.2 Octahedral Fe(II) Complexes

In the present section, the study of the four octahedral $[Fe(L)_6]^{2+}$ complexes through the externally corrected CC/DC is given, where L = H_2O, NH_3, NCH and CO. The focus is given on the computation of the spin gaps between high spin (HS) and low spin (LS) states, i.e. $\Delta E = E_{\mathrm{HS}} - E_{\mathrm{LS}}$. For d^6 complexes in the octahedral environment, the LS is given by the preference of the electrons to pair in the t_{2g} orbitals, which is here represented by a singlet, and the HS is obtained with the maximal number of unpaired electrons on t_{2g} and e_g orbitals, i.e. a quintet. In Figure 6.1, a schematic representation of these two electronic configurations is given.

A balanced description of the dynamic correlation in the different spin states represents the main computational challenge in such Fe(II) complexes. Indeed, the major difference in the electronic structure of the two spin states, namely the number of anti-parallel spin electron pairs, generates distinct contributions of the dynamic correlation for each of the states [212]. For example, the LS state ($t_{2g}{}^6 e_g{}^0$) is expected to give a larger amount of dynamic correlation than the HS ($t_{2g}{}^4 e_g{}^2$), in view of its higher number of anti-parallel intra orbitals spin pairs, see Fig. 6.1. Generally, the latter provide larger contributions to the electron repulsion than the anti-parallel inter orbital pairs and even much larger than the parallel inter orbital pairs. For that reason, a proper description of dynamic correlation in both states can not simply be recovered by cancellation of errors in the resulting energy difference, which, in turn, can lead to large deviations from the accurate results. Additionally, the slow basis set convergence

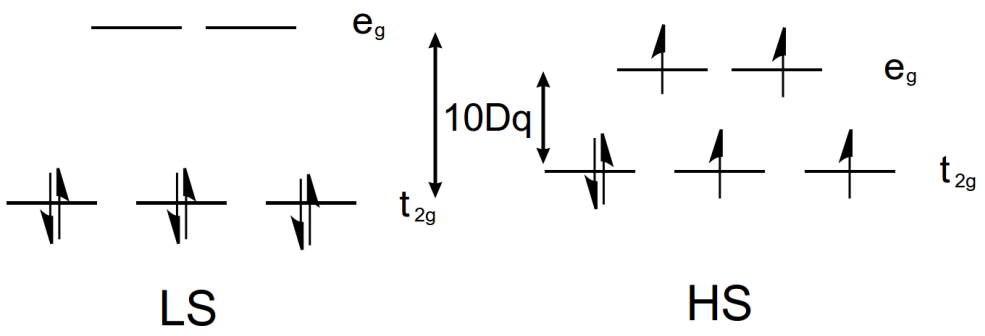

FIGURE 6.1: Schematic representation of the electronic configurations of the HS and LS d^6 octahedral complex.

that typically afflicts the dynamic correlation is not the same for different spin states. However, this problem can be alleviated by explicitly correlated techniques. The latter are used in this work in order to approach the basis set limit and to recover most of the correlation energy in each spin state.

Three different active spaces have been studied in the present work for each octahedral Fe(II)-compound. Two CASs are the same in all of the four complexes and they have been optimized by deterministic CASSCF calculations, due to the small size. First, a CAS(6,5) was evaluated consisting of only the five $3d$ orbitals of Fe together with its six electrons. Second, a bit larger CAS(6,10) has been chosen, where the five correlating d' orbitals are added to the CAS(6,5). The third is characterized by a large active space, which has been determined by DCSD NOs with occupation numbers deviating strongly from 0 and 2. And, the CI vectors are obtained from FCIQMC. The latter CAS size changed according to the system under study, but generally included over 30 electrons in more than 30 orbitals. Additionally, the consistency of the active spaces across different spin states has been maintained. This means that if the inclusion of specific orbitals must be ensured for the correct description of one spin state, these orbitals are then considered in the active spaces of both spin states.

6.2.1 $[Fe(H_2O)_6]^{2+}$

The first test system presented is the Fe(II) water ligand complex. The three active spaces introduced in Sec. 6.2 have been studied with different methods. The largest CAS consists of 42 electrons in 41 orbitals and it was determined by the most correlated

DCSD NOs. This CAS(42,41) includes the orbitals of CAS(6,5) and various σ and π type orbitals. The selected active orbitals are presented in Figure 6.2 and 6.3.

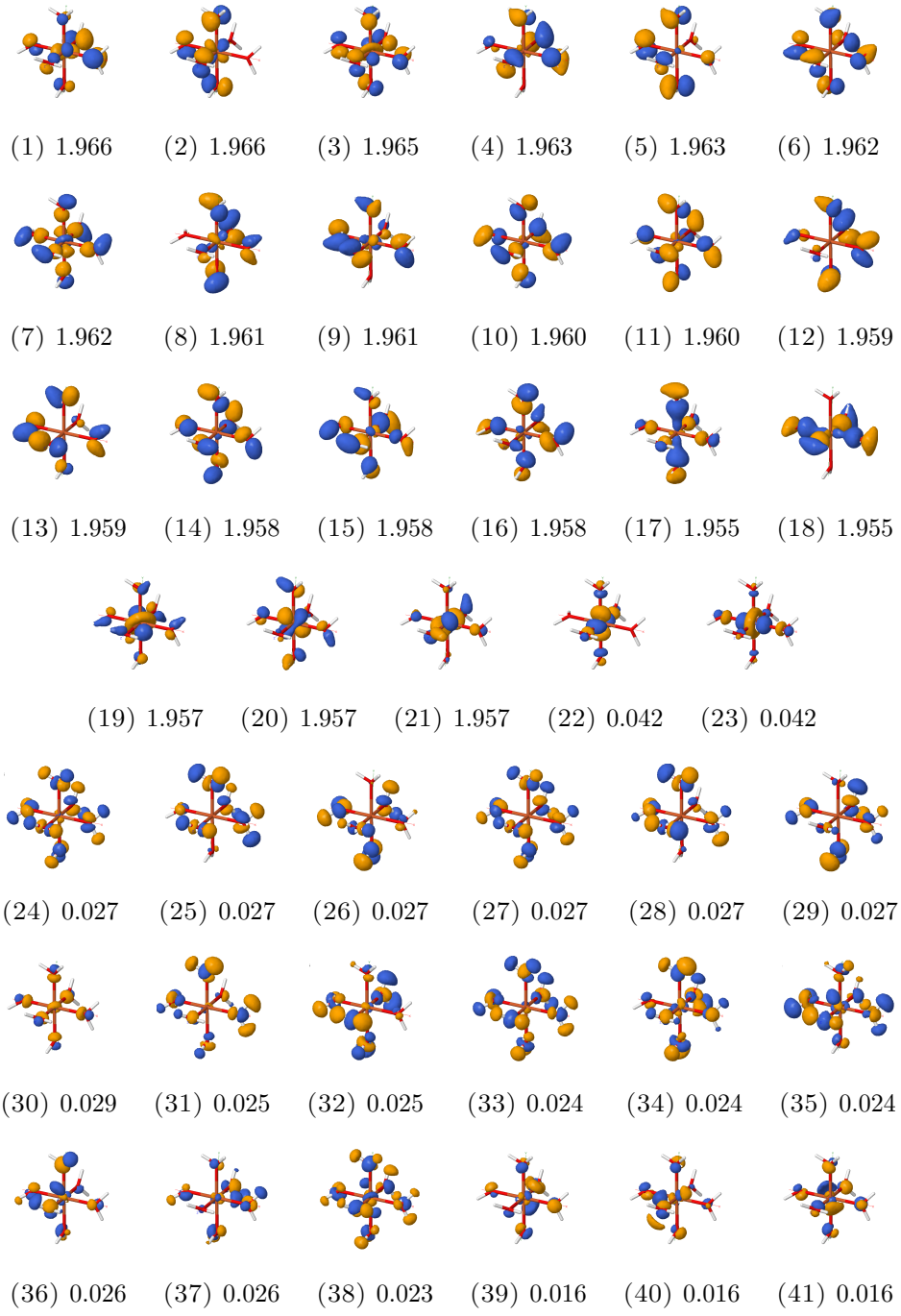

FIGURE 6.2: DCSD NOs chosen for the CAS(42,41) in the singlet state of $[Fe(H_2O)_6]^{2+}$ and their occupation numbers.

A HS ground state is expected to be found for such a compound, due to the weak ligand field strength that characterizes the octahedral Fe(II)-complex with the water

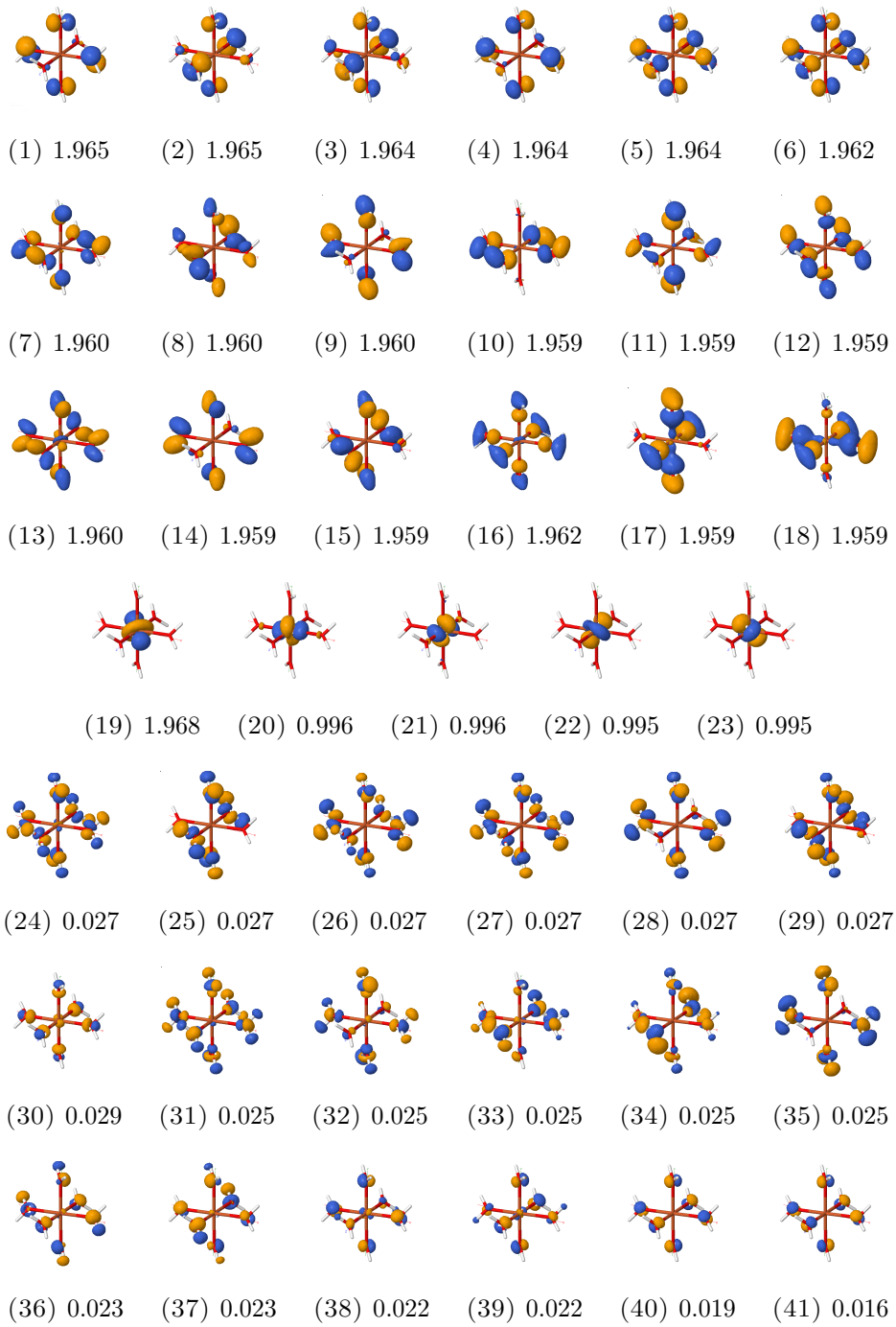

FIGURE 6.3: DCSD NOs chosen for the CAS(42,41) in the quintet state of $[Fe(H_2O)_6]^{2+}$ and their occupation numbers.

molecule as a ligand. Indeed, already at the ROHF level the correct spin state ordering is given (ΔE_{ROHF} = -78.8 kcal/mol), even though it is evident that ROHF overstabilizes the HS state. The subsequent correlated methods reduce the energy gaps. It is worth to notice in Fig. 6.4 that the tailored methods yield consistent results across the three

active spaces. Further, even a good agreement with ROHF based CC/DC and DMC calculations is visible.

A measure of the MR character can be given by the largest doubly excited CI coefficients extracted from the FCIQMC calculation in the CAS(42,41) (after intermediate normalization). The latter corresponds to 0.041 for the LS state and to 0.038 for the HS. Thus, it confirms that the complex under study shows mainly a SR character.

In Fig. 6.4 the tailored results are presented in different coloured bars relative to the specific tailored method. The corresponding basis set corrected result is shown in lighter colours. Evidently, the perturbative F12 correction further reduces the spin

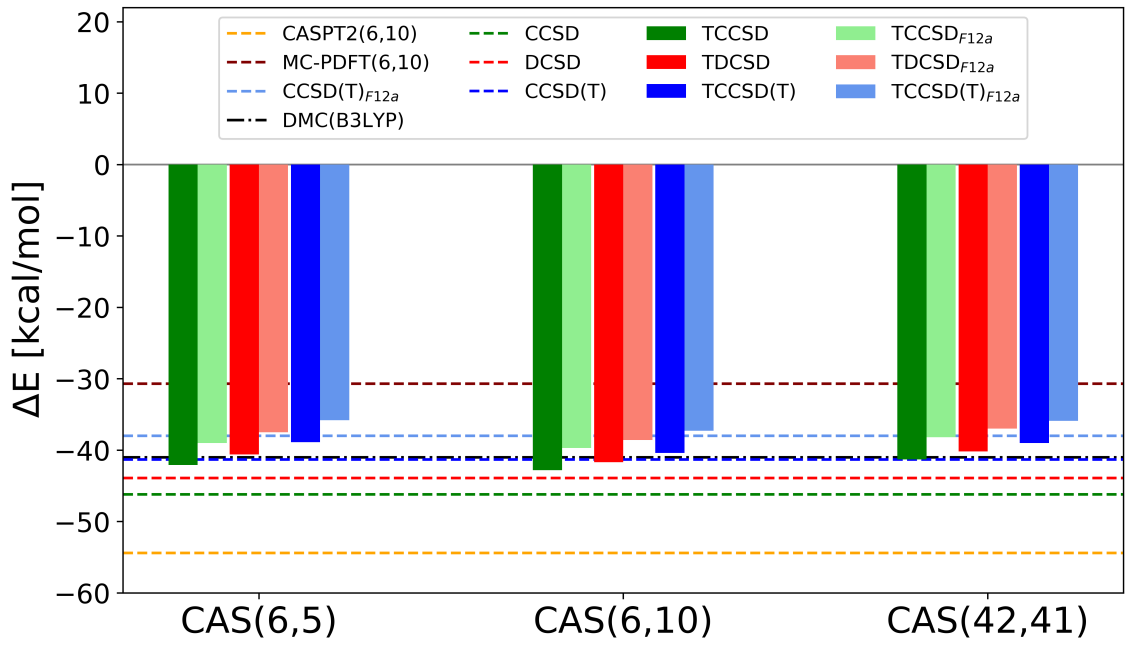

FIGURE 6.4: Spin gap estimates of $[Fe(H_2O)_6]^{2+}$ for different active spaces.

gap, moving the final value closer to the MC-PDFT(6,10) result and is also in general agreement with CCSD(T)$_{F12a}$. One one hand, the lack of higher order many-body effects seems to overstabilize HS in the CASPT2 and CCSD/DCSD methods [220]. On the other hand, DMC, MC/PDFT, CCSD(T) and TCC/TDC methods are able to describe these forms of weak correlation well and reduce the spin gap, stabilizing the LS state. Further, the TCCSD(T)$_{F12a}$ final value shown in Fig. 6.4 is found to lie in between the MC-PDFT and the DMC predictions. In this system, the size and quality of the active spaces do not show strong effects on the final TCC/TDC spin gap results.

6.2.2 $[Fe(NH_3)_6]^{2+}$

Next, the accuracy of the tailored methods is evaluated through spin gap estimations of the $[Fe(NH_3)_6]^{2+}$ complex. Again, CAS(6,5) and CAS(6,10) are defined at the CASSCF level, while the large CAS is obtained from DCSD NOs and consists of 42 electrons in 41 orbitals (see SI of Ref. [202] for further details). As for L=H_2O, an HS ground state is found already at the ROHF level and a reduction of the spin gap is introduced by electron correlation in CASSCF (or CAS-CI): $\Delta E_{CASSCF(6,5)} = -60.9$ kcal/mol; $\Delta E_{CASSCF(6,10)} = -48.1$ kcal/mol; $\Delta E_{CAS\text{-}CI(42,41)} = -40.0$ kcal/mol. In Figure 6.5, the

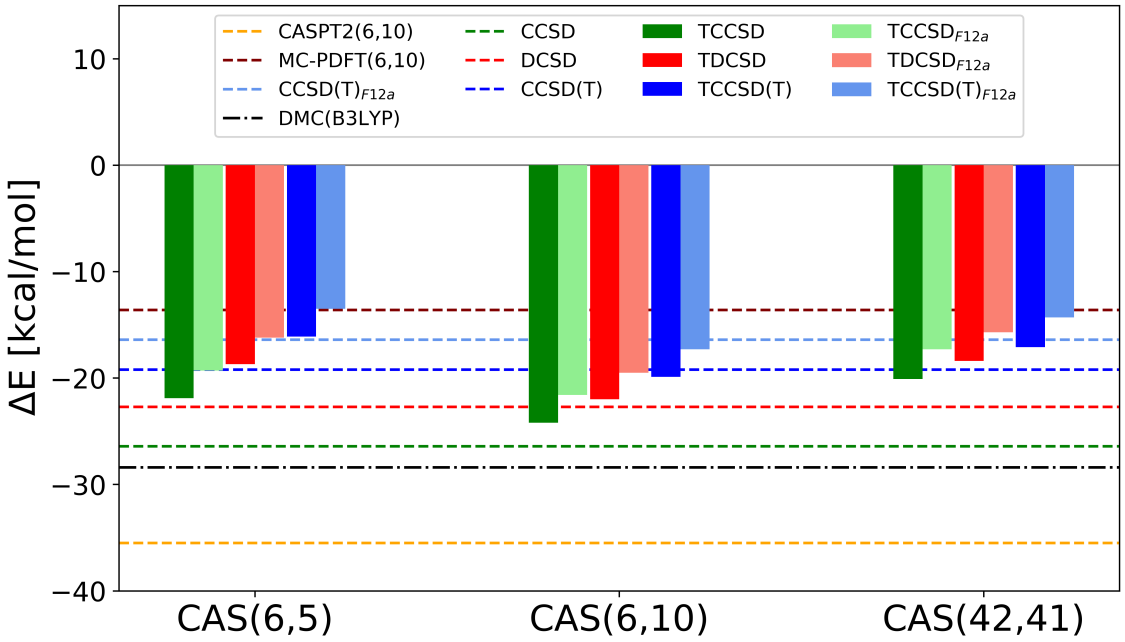

FIGURE 6.5: Spin gap estimates of $[Fe(NH_3)_6]^{2+}$ for different active spaces.

external corrections based on such active spaces reduce the relative energy even further in the corresponding tailored methods. Additionally, the results do not show a large dependence on the active space size.

The TCC/TDC spin gaps from CAS(6,5) and CAS(42,41) show a better agreement with each other than with the CAS(6,10). The latter shows results more biased towards an HS state. This bias can be explained by the missing relaxation of the CAS amplitudes. Indeed, the three t_{2g} and two e_g orbitals, shown by Fe(II) in an octahedral environment (see Figure 6.1), are all occupied in the reference determinant of the HS state, while only the t_{2g} are doubly occupied in the LS state. For that reason, the singlet state benefits from a higher flexibility of the paired electrons, if also the d' orbitals are included in

the correlation description, such as in CAS(6,10). This is confirmed by the results of CASSCF(6,5) and CASSCF(6,10). However, a ligand metal charge transfer (LMCT) is known to provide another important mechanism for LS stabilization [220–222]. Indeed, a competition of correlation between the d' orbitals and either the occupied valence $3d$ orbitals or the ligand orbitals exists. The introduction of d' orbitals into the CAS(6,10) let the coefficients be optimized without the ligand orbitals. The subsequent step of TCC/TDC to freeze the single and double amplitudes enhances the $3d$ to d' channel, which, in turn, suppresses the important ligand-metal excitations. The latter shows how a biased electron correlation description, such as the one in CAS(6,10), can be quite harmful for the LS state. Indeed, the ligand-metal and $3d \rightarrow d'$ excitations are more important to the singlet state rather than to the quintet. This confirms that the spin gap estimation of these Fe(II) compounds is not a straightforward task, as already mentioned in Sec. 6.2, even though a MR character is not involved. A measure of the multi-configurationality is here given by the largest double amplitudes within CAS(42,41): 0.041 for LS and 0.037 for HS, which is low.

In Figure 6.5 it is evident that the DMC and CASPT2 methods favor an HS state in comparison to the other methods. It is well known that CASPT2 overstabilizes the HS states due to the missing higher order correlation effects. The latter has been already shown in previous studies in the context of spin state energetics of transition metal complexes [216] and Fe(II)-porphyrin model system [220, 221]. Finally, the TDCSD$_{F12a}$ and TCCSD(T)$_{F12a}$ estimates show closer values to the CCSD(T)$_{F12a}$ and MC-PDFT(6,10) results.

6.2.3 $[Fe(NCH)_6]^{2+}$

Now, the NCH ligand is considered in the Fe(II) octahedral complex. The largest CAS is again determined from the most correlated DCSD NOs and in this case is composed by 34 electrons in 31 orbitals. This CAS(34,31) consists of twelve π_{ML} and twelve π^*_{ML} orbitals, i.e. the local π bonds between the ligands and the metal (the chosen orbitals are shown in SI of Ref. [202]).

In Figure 6.6 it is evident that the ground state is represented by the HS. However, a stabilization towards the LS state is given by electron correlation. A large deviation between the spin gaps of the non-tailored methods is shown. For example, the CCSD result is almost two times larger than CCSD(T). A better agreement is exposed among the tailored methods and mostly with a reduced spin gap. The CAS(6,10) shows

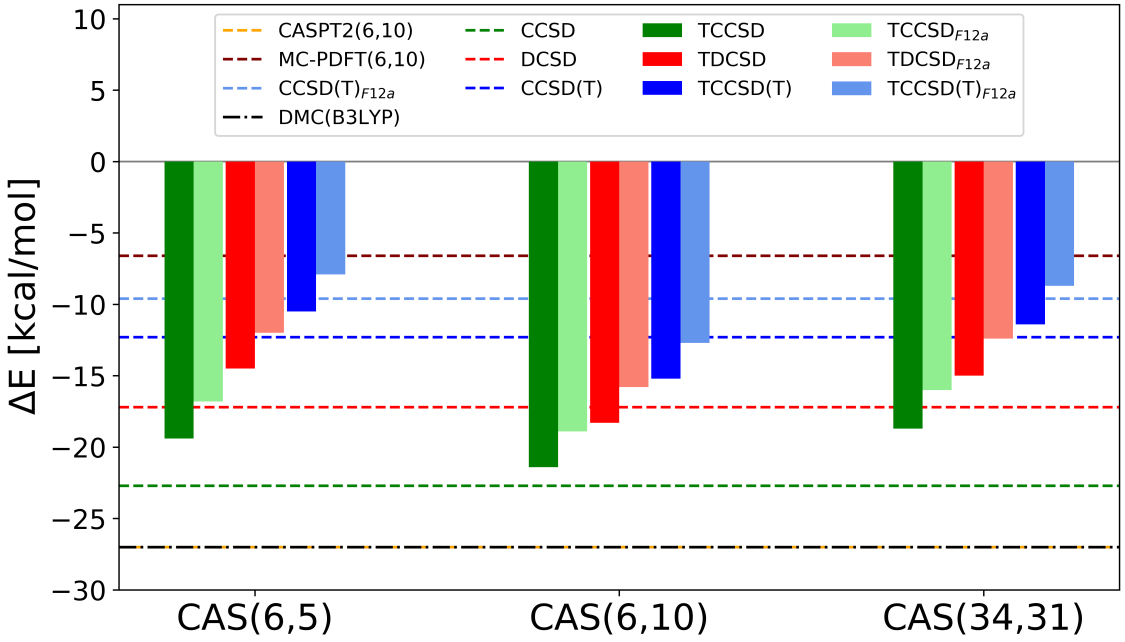

FIGURE 6.6: Spin gap estimates of $[Fe(NCH)_6]^{2+}$ for different active spaces.

once more less accurate results due to the missing relaxation of the CAS amplitudes, as explained for L=NH_3 in Sec. 6.2.2. In the largest CAS, the TCCSD(T) result remains close to CCSD(T), while TDCSD and TCCSD gaps are shifted towards the CCSD(T) value. Additionally, the TDCSD spin gaps are consistently between TCCSD and TCCSD(T) across the different CASs and also agree well with CCSD(T) values. The basis set corrected results show even smaller estimates.

The multi-configurationality of the system is again measured by the largest double amplitudes from the biggest CAS and corresponds to 0.066 and 0.038 for LS and HS states, respectively. Finally, the most negative results presented in Figure 6.6 are given by CASPT2 and DMC, which favor the HS state. On the other hand, MC-PDFT predicts a spin gap which is only ∼5 kcal/mol more stable than the LS state. The latter is interestingly very close to TCCSD(T)$_{F12a}$.

6.2.4 $[Fe(CO)_6]^{2+}$

In the last of the four octahedral Fe(II) systems studied in this work, the case with the carbon monoxide ligand is now considered. CO is well known to strongly stabilize the LS state due to the greater ligand field strength if compared to the previous cases. Such a strength is reflected in a singlet ground state as opposed to the HS in the other

three ligands. Qualitatively correct spin gaps are already obtained by the conventional CCSD, DCSD and CCSD(T) calculations based on ROHF orbitals, see Figure 6.7. The CASPT2 method is found once again to stabilize the HS, and, in this case, is also very close to the CCSD result. Large quantitative differences are evident between the methods. CCSD, for example, is five times smaller than the CCSD(T) spin gap.

In the CAS(6,5), the spin gap at the CASSCF level is equal to -47.4 kcal/mol, a HS ground state is reproduced. It is evident that the essential correlation effects that can stabilize the LS state are not included in this active space. Thus, a further electron correlation treatment is necessary. This is achieved by the tailored methods, as shown in Figure 6.7. Already in the small active space, the tailored approach recovers the

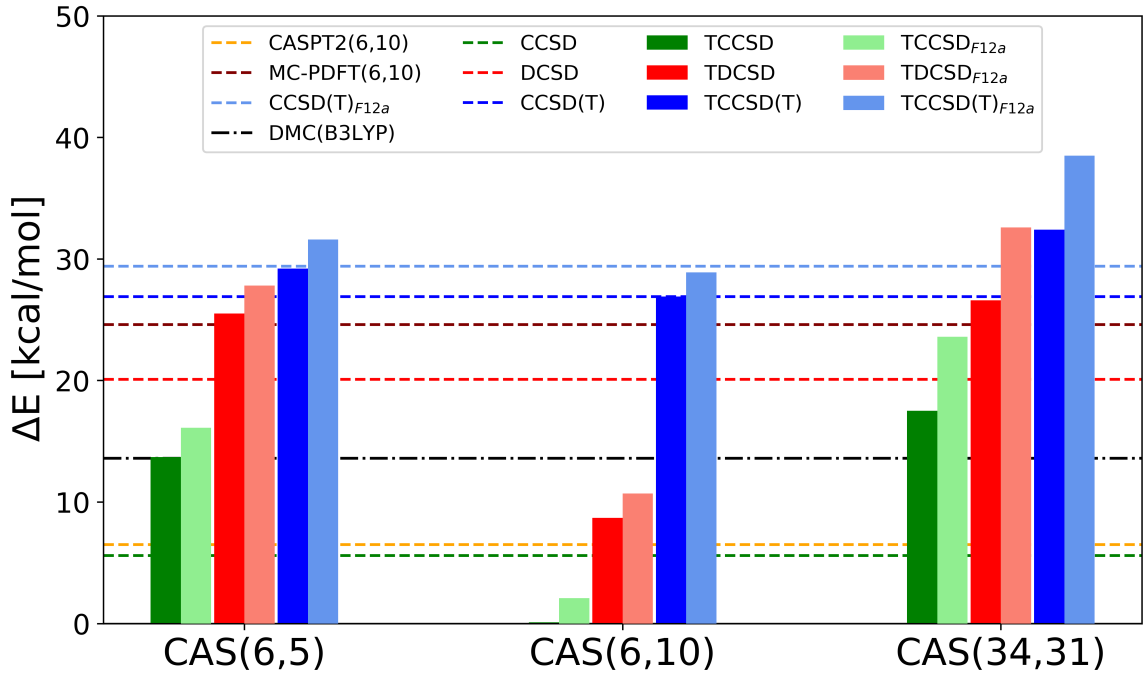

FIGURE 6.7: Spin gap estimates of $[Fe(CO)_6]^{2+}$ for different active spaces. The LS active space in CAS(6,10) has been obtained using state-averaged CASSCF, see main text.

correct spin state ordering. The latter confirms that the correlation out of the active space plays a key role in the LS stabilization. Further, a noticeable improvement in the agreement within the CC hierarchy is visible in the tailored results for CAS(6,5). The TDCSD externally corrected by CASSCF(6,5) becomes very close to TCCSD(T) and ROHF-CCSD(T). Even CCSD, which provides a LS prediction only ∼5 kcal/mol more stable than the HS state, shows the corresponding tailored method with a spin

gap increased by a factor of two. This result fortuitously matches the DMC spin gap. Further, the TDCSD gap is very close to the MC-PDFT(6,10) value.

In the CAS(6,10), the active space includes the double-shell d' orbitals of the central metal together with its five $3d$ orbitals. As shown in Figure 6.7, the external correction coming from such space results, in the TCCSD and TDCSD cases, in a large bias towards the HS state. In this active space, the necessity to provide consistent active orbitals in the two spin states under study required a state-averaging of HS and LS states at the CASSCF level. The latter made possible to obtain a CAS(6,10) for the LS state with all the d' orbitals. However, the TDCSD result is even smaller than the conventional DCSD, while the TCCSD spin states are nearly degenerate. The reason of these small spin gaps is due to the state-averaged orbitals used in the LS state and the consequent less accurate CAS amplitudes. Differently from the previous complexes discussed in this thesis, a high sensitivity of the the tailored approach to the quality and the size of the active space is evident here. The bias related to the active space choice is cured in the TCCSD(T) by the perturbative triples, which account for additional relaxation effects due to the unbalanced description of the two CASs.

The consideration of large active spaces is necessary in order to systematically improve the tailored results and to overcome the main limit related to the frozen active space amplitudes. Here, a CAS(34,31) is defined by DCSD NOs. Such an active space consists of five $3d$ orbitals of the iron center, twelve π_{ML} and twelve π^*_{ML} orbitals of the ligand, plus two σ_{ML} bonds (cf. the SI of Ref. [202] for orbitals visualization). The CAS-CI calculation yields still the wrong spin state ordering, as the previous CASSCF results. The missing orbital optimization might be the reason and could be accounted for by a Stochastic-CASSCF calculation instead of a CAS-CI. However, the tailored approach on top of such a large active space provides the qualitatively correct spin gaps. The TDCSD result almost coincides with ROHF-CCSD(T), while TCCSD(T) shows a further stabilization of the LS state. Further, the TCCSD estimate is closer to TDCSD and TCCSD(T) values. Finally, the MR character is shown to be low by the largest double amplitudes within CAS(34,31): 0.053 for LS and 0.037 for HS.

The F12 corrections further increase the final relative energies. The resulting TDCSD$_{F12a}$ and TCCSD(T)$_{F12a}$ spin gaps are shown to become larger than CCSD(T)$_{F12a}$ one, by almost 10 kcal/mol in the TCCSD(T)$_{F12a}$ case. It is worth to notice that a better agreement between CCSD(T), MC-PDFT and TCCSD(T) is demonstrated as opposed to CASPT2 and DMC, which reveal a bias for the HS state.

In this Fe(II) complex, the $\hat{T}_3^{\mathrm{CAS}}$ corrected tailored methods have also been considered.

However, negligible effects have been shown in the smaller CAS(6,5) and CAS(6,10). The latter amount to about ∼0.2 kcal/mol energy difference with the conventional tailored approaches. In the largest active space, the correction slightly increases showing an HS stabilization of ∼2 kcal/mol (TDCSD@T(34,31) = 24.5 kcal/mol and TCCSD@T(34,31) = 15.6 kcal/mol as opposed to TDCSD(34,31) = 26.6 kcal/mol and TCCSD(34,31) = 17.5 kcal/mol).

6.2.5 Overview

An overview of the results presented in the previous section for the four octahedral Fe(II) complexes is given here and compared with similar works from the literature. In Figure 6.8 the spin gap estimates calculated with the novel TDCSD are now presented along with the different complexes together with the TCCSD and TCCSD(T) methods and the corresponding explicitly correlated versions.

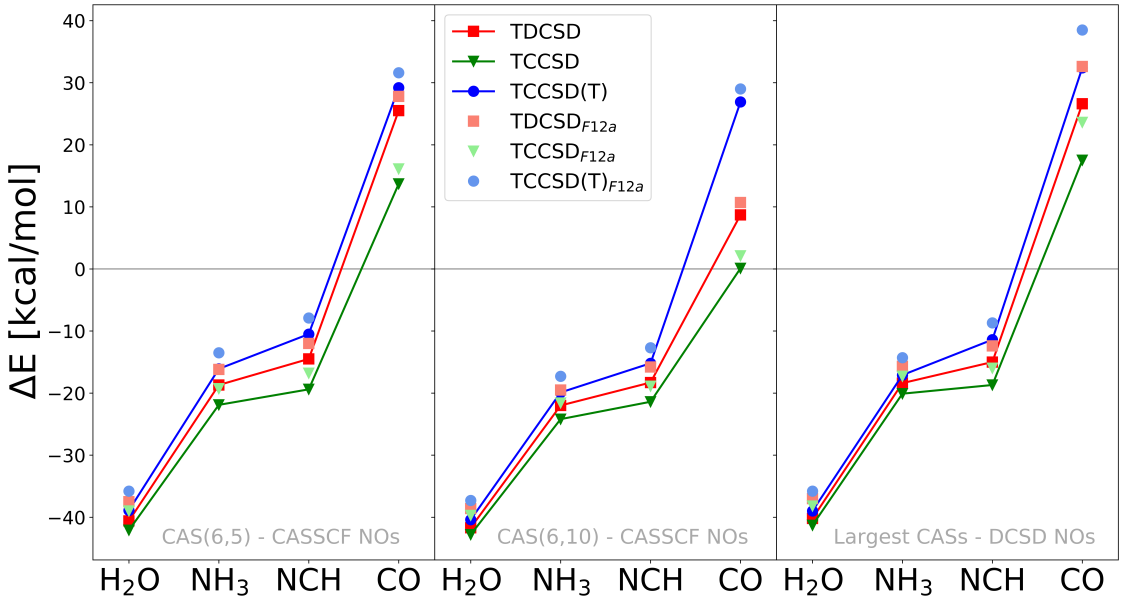

FIGURE 6.8: Spin gap estimates of the tailored methods of the four octahedral Fe(II) complexes grouped according to the active space.

In every compound, TDCSD shows results between TCCSD and TCCSD(T) and, in some cases, very close to TCCSD(T). This confirms once again a higher accuracy of TDCSD over TCCSD, as previously shown in Chapter 5, and as expected by previous studies on DCSD method [62, 64]. Figure 6.8 makes evident how the qualitative trend of spin gaps is adequately described for every active space considered in this study, even though the tailored results from CAS(6,10) seem to be not that accurate, especially in

the TCCSD case. However, a general agreement between the tailored results for each active space and complex is visible.

Table 6.1 groups the tailored results presented in this work together with some spin gap estimates available in the literature, with a focus on the most recent studies in a variety of different methods used for the same compounds.

In a recent work by Mariano et al. [214] the spin gaps of the same four Fe(II) complexes were evaluated with a new density-corrected DFT approach, DFT-PBE[U]. Such a method considers the PBE functional on the Hubbard density, whose value U is self-consistently calculated. This approach is shown to perform better than any other functional considered in their study. It is here shown in Table 6.1 together with the reference values reported in the same work, i.e. the CC corrected CASPT2 (CASPT2/CC) method. The latter method was originally proposed by Pierloot and coworkers in 2018 [223]. Indeed, it has been demonstrated how CASPT2 can provide accurate spin gap predictions as long as only the valence electrons are correlated [216]. However, a full CASPT2 treatment overstabilizes the HS state, as evident also from the CASPT2 results of the present study. Such a problem is due to the poor treatment of transition metal semi-core orbitals. In that respect, CASPT2/CC mitigates this lack of CASPT2 by including a CCSD(T) correction for the (3s3p) correlation contribution. The CASPT2/CC values shown in Table 6.1 are extrapolated to the CBS limit. Although the newly introduced DFT-PBE[U] approach is shown to perform better than any other functional considered in their study, i.e. the best mean absolute error is shown for these four octahedral Fe(II) complexes, it is clear from Table 6.1 that tailored spin gap estimates agree better with their reference values from CASPT2/CC method (except in the L=H_2O case). Indeed, in the NCH case the spin state ordering is even reversed in the DFT-PBE[U] approach, in comparison with all the other studies. However, differences in the spin gap estimates can also be related to the different geometries at hand. In this work, geometries from [211] of Burke and coworkers have been used (B3LYP optimized), allowing for direct comparison to their results. Whereas various geometry optimization strategies leading to different structural parameters have been considered in Mariano et al. [214] and the other cited works (except Ref. [208], where B3LYP geometry optimization is also used).

Another recent approach proposed by Neese and coworkers, the domain-based pair natural orbital CCSD with iterative triples (DLPNO-CCSD(T_1)) [224], has been applied to the Fe(II) complexes exhibiting a weak ligand strength, i.e. L=H_2O, NH_3 and NCH [212]. The spin gaps reported in Table 6.1 represent their basis set extrapolated

Compound	Method	ΔE	Ref.
$[\mathbf{Fe(H_2O)}_6]^{2+}$	$TDCSD_{F12a}$	-37.0	this work
	$TCCSD(T)_{F12a}$	-35.8	this work
	DLPNO-CCSD(T_1)	-33.3	[212]
	DFT-PBE[U]	-34.6	[214]
	CASPT2/CC	-42.2	[214]
	DMC	-41.0	[211]
	DMC	-58.6	[208]
$[\mathbf{Fe(NH_3)}_6]^{2+}$	$TDCSD_{F12a}$	-15.7	this work
	$TCCSD(T)_{F12a}$	-14.3	this work
	DLPNO-CCSD(T_1)	-11.3	[212]
	DFT-PBE[U]	-10.1	[214]
	CASPT2/CC	-14.9	[214]
	DMC	-28.4	[211]
	DMC	-36.7	[208]
$[\mathbf{Fe(NCH)}_6]^{2+}$	$TDCSD_{F12a}$	-12.4	this work
	$TCCSD(T)_{F12a}$	-8.7	this work
	DLPNO-CCSD(T_1)	-8.8	[212]
	DFT-PBE[U]	4.8	[214]
	CASPT2/CC	-3.8	[214]
	DMC	-27.0	[211]
	DMC	-31.8	[208]
	DMC	-19.6/-21.9	[209]
$[\mathbf{Fe(CO)}_6]^{2+}$	$TDCSD_{F12a}$	32.6	this work
	$TCCSD(T)_{F12a}$	38.5	this work
	DFT-PBE[U]	60.9	[214]
	CASPT2/CC	46.5	[214]
	DMC	13.6	[211]
	DMC	7.6	[208]

TABLE 6.1: Spin gap estimates of the four octahedral Fe(II)-complexes in kcal/mol from different studies in comparison with some tailored results.

estimates. These values are consistent with the $TCCSD(T)_{F12a}$ and $TDCSD_{F12a}$ results within a few kcal/mol. However, it must be noted that the DLPNO-CCSD(T_1) results

include scalar relativistic effects, which, according to Ref. [212], account for a further lowering of 2-3 kcal/mol in the final spin gap estimates. Interestingly, such DLPNO-CCSD(T_1) values without the relativistic correction are expected to show results in between the TDCSD$_{F12a}$ and TCCSD(T)$_{F12a}$ spin gaps.

Multiple works have attempted to provide reliable benchmark values through DMC calculations. The latter are commonly used as reference data in DFT studies with the application of various different functionals. However, the DMC estimates from Song et al. [211] show a tendency to favor the HS state in comparison to the results of the present work. The same tendency is evident for every other DMC value presented in Table 6.1.

This overview demonstrates once more the difficult problem at hand. Many different studies exploiting various methods, from DFT to *ab-initio*, have been showing a scattering of the results in a wide range of energies. Indeed, large deviations of the spin gap estimates are evident with respect to DMC results, even in comparison with each other, thus, not providing a solid consistent reference to rely on. The same problem has been seen for the different DFT approaches. For example, Mariano et al. [214] and Neese and coworkers [212], study many popular functionals which give rise to deviations up to tens of kcal/mol. As already stated by Droghetti et al. in 2012 [208], a "universal" functional which would properly describe the energetics of every Fe(II) complex is unlikely to be found and, even though these systems do not represent a challenging MR character (as also shown in the previous sections by their largest double amplitudes within the large CAS), their electronic structure makes a balanced description not a trivial task to be accomplished.

6.3 Fe(II)-Porphyrin

The Fe(II)-porphyrin model system is evaluated here with the tailored DCSD approach. Such a molecular system has been extensively studied over the past years [216, 217, 219–222, 225]. It has been demonstrated by Li Manni et al. [220, 221], using Stochastic-CASSCF and high order CC methods, that the FeP model shows a stable intermediate state (^3E_g) over the high spin state ($^5A_{1g}$). Further, the stabilization process of the triplet state has also been thoroughly investigated through the leading key excitations [222]. As in the previous octahedral Fe(II) complexes, the focus is on the spin gap estimate, here given by $\Delta E = E_Q - E_T$. However, in this case a number of nearly

degenerate spin states are present and this also characterizes the system with a ΔE which ranges in a few kcal/mol.

The analysis of such system is carried in the present work through four different active spaces. The first considered is CAS(8,11), which consists of the five $3d$ orbitals of central Fe, together with its five empty correlating d' orbitals and one σ Fe-N orbital. The second active space is CAS(12,15), which adds the four Gouterman π orbitals on top of the CAS(8,11). Such π-frontier orbitals are shown in Ref. [220] to play a decisive role in the triplet state stabilization, even though such an effect is present only when the largest CAS is considered. Next, the CAS(14,18) is evaluated. The latter is composed of the orbitals in CAS(8,11) with additional orbitals from the iron atom, four $4s4p$, and from the remaining three σ Fe-N bonding orbitals. The last studied active space includes the entire π system of the FeP model on top of the CAS(14,18), resulting in the CAS(32,34). All these CASs are optimized at the CASSCF level. However, the last defined active space is computationally too expensive for a conventional CASSCF. Thus, the Stochastic-CASSCF has been applied for the CAS(32,34). Such a choice of active spaces has already been evaluated in previous studies [220, 221]. Differently from the four octahedral Fe(II) complexes, the multi-configurationality of FeP is more pronounced as shown by the largest amplitudes given by the calculation in CAS(32,34): 0.242 for the triplet and 0.221 for the quintet state.

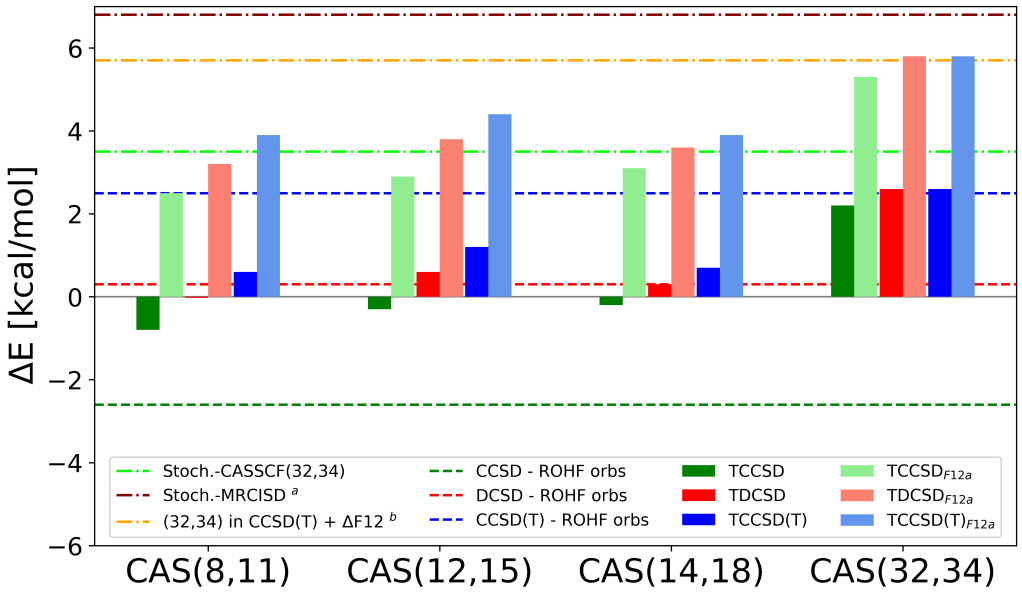

FIGURE 6.9: Spin gap estimates of the Fe(II)-porphyrin over different active spaces. [a] Stochastic-MRCISD (6.8 kcal/mol) on top of CAS(32,34), Ref.[225]. [b] best estimate from a subtractive embedding scheme, Ref. [221].

Figure 6.9 presents the spin gap estimates for this work, together with two additional results from the literature. Further, the conventional DCSD, CCSD and CCSD(T) on ROHF orbitals are also shown. All the tailored calculations are performed on (Stochastic-) CASSCF NOs.

The ROHF-CC/DC calculations show evident differences from each other in the final results. For example, CCSD even shows a quintet ground state with a $\Delta E = -2.6$ kcal/mol. However, such deviations are reduced in the corresponding tailored methods. Indeed the conventional CC approaches differ in a range of values up to 5 kcal/mol, while the results from tailored methods differ only by up to 1.5 kcal/mol in every chosen CAS.

In Figure 6.9 it is worth noticing how the frozen amplitudes in the three smallest CASs negatively affect the accuracy of the tailored methods. For example, the TDCSD spin gap in CAS(8,11) is degenerate and it does not seem to improve much from its conventional counterpart in the next two CASs. This problem is especially evident in the TCCSD(T) results, which are much smaller than the CCSD(T) estimate in the first three CASs. This confirms that the reliability of the tailored methods is also related to the size of the considered active space, especially when MR systems are under study.

A change in the correlation description is clear in the largest CAS. In this case, the Stochastic-CASSCF calculation produces a triplet ground state, whose result is presented as a light green line in Figure 6.9, $\Delta E = 3.8$ kcal/mol, while the smaller three CASs show a negative CASSCF spin gap prediction. It demonstrates that the inclusion of the entire π system in the CAS(32,34) is crucial for the stabilization of the triplet state. The tailored approaches together with the basis set correction enlarge the spin gap predictions even further, showing that the dynamic correlation effects out of the active space play a significant role, while the basis set incompleteness error is greatly reduced.

The final results of TDCSD, TCCSD and TCCSD(T) in CAS(32,34) are in general good agreement with CCSD(T) and give further evidence in favor of the triplet ground-state in this long dispute about the lowest energetic spin state of the Fe(II)-porphyrin model system [220].

In a recent study from Weser et al. [225] the spin gap of the FeP model system has been calculated using a stochastic MRCISD which correlates 96 electrons into 159 orbitals on top of the same largest active space considered here. The spin gap prediction of 6.8 kcal/mol further favors the triplet state and the difference with the tailored results can be understood as a possible bias towards the quintet state due to the SR

framework the tailored approach works in, unlike a true MR method, as well as the neglect of higher order contributions beyond (T). On the other hand, the MRCISD method presents issues such as size-extensivity. In addition, the 159 orbitals used for the spin gap calculation are still far from approaching the CBS limit.

In another work from Li Manni et al.[221], a subtractive embedding scheme accounts for an attempt to include all the correlation effects beyond the active space. The resulting DCSD-embedded CAS(32,34)+ΔF12 amounted to 3.6 kcal/mol, while CCSD(T)-embedded CAS(32,34)+ΔF12 to 5.7 kcal/mol. Interestingly, the latter shows a very good agreement with the results at the highest level of theory given by TCCSD(T)$_{F12a}$ and TDCSD$_{F12a}$, i.e. 5.8 kcal/mol.

6.4 Conclusions

In this chapter, the tailored DC approach has been applied to the open-shell systems in order to assess its validity and accuracy in the study of Fe(II) transition metal complexes, whose relevance in many different fields made it an interesting case for predictive electronic structure calculations. Natural orbitals have defined every active space, either from DCSD or (Stochastic-)CASSCF methods. The potential errors introduced in the tailored formalism, i.e. the bias towards a specific reference determinant and the frozen CAS amplitudes, are compensated by a study of various active space sizes, where the very large ones have been evaluated with the FCIQMC method.

The TCCSD(T) is the highest level in the TCC hierarchy considered in this work. Its results are consistently closer to the TDCSD estimates than to TCCSD, demonstrating once more the accuracy of the TDCSD method over the TCCSD also in the open-shell cases. Further, a better quantitative agreement can be noticed between TDCSD, TCCSD(T) and MC-PDFT, in comparison with the CASPT2 and DMC methods.

The assumption that the larger active spaces correspond to higher accuracy is not always found. For example, the inclusion of the correlating double-shell d' orbitals on top of the CAS(6,5) did not increase the quality of the results, but instead introduced a certain bias towards the HS state. This has been explained in view of the artificial amplification of the $3d \rightarrow d'$ excitation and the consequent neglect of the important ligand to metal excitations. Further, a tendency towards the HS has been clearly shown also by the CASPT2 results. Interestingly, even the TDCSD@T and TCCSD@T results have shown an additional slight HS stabilization in the L=CO case. However, the

tailored results improve consistently in every system if the active spaces are expanded in a systematic and balanced way.

Another confirmation of the triplet ground state has been added in the long search for an incontrovertible spin gap prediction in the Fe(II)-porphyrin model system. The largest active space shows very close spin gap estimates between the tailored results, and even an overlapping result between TCCSD(T) and TDCSD. This demonstrates the convergence of the tailored results with respect to the active space size. Additionally, the confirmation from the subtractive embedding scheme in the same CAS(32,34) further supports the calculated spin gaps.

The explicitly correlated corrections have been applied in every Fe(II) complex in order to approach the complete basis set limit. As shown in all the spin gap estimates, the F12 correction accounted for an additional LS stabilization in every system (and triplet stabilization in Fe(II)-Porphyrin case). Further, the CCSD(T) calculations are found to yield quite accurate results, providing a good agreement with the best tailored spin gaps. However, the advantage of the tailored method is a systematically improvable approach, which is obtained from the combination of coupled cluster or distinguishable cluster with FCIQMC.

Chapter 7

Hydrogen systems

Strong correlation effects observed in many-body systems are challenging to treat in QC for every approximate correlated method. In Chapter 5, the novel TDCSD method was demonstrated to perform well in dissociating regimes in comparison to true MR methods. In this Chapter, model systems are evaluated through the application of the screened embedding method. These benchmark quantum chemical systems, such as the H_n clusters consisting of n hydrogen atoms in various configurations, are of essential importance for understanding the mechanism behind strong correlation effects.

The H chain (meant as a 1 dimensional arrangement with uniform interatomic spacing) has been extensively studied in the past years [226–235]. Despite its simple structure, it captures the main features of the many-electron problems in real materials, without the need to include core electrons or scalar relativistic effects [232]. The works on such a system revealed a metal-insulator transition (MIT) mechanism [226], which occurs at a critical bond length in the intermediate region between the compressed and equilibrium geometries. Indeed, the hydrogen chain can be seen as a good compromise between a still physically and chemically relevant system, but with the advantage of an approachable computational tractability. This makes such a model an ideal case study to assess the ability of theoretical methods.

The evaluation of potential energy curves in the H-systems leads to degeneracies which are usually described by MR methods. In the present Chapter, a screened embedding on top of DCSD and tailored DCSD is presented and its application on representative H-systems is analyzed.

7.1 Computational Details

Three hydrogen systems have been investigated in order to evaluate the efficiency of the TDCSD approach and the screened embedding. Namely, the systems under study are an H-chain composed of 10 atoms, an H-ring with 10 atoms as well and an H-plane with 4x3 H atoms. The study has been focused on the computation of PECs of these systems in the cc-pVTZ basis set.

MRCISD with Davidson correction (MRCI+Q) has been calculated in all the systems as a reference value, starting from a CASSCF with the same active space of the size of the embedded space. The latter was always defined equal to the minimal active space. The same applies to the CAS included in the TDCSD method.

All the calculations of the screened embedding have been performed on top of natural orbitals, either CASSCF or DCSD NOs. In case of CASSCF NOs, first the CI coefficients and the natural orbitals are generated in the corresponding CASSCF calculation, then the TDCSD computation is performed and, finally, the dressed integrals are produced starting from the CC amplitudes of the TDCSD calculation. In case of DCSD NOs, a simple DCSD is first performed to generate the relative NOs and the embedded fragment is chosen from those. Again, the dressed integrals are generated starting from the amplitudes of the previous calculation, in this case DCSD. However, when the DCSD NOs were used, it turned out to be important to sort the orbitals in order to define a good reference determinant, with a lower energy. This can be done semi-automatically by calculating Fock matrix elements in the natural orbital basis using the full correlated density matrix instead of the usual orbital-density matrix and ordering the orbitals according to the diagonal elements of this Fock matrix.

All the screened integrals are generated in the Molpro software [123–125] in the form of non-Hermitian FCIDUMPs. The latter are read in by the NECI algorithm [108], where the corresponding embedding calculations take place.

7.2 H-chain (H_{10})

First, the uniform dissociation of the H chain composed of 10 H atoms is considered. The system is constructed as a 1 dimensional chain, where the only characterizing parameter is the distance between two adjacent atoms. Here, the active space is taken equal to the minimal active space, i.e. 10 electrons in 10 orbitals.

In Figure 7.1, the TDCSD and TCCSD approaches provide very similar PECs. All the tailored methods, regardless of the NOs used, show an overestimation of the electron correlation in the intermediate stretched region, in comparison to the MRCI+Q results. However, a slight improvement is possible to be noticed in the tailored results using DCSD NOs, with respect to the ones using CASSCF NOs. Even in comparison with the conventional DCSD, the TDCSD method seems less accurate. This low accuracy can be again related to the frozen amplitudes in the active space.

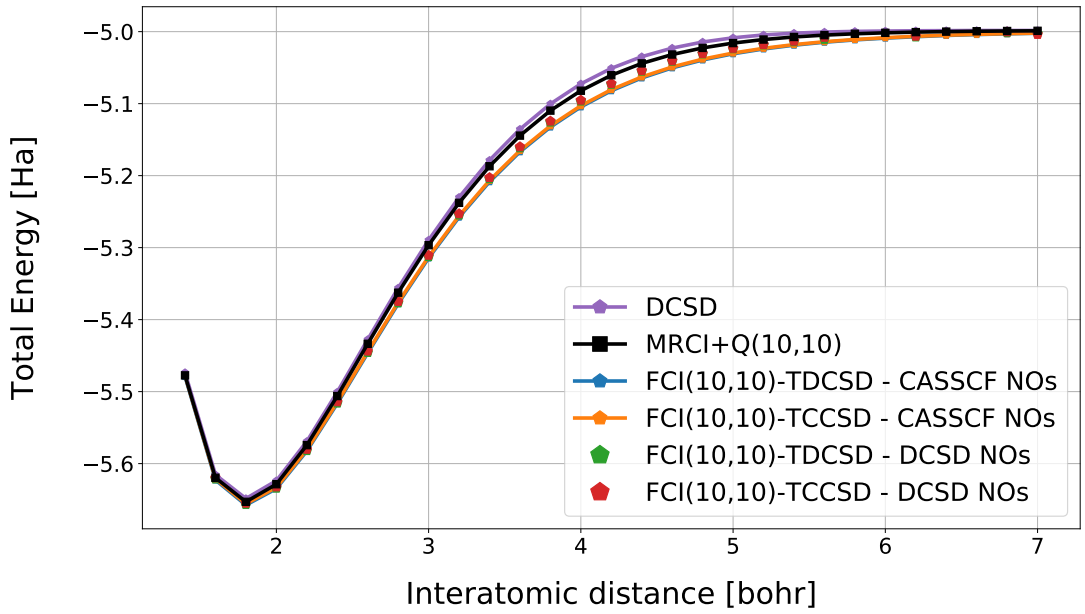

FIGURE 7.1: Potential energy curves for H-chain with (10,10) active space in the cc-pVTZ basis set

In this case, a larger active space has been also studied, including 10 more virtual DCSD NOs with the largest occupation numbers. In Figure 7.2, it is possible to notice that the relative TDCSD curve shows only a slightly better result than the (10,10) values. The intermediate region approach, already proposed in the closed shell molecules studied in Chapter 5, has been applied also here. A buffer region between the largest CAS(10,20) and the minimal space CAS(10,10) is defined, denoted as FCIQMC$_{(10,20)}$(10, 10)-TDCSD in Figure 7.2. The resulting curve shows a slight further improvement towards the reference MRCI+Q PEC. This suggests that the missing relaxation in the tailored approach represents an issue in the study of such systems. Finally, a simple subtractive embedding scheme has been also applied, denoted in Figure 7.2 as FCI(10,10)+ΔDCSD, and shows a remarkable overlap with the reference values.

Although the tailored formalism was shown to be successful in the dissociation of case studies in Chapter 5, it is evident at this point that the DCSD method does not

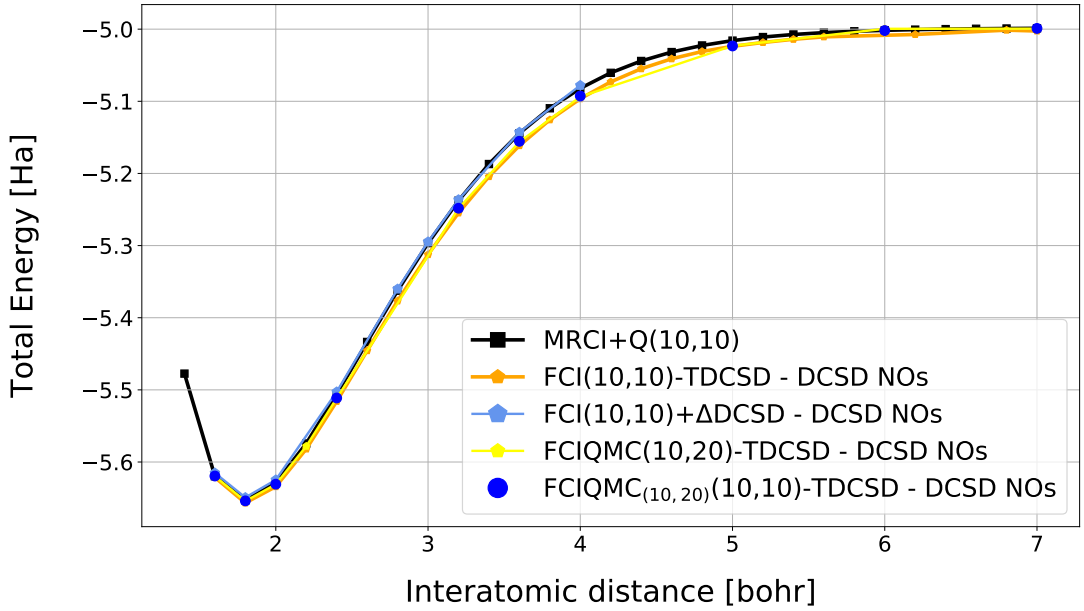

FIGURE 7.2: Comparison of the H-chain PECs from various TDCSD methods with MRCI+Q and subtractive embedding in cc-pVTZ basis

benefit from its application in the evaluation of this model system, even when larger active spaces are considered. In Figure 7.3, the TDCSD and DCSD methods based on CASSCF NOs and RHF orbitals, respectively, are shown along the dissociation path according to the energy differences with respect to the MRCI+Q(10,10) values. It is interesting to see how the plain DCSD shows a trend similar to TDCSD, but characterized by an underestimation of the correlation energy.

These two calculations can now be used as starting points to evaluate the performance of the new screened embedding. After the TDCSD or DCSD calculations, integrals in the embedded fragment can be generated starting from the CC amplitudes of the previous calculations on top of the NOs of choice. Dressed FCIDUMPs are then produced, using again the minimal active space, CAS(10,10), as in the tailored approach. The resulting PECs are shown in Figure 7.3 relative to the MRCI+Q reference.

The effect of this dressing is remarkable in both cases. First, the screening applied on top of the plain DCSD (green line in Figure 7.3) shows absolute values much closer to the reference energy. Further, the oscillations of the PEC get smaller the more stretched the H-chain becomes, until they will eventually overlap with the MRCI+Q values. Same effect is visible on the dressing applied on top of TDCSD (red line in Figure 7.3). In this case there is also a semblance of oscillations, but the limited region shown in the graph does not make it straightforward to notice. However, what looks

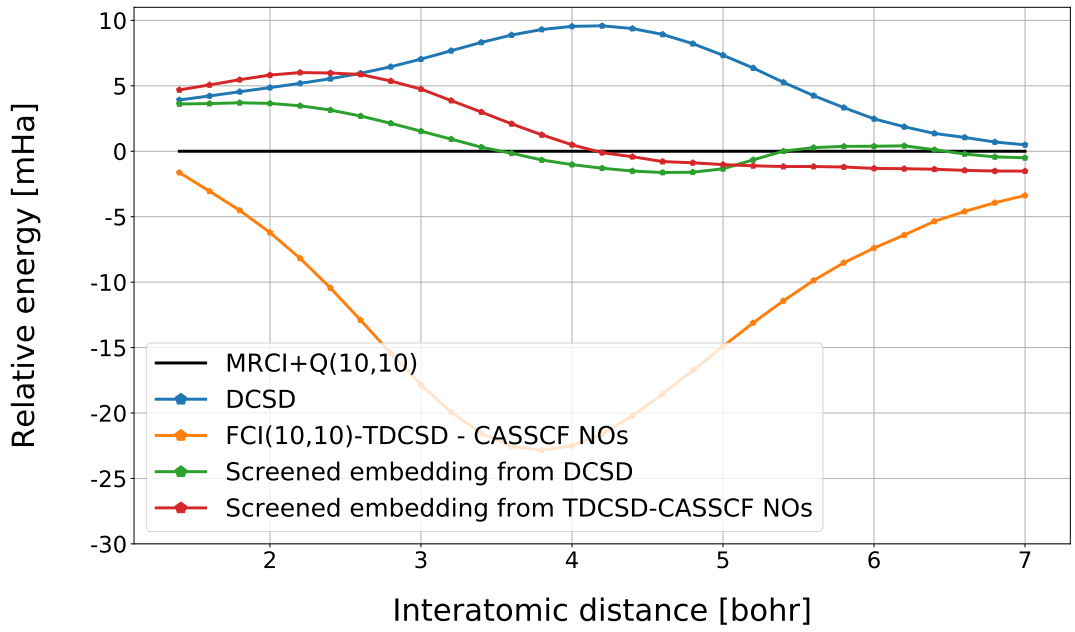

FIGURE 7.3: Relative energies of H_{10}-chain in different PECs with respect to the MRCI+Q(10,10) values

like a divergent trend might represent a wider oscillation and eventually converge onto the same MRCI+Q values at larger distances. Interestingly, the dressed values in the compressed and equilibrium region (1.4 bohr $< r <$ 2.0 bohr) show a decreased accuracy compared to the initial TDCSD (orange line in Figure 7.3).

7.3 H-ring (H_{10})

Next, the ring compound of 10 hydrogen atoms has been taken into account. Here, the 10 atoms are fixed to have always the same internuclear angle of 144 degree and the only parameter is again the interatomic distance.

The initial calculations of DCSD and TDCSD show again an underestimation and overestimation of the MRCI+Q values, respectively. However, the screened embedding applied on top of these two methods in the minimal active space of 10 electrons in 10 orbitals introduce an evident improvement in both cases, especially in the stretched region. Further, Figure 7.4 shows an oscillation of the dressed calculations that is more visible in the DCSD case, but it can be present also in the TDCSD case at larger distances.

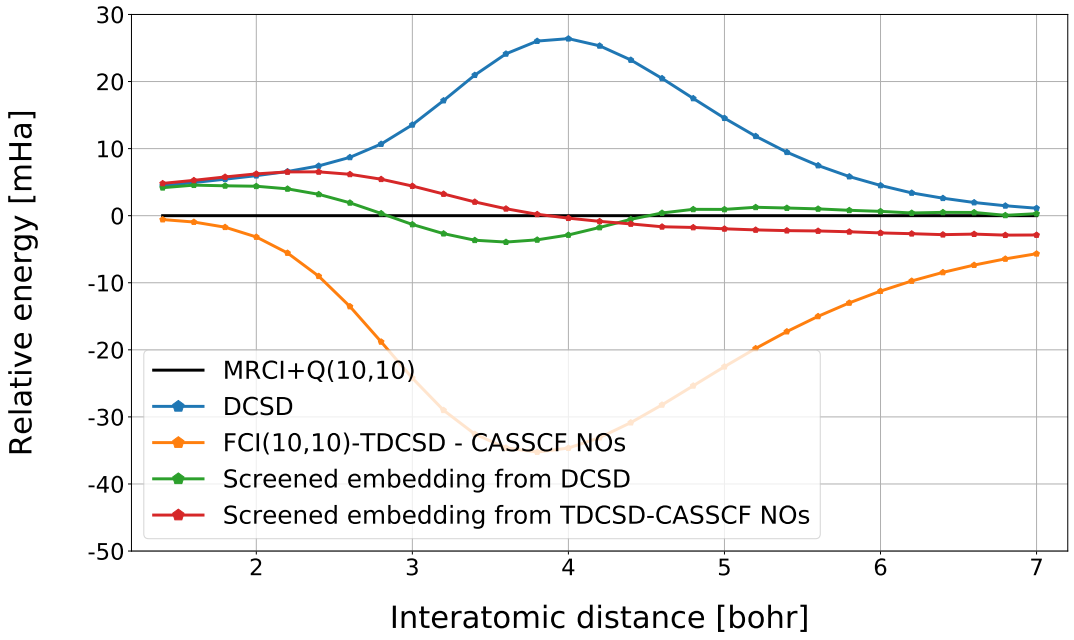

FIGURE 7.4: Relative energies of H_{10}-ring in different PECs with respect to the MRCI+Q(10,10) values

It is worth to notice that the DCSD-based screened embedding shows a PEC that is more accurate compared to the initial DCSD at any point in Figure 7.4, whereas the TDCSD PEC has again a higher accuracy for small interatomic distances with respect to its screened version.

7.4 H-plane ($H_{4\times3}$)

The last test system is a two dimensional hydrogen system, whose geometry is structured as a rectangle composed by 12 H atoms. The latter are arranged in 4 lines and 3 columns, giving rise to a 2D system, where the only parameter that describes the PEC is represented by the distance between 1 H atom and all the first adjacent atoms.

The first two initial calculations, DCSD and TDCSD, give again an under- and over-estimation of correlation energy, respectively. The embedding scheme is applied here on the minimal active space of 12 electrons in 12 orbitals.

The screening applied to the two calculations gives rise to a noticeable improvement of the PECs when compared to the reference MRCI+Q in a CAS(12,12), as shown in Figure 7.5. Further, a similar pattern is visible for both dressed variants, with DCSD-based results showing smaller oscillations around the reference curve and TDCSD-based

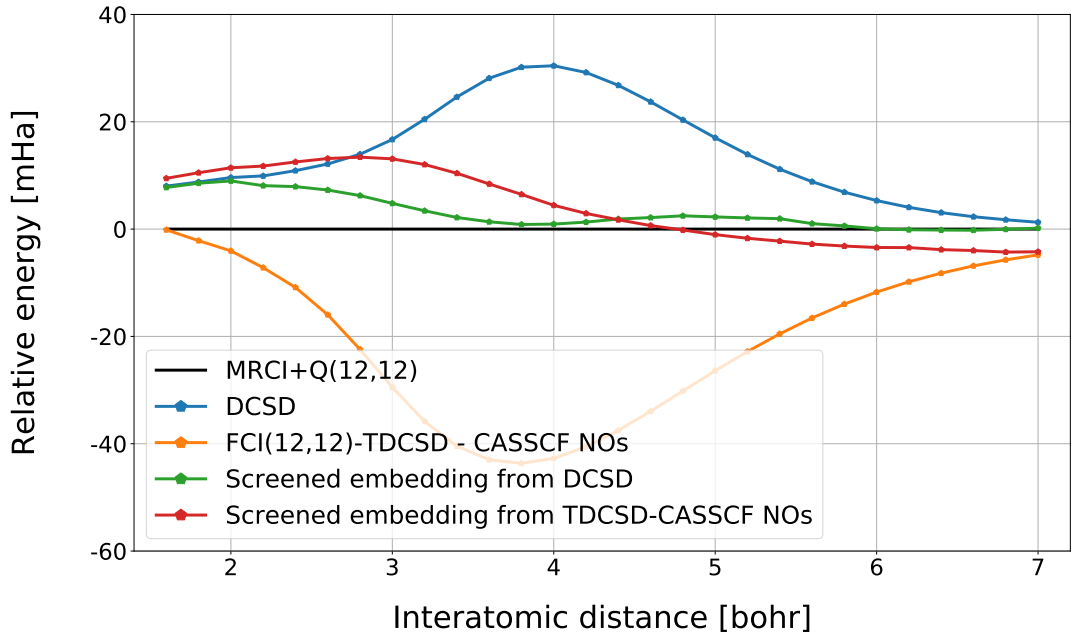

FIGURE 7.5: Relative energies of $H_{4\times3}$-plane in different PECs with respect to the MRCI+Q(12,12) values

ones performing similar to the two previous model systems. Again, the accuracy of the PEC at small interatomic distances is better in the plain TDCSD rather than in the screened version.

7.5 Conclusions

In all the three H-systems shown in this Chapter, the methods have very similar behaviors. On the one hand, TDCSD always appears with an evident miscalculation of the intermediate stretched region up to ∼40 mHa error in the worst case. On the other hand, DCSD shows smaller absolute errors but still far from reproducing a correct curve in the same intermediate distances. However, the application of a simple subtractive embedding scheme to the H-chain produces an accurate PEC.

The screened embedding can dramatically improve the description of these strongly correlated systems. Indeed, the plotted relative energies show an accuracy that tackles MRCI+Q in every case. The different oscillations around the reference value distinguish the two screened embeddings, and a common trend can be seen across the three systems.

The calculations on TDCSD-dressed fragments show good accuracy all along the dissociation path of the three H systems, even though the plain TDCSD provides better

results in the region around the equilibrium. The same higher accuracy is seen in the DCSD-screened embedding PECs, in comparison with the corresponding plain DCSD method. However, the improvement is generalized over the entire dissociation curve in this case.

Part IV

Conclusions

Chapter 8

Summary and Outlook

In this thesis, the developments and applications of embedded methods in the context of coupled cluster theory and FCIQMC were explored to extend their accuracy and applicability in strongly and weakly correlated systems. Two distinct embedding schemes were introduced, and their applications to various systems were presented.

A novel tailored distinguishable cluster approach has been implemented and combined with the stochastic CI eigensolver, FCIQMC. The tailored formalism allowed to quantitatively increase the accuracy of the DCSD method in most cases and to extend the applicability of FCIQMC to larger problems than normally possible. The motivations for developing the novel method were based on the remarkable performance of DCSD, in comparison to CCSD, and on the benefits provided by a large CI problem solver. In addition, a perturbative explicit correlation correction was also considered in this work to investigate the issue of basis set incompleteness error for *ab-initio* methods. This includes the introduction of a new explicitly correlated FCIQMC approach.

The FCIQMC tailored DCSD (TDCSD) method was benchmarked on various closed-shell molecular systems against true MR methods and other established approaches. For the examples of N_2, F_2 and H_2O dissociation curves, the new method provided quite accurate results in comparison with the reference values. Further, the torsion curves of ethylene and the automerization reaction of cyclobutadiene were analyzed, highlighting once more the accuracy of TDCSD in systems away from the equilibrium geometry. Finally, the relative energies of the ozone states were considered, giving results in good agreement with best available estimates.

The application of the FCIQMC-TDCSD was further extended to larger open-shell molecular systems, where a quantitatively accurate calculation of spin gaps is not a trivial task in QC. This has expanded the applicability of the novel method to both strongly and weakly correlated systems and made the estimation of spin state energetics

an interesting assessment. The single-center transition metal complexes considered in this work are defined mainly by dynamic electron correlation, for which higher than double excitations are typically required to achieve high (sub kcal/mol) accuracy.

The TDCSD method was shown to provide more accurate results than the simple DCSD and its CC counterpart, TCCSD. In the closed-shell systems, the better performance of TDCSD was acknowledged by the very good agreement it has with the reference results (except in the H model systems). Remarkable accuracy was found in systems characterized by a large amount of static correlation. In the open-shell systems, TDCSD provided estimates of the spin gap, which are consistent with the CCSD(T) results and are even close to the TCCSD(T) values in some cases. Although a good agreement was found with similar studies, e.g. with CASPT2/CC, establishing consistent reliable reference values is hard and is still a matter of debate. However, an overall agreement of the spin gaps given by the tailored methods in the largest CASs validates an improved accuracy given by the tailored formalism, as opposed to the larger deviations between the simple CC/DC approaches.

The FCIQMC-TDCSD method provides a valuable approach to study strongly and weakly correlated systems. Although in some cases the current scheme is still plagued by the missing relaxation of the CAS amplitudes and an inherent bias towards a SR determinant, the novel method is computationally favorable, in comparison with true MR methods or high-level SR approaches, and systematically improvable. The addition of a further external correction represented by the triple amplitudes in the active space was found to accelerate the convergence with respect to the active space size. Further, the DCSD natural orbitals have been confirmed to be a good alternative to CASSCF NOs in order to select large active spaces without accounting for a full CASSCF optimization.

Another embedded method based on the screened Coulomb formalism was explored in this thesis as a further scheme to describe strongly correlated systems. The additional information included in the one- and two-electron integrals was introduced by a screened fluctuation density obtained in a dRPA manner. These screened embedding approaches properly described the degeneracies found in the dissociation of the hydrogen model systems. This was confirmed by the corresponding results approaching the MRCI+Q reference values.

Future developments of both of the embedded methods are possible, for example, in the open-shell systems. FCIQMC-TDCSD can be extended to study complexes represented by spin-broken reference determinants. This would further increase the

applicability of the method in open-shell systems characterized by strong multi-reference character. On the other hand, the application of the screened embedding in such systems might be valuable as shown in closed-shell cases.

Part V

Appendix

Appendix A

Derivation of the energy of a single Slater Determinant

The energy associated with a single Slater Determinant can be expressed by the expectation value of the Hamiltonian operator. Further, when the N-electron wave function $|\Psi\rangle$ (Eq. 1.9) is expanded by N orthonormal spin orbitals, the energy equation can be written as,

$$\begin{aligned} E &= \frac{\langle\Psi|\hat{H}|\Psi\rangle}{\langle\Psi|\Psi\rangle} = \langle\phi_1\phi_2\dots\phi_N|\hat{H}|\phi_1\phi_2\dots\phi_N\rangle \\ &= \langle\phi_i\phi_j\dots\phi_N|\sum_m \hat{h}_1(\mathbf{x}_m) + \sum_{m,q>m} \hat{h}_2(\mathbf{x}_m,\mathbf{x}_q) + \hat{V}_{nuc}|\phi_i\phi_j\dots\phi_N\rangle. \end{aligned} \tag{A.1}$$

where the Hamiltonian is reported by its one- and two-electron operators (Eq. 1.11), and also the nuclear energy operator is included.

The expression in Eq. A.1 becomes quickly complex due to the large number of terms arising from the SDs. Indeed, each SD generates N! permutations, which, in turn, produce $(N!)^2$ integrals. However, if orthonormality conditions of spatial orbitals and spin functions are applied, the energy equation can be simplified.

First, let us consider the one-electron operator in Eq. A.1:

$$E_1 = \sum_m^N \langle\Psi|\hat{h}_1(\mathbf{x}_m)|\Psi\rangle. \tag{A.2}$$

An example is here given for the m-th electron, $\mathbf{x}_m$:

$$\begin{aligned}
&\langle\Psi|\hat{h}_1(\mathbf{x}_m)|\Psi\rangle = \\
&\frac{1}{N!}\left[\int \phi_i^*(\mathbf{x}_1)\dots\phi_k^*(\mathbf{x}_m)\dots\phi_N^*(\mathbf{x}_N)\hat{h}_1(\mathbf{x}_m)\phi_i(\mathbf{x}_1)\dots\phi_k(\mathbf{x}_m)\dots\phi_N(\mathbf{x}_N)d\mathbf{x}_1\dots d\mathbf{x}_m\dots d\mathbf{x}_N+\dots\right] \\
&= \frac{1}{N!}\left[\int \phi_i^*(\mathbf{x}_1)\phi_i(\mathbf{x}_1)d\mathbf{x}_1\int\dots\int \phi_k^*(\mathbf{x}_m)\hat{h}_1(\mathbf{x}_m)\phi_k(\mathbf{x}_m)d\mathbf{x}_m\int\dots\int \phi_N^*(\mathbf{x}_N)\phi_N(\mathbf{x}_N)d\mathbf{x}_N+\dots\right] \\
&= \frac{1}{N!}\left[\langle\phi_i|\phi_i\rangle\dots\langle\phi_k|\hat{h}_1|\phi_k\rangle\dots\langle\phi_N|\phi_N\rangle+\dots\right] \qquad \text{(A.3)}
\end{aligned}$$

The latter is only the first term of $(\mathrm{N!})^2$ in total. Since the one-electron Hamiltonian depends only on the m-th electron, only the spin orbitals containing $\mathbf{x}_m$ are to be integrated with it. Every other term can be separated into individual inner products, which correspond to Kroenecker deltas due to orthonormality of the chosen spin orbitals. The only non-zero contributions are the N! permutations where the bra and ket parts of every inner product are the same (e.g., the term shown in Eq. A.3). Further, these non-zero contributions result into $(N-1)!$ equivalent integrals. So, the energy of the one-electron operator for the m-th electron can be simplified as,

$$\langle\Psi|\hat{h}_1(\mathbf{x}_m)|\Psi\rangle = \ = \frac{1}{N!}\left[(N-1)!\sum_k^N\langle\phi_k|\hat{h}_1|\phi_k\rangle\right] = \frac{1}{N}\sum_k^N h_{kk}. \qquad \text{(A.4)}$$

The same result is found regardless of which electron is considered. Thus, the sum over all the electrons in Eq. A.2 can be replaced by the factor N in the final expression of E_1 where Eq. A.4 is inserted,

$$E_1 = \sum_m^N\left[\frac{1}{N}\sum_k^N h_{kk}\right] = \sum_k^N h_{kk}. \qquad \text{(A.5)}$$

Next step is to consider the two-body part of the Hamiltonian in Eq. A.1,

$$E_2 = \frac{1}{2}\sum_{m\neq q}^N\langle\Psi|\hat{h}_2(\mathbf{x}_m,\mathbf{x}_q)|\Psi\rangle. \qquad \text{(A.6)}$$

A similar process to h_1 is followed, where the only non-zero terms are given by the inner products involving the same orbital in bra and ket. Let us assume the $\hat{h_2}$ operator

acting on the m- and q-th electrons,

$$\begin{aligned}
&\langle\Psi|\hat{h}_2(\mathbf{x}_m,\mathbf{x}_q)|\Psi\rangle = \\
&\frac{1}{N!}\left[\int \phi_i^*(\mathbf{x}_1)\dots\phi_k^*(\mathbf{x}_m)\phi_l^*(\mathbf{x}_q)\dots\phi_N^*(\mathbf{x}_N)\hat{h}_2(\mathbf{x}_m,\mathbf{x}_q)\phi_i(\mathbf{x}_1)\dots\phi_k(\mathbf{x}_m)\phi_l(\mathbf{x}_q)\dots\phi_N(\mathbf{x}_N)d\mathbf{x}_1\dots d\mathbf{x}_m d\mathbf{x}_q\dots d\mathbf{x}_N+\dots\right] \\
&= \frac{1}{N!}\left[\int \phi_i^*(\mathbf{x}_1)\phi_i(\mathbf{x}_1)d\mathbf{x}_1\int\dots\int \phi_k^*(\mathbf{x}_m)\phi_l^*(\mathbf{x}_q)\hat{h}_2(\mathbf{x}_m,\mathbf{x}_q)\phi_k(\mathbf{x}_m)\phi_l(\mathbf{x}_q)d\mathbf{x}_m d\mathbf{x}_q\int\dots\int \phi_N^*(\mathbf{x}_N)\phi_N(\mathbf{x}_N)d\mathbf{x}_N+\dots\right].
\end{aligned} \tag{A.7}$$

Here, again only the first term of the $(N!)^2$ possible ones is represented. This time, two different integrals arise since $\hat{h}_2$ depends on two electrons. However, simplifications due to orthonormal spin orbitals and equal integrals result as,

$$\begin{aligned}
\langle\Psi|\hat{h}_2(\mathbf{x}_m,\mathbf{x}_q)|\Psi\rangle &= \frac{1}{N!}\left[(N-2)!\sum_{kl}^{N}(\langle\phi_k\phi_l|\hat{h}_2|\phi_k\phi_l\rangle - \langle\phi_k\phi_l|\hat{h}_2|\phi_l\phi_k\rangle)\right] \\
&= \frac{1}{N(N-1)}\sum_{kl}^{N}\left[\langle kl|kl\rangle - \langle kl|lk\rangle\right] = \frac{1}{N(N-1)}\sum_{kl}^{N}\langle kl||kl\rangle,
\end{aligned} \tag{A.8}$$

where a short-hand notation has been introduced, i.e. $|\phi_k\rangle \equiv |k\rangle$ and $\langle\phi_k| \equiv \langle k|$. Two integrals are found in the energy expression of the two-electrons Hamiltonian. The first is the so called Hartree term (J_{kl}), where the Coulomb potential arising from N charges is calculated. This also includes an unphysical self-interaction when $k = l$. This term is canceled by the second integral, so called exchange term (K_{kl}). The exchange term has a minus sign from the antisymmetry guaranteed by the SD and represents the inclusion of the Pauli principle in the Hartree method. This term accounts for the repulsion given by electrons with parallel spins in different orbitals. The latter follows from the orthogonality of the spin function introduced in Eq. 1.8. This ensures that in the surrounding of a given electron no other electrons with same spin is found, that is also called "exchange/Fermi hole". The equation A.8 is independent of the specific electrons pair under consideration. Indeed, the same result is obtained for all the $N(N-1)$ pairs of electrons of the system. The final expression can be written inserting Eq. A.8 into Eq. A.6,

$$E_2 = \frac{1}{2}\sum_{m\neq q}^{N}\left[\frac{1}{N(N-1)}\sum_{kl}^{N}(J_{kl}-K_{kl})\right] = \frac{1}{2}\sum_{kl}^{N}(J_{kl}-K_{kl}). \tag{A.9}$$

Finally, the energy of a single SD in a system with N electrons can be written as a sum of Eq. A.5 and A.9 plus the nuclear energy:

$$\langle\Psi|\hat{H}|\Psi\rangle = \sum_{i}^{N}h_{ii} + \frac{1}{2}\sum_{i,j}^{N}(J_{ij}-K_{ij}) + E_{nuc}, \tag{A.10}$$

where the indices k and l are replaced by the more conventional i and j. Further, the last term is trivially obtained since no dependence on electronic coordinates is shown (i.e. $\langle\Psi|\hat{V}_{nuc}|\Psi\rangle = E_{nuc}\langle\Psi|\Psi\rangle = E_{nuc}$) and can be added as a constant.

Appendix B

Variational Principle

In the HF method, the orbitals are optimized by the variational principle, which gives the best set of orbitals. This principle guarantees that any approximate wave function provides an upper bound to the exact ground state energy, E_{exact}. Let us assume that we have an approximate wave function, Φ, of the unknown exact solution, Ψ. This can be easily demonstrated.

Proof. The energy of an approximate wave function can be written as an expectation value of the Hamiltonian operator:

$$E = \langle \Phi | \hat{H} | \Phi \rangle, \tag{B.1}$$

where a normalized wave function is assumed. Then the variational principle would state:

$$\langle \Psi | \hat{H} | \Psi \rangle = E_{exact} \leq \langle \Phi | \hat{H} | \Phi \rangle, \tag{B.2}$$

which holds for any $|\Phi\rangle$. Let us assume that we have the full set of eigenfunctions of the electronic Schrödinger equation, $\hat{H}|\Phi_i\rangle = E_i|\Phi_i\rangle$, that is the solutions for every electronic state $i = 1, 2, ..., \infty$. We can then write the total wave function $|\Phi\rangle$ as a linear combination of this orthonormal basis. The latter can be orthonormal because the eigenfunctions of an hermitian operator are orthogonal, and the normalization can be explicitly guaranteed:

$$\langle \Phi_i | \Phi_j \rangle = \delta_{ij}. \tag{B.3}$$

Thus, the total wave function $|\Phi\rangle$ can be expressed as a linear combination of the eigenfunctions of $\hat{H}$ without introducing any approximation:

$$|\Phi\rangle = \sum_{i}^{\infty} C_i |\Phi_i\rangle, \quad \sum_{i}^{\infty} |C_i|^2 = 1. \tag{B.4}$$

The expansion coefficients, C_i, are the variational parameters, whose minimization would give the best estimate for the energy. If we now evaluate the energy (Eq. B.1) using the eigendecomposition of $|\Phi\rangle$ (Eq. B.4),

$$\begin{aligned} E &= \langle\Phi|\hat{H}|\Phi\rangle \\ &= \sum_{ij} C_i^* C_j \langle\Phi_i|\hat{H}|\Phi_j\rangle \\ &= \sum_{ij} C_i^* C_j E_j \delta_{ij} \\ &= \sum_{i} |C_i|^2 E_i \\ &= \sum_{i} |C_i|^2 E_i \geq \sum_{i} |C_i|^2 E_{exact} = E_{exact} \end{aligned} \tag{B.5}$$

□

Appendix C

Normal ordered second quantized operators (Wick's theorem)

The computation of the different integrals involved in the expectation values, such as the energy, is an important aspect of QC calculations. In second quantization an expectation value can be evaluated with respect to the vacuum state. However, every matrix element involving any other determinant can also be written as a vacuum expectation value:

$$\langle\psi_p|\hat{A}|\psi_q\rangle = \langle|a_p\hat{A}a_q^\dagger|\rangle,^{\text{a}} \tag{C.1}$$

given that $\hat{A}$ is any arbitrary second quantized operator composed by a string of annihilation/creation operators. A convenient way to compute these matrix elements is making use of normal ordered operators. Normal ordering is a useful tool of second quantization to make mathematical analysis less arduous. Indeed, matrix elements can give rise to many possible terms and tedious calculations. Instead, the vacuum expectation value of a normal ordered operator provides information about the only non-zero terms contained in the equation.

A normal ordered string is defined as one where *all the annihilation operators stand to the right of all creation operators*. Conventionally, curly brackets indicate a normal ordered form to be assigned. For example,

$$\{a_p a_q^\dagger\} = -a_q^\dagger a_p \quad ; \quad \{a_p^\dagger a_q\} = a_p^\dagger a_q, \tag{C.2}$$

where the sign changes since an odd number of permutations takes place to reorder the pair and the second pair is the same because already normal ordered. Any second quantized operator can simply be turned into a normal ordered by applying the

[a] The annihilation operator a_p is the Hermitian conjugate of the creation operator $a_p^\dagger$: $\langle\psi_p| = \langle|a_p = (a_p^\dagger|\rangle)^\dagger = (|\psi_p\rangle)^\dagger$

anticommutation relations shown in Eq. 2.5-2.7. However, another valid option is given by the Wick's theorem.

The Wick's theorem provides a recipe to get a linear combination of normal ordered strings as a result of all the possible pairwise contractions between annihilation/creation operators. A contraction is simply the initial order of the operator pair minus the normal ordered version of it, e.g. $\overbracket{AB} = AB - \{AB\}$. Four possible pairs can be obtained out of two second quantization operators. For example, let us consider the only pair whose contraction is not zero:

$$\overbracket{a_p a_q^\dagger} = a_p a_q^\dagger - \{a_p a_q^\dagger\} = a_p a_q^\dagger + a_q^\dagger a_p = \delta_{pq}. \tag{C.3}$$

While the other three possible pairs, $a_p a_q$, $a_p^\dagger a_q^\dagger$ and $a_p^\dagger a_q$, give all a contraction equal to zero because already normal ordered.

As already presented in Eq. C.1, any matrix element can be written as an expectation value in the true vacuum state. It can be shown that Wick's theorem provide the only non-zero contributions given by a vacuum expectation value of a normal ordered operator. For example, let us consider an arbitrary string of annihilation/creation operators, $\hat{A} = a_p a_q^\dagger a_r a_s^\dagger$. The non-zero contractions arising from the Wick's theorem can be written as:

$$\begin{aligned}\hat{A} &= \{a_p a_q^\dagger a_r a_s^\dagger\} + \{\overbracket{a_p a_q^\dagger} a_r a_s^\dagger\} + \{\overbracket{a_p a_q^\dagger a_r a_s^\dagger}\} + \{a_p a_q^\dagger \overbracket{a_r a_s^\dagger}\} + \{\overbracket{a_p a_q^\dagger}\overbracket{a_r a_s^\dagger}\} \\ &= \{a_p a_q^\dagger a_r a_s^\dagger\} + \delta_{pq}\{a_r a_s^\dagger\} + \delta_{ps}\{a_q^\dagger a_r\} + \delta_{rs}\{a_p a_q^\dagger\} + \delta_{pq}\delta_{rs} \\ &= a_q^\dagger a_s^\dagger a_p a_r - \delta_{pq} a_s^\dagger a_r + \delta_{ps} a_q^\dagger a_r - \delta_{rs} a_q^\dagger a_p + \delta_{pq}\delta_{rs}. \end{aligned} \tag{C.4}$$

It is evident to see how all the strings in the final line are all normal ordered. However, only the last term would give a non-zero contribution in a vacuum expectation value,

$$\langle|\hat{A}|\rangle = \delta_{pq}\delta_{rs}. \tag{C.5}$$

Indeed, all the other terms would be zero following by Eq. 2.9. Such a result allows to generalize that only the fully contracted terms give a non-zero matrix element.

However, in QC it is not convenient to work with expectation values in the true vaccum state, but rather with the N-electrons reference determinant $|\Phi_0\rangle$. For this reason, the particle-hole formalism is introduced. This formalism is based on the definitions of *particle* and *hole* states, which respectively refer to the presence of electrons in the unoccupied orbitals in $|\Phi_0\rangle$ and to the absence of electrons in those

occupied in $|\Phi_0\rangle$. In this picture, the HF reference determinant (also called the Fermi vacuum) can be seen as a vacuum where there are no particles and no holes.

In the particle-hole formalism the pairwise contractions change according to the considered orbital. Before, the second quantized operators were defined by their ability to create or remove a specific spin orbital in a SD. Now, the creation/annihilation operators are defined as *quasiparticle* (q) construction operators. The q-annihilation operators are determined as those that annihilate holes ($a_i^\dagger$) and particles (a_a). And, the q-creation operators are those that create holes (a_i) and particles ($a_a^\dagger$). The indices for occupied $(i, j, k, ...)$ and unoccupied $(a, b, c, ...)$ spin orbitals are used. The normal ordered string is now given by *all the q-annihilation operators standing to the right of all q-creation operators*. The only non-zero contractions are:

$$\overbrace{a_i^\dagger a_j} = a_i^\dagger a_j - \{a_i^\dagger a_j\} = a_i^\dagger a_j + a_j a_i^\dagger = \delta_{ij}, \tag{C.6}$$

$$\overbrace{a_a a_b^\dagger} = a_a a_b^\dagger - \{a_a a_b^\dagger\} = a_a a_b^\dagger + a_b^\dagger a_a = \delta_{ab}. \tag{C.7}$$

While every other possible pair gives a zero contraction, e.g. $\overbrace{a_a^\dagger a_b} = \overbrace{a_i a_j^\dagger} = 0$. Thus, the particle-hole definition changes only slightly the second quantization formalism, turning the roles of the operators in the occupied space, while leaving untouched those operating in the unoccupied space (see similarity Eq. C.3 and Eq. C.7). Further, a more general version of the Wick's theorem is also available, where one can evaluate the contractions between normal ordered strings.

$$\{ABC\ldots\}\{XYZ\ldots\} = \{ABC\ldots XYZ\ldots\} + \sum_{\substack{\text{single}\\ \text{contractions}}} \{\overbrace{ABC\ldots XYZ}\ldots\} +$$

$$\sum_{\substack{\text{double}\\ \text{contractions}}} \{\overbrace{ABC\ldots XYZ}\ldots\} + \sum_{\substack{\text{triple}\\ \text{contractions}}} \{\overbrace{ABC\ldots XYZ}\ldots\} + \ldots \tag{C.8}$$

where the intersection of the contraction lines over the second quantization operators gives the sign to the term (i.e. an odd number of crossings gives a minus sign, while an even number gives a plus sign). Such a version is useful to calculate the non-zero expectation value arising from the products of operators strings, such as shown in section 2.2.1. And, together with the particle-hole formalism allows to obtain a matrix element relative to the reference determinant rather than to the vacuum state.

Bibliography

[1] W. Heisenberg. “Kapitel 5 - Die Quantenmechanik und ein Gespräch mit Einstein (1925-1926)”. In: *Der Teil und das Ganze - Gespräche im Umkreis der Atomphysik*. Ed. by R. P. und Co. Verlag. 1969.

[2] W. Heisenberg. “Chapter 5 - Quantum Mechanics and a Talk with Einstein (1925-1926)”. In: *Physics and Beyond - Encounters and Conversations*. Ed. by P. Harper & Row. 1971.

[3] W. Heisenberg. “Über quantentheoretische Umdeutung kinematischer und mechanischer Beziehungen”. In: *Z. Phys.* 33 (1925), pp. 879–893. DOI: 10.1007/BF01328377.

[4] M. Planck. “Über Das Gesetz Der Energieverteilung Im Normalspectrum”. In: *Ann. Phys.* 309.3 (1901), pp. 553–563. DOI: 10.1002/andp.19013090310.

[5] A. Einstein. “Über einem die Erzeugung und Verwandlung des Lichtes betreffenden heuristischen Gesichtspunkt”. In: *Ann. Phys.* 4 (1905), pp. 132–148.

[6] E. Rutherford. “The scattering of α and β particles by matter and the structure of the atom”. In: *Phil. Mag.* 92.4 (1911), pp. 379–398. DOI: 10.1080/14786435.2011.617037.

[7] E. Rutherford. “LVII. The structure of the atom”. In: *Lond. Edinb. Dubl. Phil. Mag.* 27.159 (1914), pp. 488–498. DOI: 10.1080/14786440308635117.

[8] N. Bohr. “I. On the constitution of atoms and molecules”. In: *Lond. Edinb. Dubl. Phil. Mag.* 26.151 (1913), pp. 1–25. DOI: 10.1080/14786441308634955.

[9] N. Bohr. “II. Systems containing only a Single Nucleus”. In: *Lond. Edinb. Dubl. Phil. Mag.* 26.151 (1913), p. 476.

[10] N. Bohr. “The Spectra of Helium and Hydrogen”. In: *Nature* 92 (1913), pp. 231–232. DOI: 10.1038/092231d0.

[11] M. Born, W. Heisenberg, and P. Jordan. “Zur Quantenmechanik. II.” In: *Z. Phys.* 35 (1926), pp. 557–615. DOI: 10.1007/BF01379806.

[12] P. A. M. Dirac and R. H. Fowler. "The fundamental equations of quantum mechanics". In: *Proc. Roy. Soc. London A* 109.752 (1925), pp. 642–653. DOI: 10.1098/rspa.1925.0150.

[13] W. Pauli. "Über das Wasserstoffspektrum vom Standpunkt der neuen Quantenmechanik". In: *Z. Phys.* 36 (1926), pp. 336–363. DOI: 10.1007/BF01450175.

[14] N. Bohr. "Part I. On the general theory". In: *On the quantum theory of line-spectra*. Ed. by I. Dover Publications. 1918.

[15] E. Schrödinger. "An Undulatory Theory of the Mechanics of Atoms and Molecules". In: *Phys. Rev.* 28.6 (1926), pp. 1049–1070. DOI: 10.1103/PhysRev.28.1049.

[16] L. de Broglie. "Recherches sur la théorie des Quanta". In: *Ann. Phys.* 3.22 (1925). DOI: 10.1119/1.10583.

[17] D. C. Mattis. In: *The Many-Body Problem: An Encyclopedia of Exactly Solved Models in One Dimension*. Ed. by W. Scientific. 1993.

[18] M. Born and R. Oppenheimer. "Zur Quantentheorie der Molekeln". In: *Ann. Phys.* 389.20 (1927), pp. 457–484. DOI: 10.1002/andp.19273892002.

[19] D. R. Hartree. "The Wave Mechanics of an Atom with a Non-Coulomb Central Field. Part I. Theory and Methods". In: *Math. Proc. Camb. Philos. Soc.* 24.1 (1928), pp. 89–110. DOI: 10.1017/S0305004100011919.

[20] D. R. Hartree. "The Wave Mechanics of an Atom with a Non-Coulomb Central Field. Part II. Some Results and Discussion". In: *Math. Proc. Camb. Philos. Soc.* 24.1 (1928), pp. 111–132. DOI: 10.1017/S0305004100011920.

[21] V. Fock. "Näherungsmethode zur Lösung des quantenmechanischen Mehrkörperproblems". In: *Z. Phys.* 61.1-2 (1930), pp. 126–148. DOI: 10.1007/BF01340294.

[22] J. C. Slater. "Note on Hartree's Method". In: *Phys. Rev.* 35 (2 1930), pp. 210–211. DOI: 10.1103/PhysRev.35.210.2.

[23] W. Heitler and F. London. "Wechselwirkung neutraler Atome und homöopolare Bindung nach der Quantenmechanik". In: *Z. Phys.* 44.6-7 (1927), pp. 455–472. DOI: 10.1007/BF01397394.

[24] T. Helgaker, P. Jørgensen, and J. Olsen. "Chapter 11 - Configuration-Interaction Theory". In: *Molecular Electronic-Structure Theory*. John Wiley & Sons, 2014. DOI: 10.1063/1.1445550.

[25] J. Čížek. "On the Correlation Problem in Atomic and Molecular Systems. Calculation of Wavefunction Components in Ursell-Type Expansion Using Quantum-Field Theoretical Methods". In: *J. Chem. Phys.* 45 (1966), p. 4256. DOI: 10.1063/1.1727484.

[26] J. Čížek. "On the Use of the Cluster Expansion and the Technique of Diagrams in Calculations of Correlation Effects in Atoms and Molecules". In: *Adv. Chem. Phys.* 14 (1969), p. 35. DOI: 10.1002/9780470143599.ch2.

[27] J. Čížek and J. Paldus. "Correlation problems in atomic and molecular systems. III. Rederivation of the coupled-pair many-electron theory using the traditional quantum chemical methods". In: *Int. J. Quantum Chem.* 5 (1971), p. 359. DOI: 10.1002/qua.560050402.

[28] J. Paldus, J. Čížek, and I. Shavitt. "Correlation Problems in Atomic and Molecular Systems. IV. Extended Coupled-Pair Many-Electron Theory and Its Application to the BH_3 Molecule". In: *Phys. Rev. A* 5 (1 1972), pp. 50–67. DOI: 10.1103/PhysRevA.5.50.

[29] K. Raghavachari, G. W. Trucks, J. A. Pople, and M. Head-Gordon. "A fifth-order perturbation comparison of electron correlation theories". In: *Chem. Phys. Lett.* 157.6 (1989), pp. 479–483. ISSN: 0009-2614. DOI: https://doi.org/10.1016/S0009-2614(89)87395-6.

[30] B. O. Roos, P. R. Taylor, and P. E. M. Siegbahn. "A complete active space SCF method (CASSCF) using a density matrix formulated super-CI approach". In: *Chem. Phys.* 48.2 (1980), pp. 157–173. DOI: 10.1016/0301-0104(80)80045-0.

[31] B. O. Roos. "The complete active space SCF method in a fock-matrix-based super-CI formulation". In: *Int. J. Quantum Chem.* 18.S14 (1980), pp. 175–189. DOI: https://doi.org/10.1002/qua.560180822.

[32] P. Siegbahn, A. Heiberg, B. O. Roos, and B. Levy. "A Comparison of the Super-CI and the Newton-Raphson Scheme in the Complete Active Space SCF Method". In: *Physica Scripta* 21.3-4 (1980), pp. 323–327. DOI: 10.1088/0031-8949/21/3-4/014.

[33] H.-J. Werner and W. Meyer. "A quadratically convergent multiconfiguration-self-consistent field method with simultaneous optimization of orbitals and CI coefficients". In: *J. Chem. Phys.* 73.5 (1980), pp. 2342–2356. DOI: 10.1063/1.440384.

[34] P. E. M. Siegbahn, J. Almlöf, A. Heiberg, and B. O. Roos. "The complete active space SCF (CASSCF) method in a Newton-Raphson formulation with application to the HNO molecule". In: *J. Chem. Phys.* 74.4 (1981), pp. 2384–2396. DOI: 10.1063/1.441359.

[35] S. R. White. "Density matrix formulation for quantum renormalization groups". In: *Phys. Rev. Lett.* 69 (19 1992), pp. 2863–2866. DOI: 10.1103/PhysRevLett.69.2863.

[36] S. R. White. "Density-matrix algorithms for quantum renormalization groups". In: *Phys. Rev. B* 48 (14 1993), pp. 10345–10356. DOI: 10.1103/PhysRevB.48.10345.

[37] S. R. White and R. L. Martin. "Ab initio quantum chemistry using the density matrix renormalization group". In: *J. Chem. Phys.* 110.9 (1999), pp. 4127–4130. DOI: 10.1063/1.478295.

[38] G. K.-L. Chan and D. Zgid. "Chapter 7 - The Density Matrix Renormalization Group in Quantum Chemistry". In: ed. by R. A. Wheeler. Vol. 5. Annual Reports in Computational Chemistry. Elsevier, 2009, pp. 149–162. DOI: https://doi.org/10.1016/S1574-1400(09)00507-6.

[39] G. K.-L. Chan and S. Sharma. "The Density Matrix Renormalization Group in Quantum Chemistry". In: *Annu. Rev. Phys. Chem.* 62.1 (2011), pp. 465–481. DOI: 10.1146/annurev-physchem-032210-103338.

[40] K. H. Marti and M. Reiher. "The Density Matrix Renormalization Group Algorithm in Quantum Chemistry". In: *Progress in Physical Chemistry Volume 3: Modern and Universal First-principles Methods for Many-electron Systems in Chemistry and Physics*. Ed. by F. M. Dolg. Oldenbourg Wissenschaftsverlag, 2011, pp. 293–309. DOI: 10.1524/9783486711639.293.

[41] L. Freitag and M. Reiher. "Chapter 7 - The density matrix renormalization group for strong correlation in ground and excited states". In: *Quantum Chemistry and Dynamics of Excited States: Methods and Applications*. Ed. by L. González and R. Lindh. Vol. 1. John Wiley & Sons, 2020, p. 205. DOI: https://doi.org/10.1016/S1574-1400(09)00507-6.

[42] G. Booth, A. Thom, and A. Alavi. "Fermion monte carlo without fixed nodes: A game of life, death, and annihilation in slater determinant space". In: *J. Chem. Phys.* 131 (2009), p. 054106. DOI: 10.1063/1.3193710.

[43] D. Cleland, G. H. Booth, and A. Alavi. "Communications: Survival of the fittest: Accelerating convergence in full configuration-interaction quantum Monte Carlo". In: *J. Chem. Phys.* 132.4 (2010), p. 041103. DOI: 10.1063/1.3302277.

[44] C. Overy, G. Booth, N. S. Blunt, J. Shepherd, D. Cleland, and A. Alavi. "Unbiased reduced density matrices and electronic properties from full configuration interaction quantum Monte Carlo". In: *J. Chem. Phys.* 141 (2015), p. 244117. DOI: 10.1063/1.4904313.

[45] G. Booth, S. D. Smart, and A. Alavi. "Linear-scaling and parallelizable algorithms for stochastic quantum chemistry". In: *Mol. Phys.* 112 (2014), pp. 1855–1869. DOI: 10.1080/00268976.2013.877165.

[46] T. Jiang, Y. Chen, N. A. Bogdanov, E. Wang, A. Alavi, and J. Chen. "A full configuration interaction quantum Monte Carlo study of ScO, TiO, and VO molecules". In: *J. Chem. Phys.* 154.16 (2021), p. 164302. DOI: 10.1063/5.0046464.

[47] D. Zgid and M. Nooijen. "The density matrix renormalization group self-consistent field method: Orbital optimization with the density matrix renormalization group method in the active space". In: *J. Chem. Phys.* 128.14 (2008), p. 144116. DOI: 10.1063/1.2883981.

[48] S. Wouters, T. Bogaerts, P. Van Der Voort, V. Van Speybroeck, and D. Van Neck. "Communication: DMRG-SCF study of the singlet, triplet, and quintet states of oxo-Mn(Salen)". In: *J. Chem. Phys.* 140.24 (2014), p. 241103. DOI: 10.1063/1.4885815.

[49] S. Wouters, W. Poelmans, S. De Baerdemacker, P. W. Ayers, and D. Van Neck. "CheMPS2: Improved DMRG-SCF routine and correlation functions". In: *Comput. Phys. Commun.* 191 (2015), pp. 235–237. ISSN: 0010-4655. DOI: https://doi.org/10.1016/j.cpc.2015.01.007.

[50] G. Li Manni, S. D. Smart, and A. Alavi. "Combining the Complete Active Space Self-Consistent Field Method and the Full Configuration Interaction Quantum Monte Carlo within a Super-CI Framework, with Application to Challenging Metal-Porphyrins". In: *J. Chem. Theory Comput.* 12.3 (2016), pp. 1245–1258. DOI: 10.1021/acs.jctc.5b01190.

[51] J. Paldus. "Externally and internally corrected coupled cluster approaches: an overview". In: *J. Math. Chem.* 55 (2017), pp. 477–502. DOI: 10.1007/s10910-016-0688-6.

[52] K. Jankowski and J. Paldus. "Applicability of coupled-pair theories to quasidegenerate electronic states: A model study". In: *Int. J. Quantum Chem.* 18.5 (1980), pp. 1243–1269. DOI: https://doi.org/10.1002/qua.560180511.

[53] R. A.Chiles and C. E.Dykstra. "An efficient and accurate approximation to double substitution coupled cluster wavefunctions". In: *Chem. Phys. Lett.* 80 (1981), pp. 69–72. DOI: 10.1016/0009-2614(81)80059-0.

[54] J. Paldus, J. Čížek, and M. Takahashi. "Approximate account of the connected quadruply excited clusters in the coupled-pair many-electron theory". In: *Phys. Rev. A* 30 (5 1984), pp. 2193–2209. DOI: 10.1103/PhysRevA.30.2193.

[55] J. Paldus, M. Takahashi, and R. W. H. Cho. "Coupled-cluster approach to electron correlation in one dimension: Cyclic polyene model in delocalized basis". In: *Phys. Rev. B* 30 (1984), p. 4267. DOI: 10.1103/PhysRevB.30.4267.

[56] P. Piecuch and J. Paldus. "On the solution of coupled-cluster equations in the fully correlated limit of cyclic polyene model". In: *Int. J. Quantum Chem.* 40.S25 (1991), pp. 9–34. DOI: 10.1002/qua.560400807.

[57] P. Piecuch, R. Tobola, and J. Paldus. "Approximate account of connected quadruply excited clusters in single-reference coupled-cluster theory via cluster analysis of the projected unrestricted Hartree-Fock wave function". In: *Phys. Rev. A* 54.2 (1996), pp. 1210–1241. DOI: 10.1103/PhysRevA.54.1210. URL: http://link.aps.org/doi/10.1103/PhysRevA.54.1210.

[58] R. J. Bartlett and M. Musiał. "Addition by subtraction in coupled-cluster theory: A reconsideration of the CC and CI interface and the nCC hierarchy". In: *J. Chem. Phys.* 125.20 (2006), p. 204105. ISSN: 00219606. DOI: 10.1063/1.2387952.

[59] L. M. J. Huntington and M. Nooijen. "pCCSD: Parameterized coupled-cluster theory with single and double excitations". In: *J. Chem. Phys.* 133.18 (2010), p. 184109. DOI: doi:10.1063/1.3494113.

[60] J. B. Robinson and P. J. Knowles. "Quasi-variational coupled cluster theory". In: *J. Chem. Phys.* 136 (2012), p. 054114. DOI: 10.1063/1.3680560.

[61] D. Kats and F. R. Manby. "Communication: The distinguishable cluster approximation". In: *J. Chem. Phys.* 139 (2013), p. 021102. DOI: 10.1063/1.4813481.

[62] D. Kats. "Communication: The distinguishable cluster approximation. II. The role of orbital relaxation". In: *J. Chem. Phys.* 141 (2014), p. 061101. DOI: 10.1063/1.4892792.

[63] D. Kats. "The distinguishable cluster approach from a screened Coulomb formalism". In: *J. Chem. Phys.* 144 (2016), p. 044102. DOI: 10.1063/1.4940398.

[64] D. Kats, D. Kreplin, H. J. Werner, and F. Manby. "Accurate thermochemistry from explicitly correlated distinguishable cluster approximation". In: *J. Chem. Phys.* 142 (2015), p. 064111. DOI: 10.1063/1.4907591.

[65] T. Tsatsoulis, F. Hummel, D. Usvyat, M. Schütz, G. H. Booth, S. S. Binnie, M. J. Gillan, D. Alfé, A. Michaelides, and A. Grüneis. "A comparison between quantum chemistry and quantum Monte Carlo techniques for the adsorption of water on the (001) LiH surface". In: *J. Chem. Phys.* 146.20 (2017), p. 204108. DOI: 10.1063/1.4984048.

[66] M. K. Kesharwani, N. Sylvetsky, and J. M. L. Martin. "Surprising performance for vibrational frequencies of the distinguishable clusters with singles and doubles (DCSD) and MP2.5 approximations". In: *AIP Conf. Proc.* 1906.1 (2017), p. 030005. DOI: 10.1063/1.5012284.

[67] D. G. Khomyakov and Q. K. Timerghazin. "Toward Reliable Modeling of S-Nitrosothiol Chemistry: Structure and Properties of Methyl Thionitrite (CH3SNO), an S-Nitrosocysteine Model". In: *J. Chem. Phys.* 147.4 (2017), p. 044305. ISSN: 0021-9606. DOI: 10.1063/1.4995300.

[68] D. Kats. "Improving the distinguishable cluster results: spin-component scaling". In: *Mol. Phys.* 116 (2018), p. 1435. DOI: 10.1080/00268976.2017.1417646.

[69] J. A. Black and P. J. Knowles. "Statistical Analysis of Activation and Reaction Energies with Quasi-Variational Coupled-Cluster Theory". In: *Mol. Phys.* 116.11 (2018), pp. 1421–1427. ISSN: 0026-8976. DOI: 10.1080/00268976.2017.1400698.

[70] T. Petrenko and G. Rauhut. "Refined Analysis of the $\tilde{X}\,2A2 \leftarrow \tilde{X}\,1A1$ Photoelectron Spectrum of Furan". In: *J. Chem. Phys.* 148.5 (2018), p. 054306. ISSN: 0021-9606. DOI: 10.1063/1.5018928.

[71] P. Piecuch, N. Oliphant, and L. Adamowicz. "A state-selective multireference coupled-cluster theory employing the single-reference formalism". In: *J. Chem. Phys.* 99 (1993), p. 1875. DOI: 10.1063/1.466179.

[72] P. Piecuch and L. Adamowicz. "State-selective multireference coupled-cluster theory employing the single-reference formalism: Implementation and application to the H_8 model system". In: *J. Chem. Phys.* 100 (1994), p. 5792. DOI: 10.1063/1.467143.

[73] J. Paldus and J. Planelles. "Valence bond corrected single reference coupled cluster approach. I. General formalism". In: *Theor. Chim. Acta* 89 (1994), pp. 13–31. DOI: 10.1007/BF01123868.

[74] J. Planelles, J. Paldus, and X. Li. "Valence bond corrected single reference coupled cluster approach. II. Application to PPP model systems". In: *Theor. Chim. Acta* 89 (1994), pp. 33–57. DOI: 0.1007/BF01167280.

[75] X. Li and J. Paldus. "Reduced multireference CCSD method: An effective approach to quasidegenerate states". In: *J. Chem. Phys.* 107.16 (1997), pp. 6257–6269. DOI: 10.1063/1.474289.

[76] X. Li and J. Paldus. "Reduced multireference couple cluster method. II. Application to potential energy surfaces of HF, F2, and H2O". In: *J. Chem. Phys.* 108.2 (1998), pp. 637–648. DOI: 10.1063/1.475425.

[77] G. Peris, J. Planelles, and J. Paldus. "Single-reference CCSD approach employing three- and four-body CAS SCF corrections: A preliminary study of a simple model". In: *Int. J. Quantum Chem.* 62.2 (1997), pp. 137–151. DOI: https://doi.org/10.1002/(SICI)1097-461X(1997)62:2<137::AID-QUA2>3.0.CO;2-X.

[78] X. Li, G. Peris, J. Planelles, F. Rajadall, and J. Paldus. "Externally corrected singles and doubles coupled cluster methods for open-shell systems". In: *J. Chem. Phys.* 107.1 (1997), pp. 90–98. DOI: 10.1063/1.474355.

[79] G. Peris, F. Rajadell, X. Li, J. Planelles, and J. Paldus. "Externally corrected singles and doubles coupled cluster methods for open-shell systems. II. Applications to the low lying doublet states of OH, NH2, CH3 and CN radicals". In: *Mol. Phys.* 94.1 (1998), pp. 235–248. DOI: 10.1080/002689798168529.

[80] T. Kinoshita, O. Hino, and R. J Bartlett. "Coupled-cluster method tailored by configuration interaction". In: *J. Chem. Phys.* 123 (2005), p. 074106. DOI: 10.1063/1.2000251.

[81] L. Veis, A. Antalík, J. Brabec, F. Neese, Ö. Legeza, and J. Pittner. "Coupled Cluster Method with Single and Double Excitations Tailored by Matrix Product State Wave Functions". In: *J. Phys. Chem. Lett.* 7 (2016), p. 4072. DOI: 10.1021/acs.jpclett.6b01908.

[82] L. Veis, A. Antalík, Ö. Legeza, A. Alavi, and J. Pittner. "The Intricate Case of Tetramethyleneethane: A Full Configuration Interaction Quantum Monte Carlo Benchmark and Multireference Coupled Cluster Studies". In: *J. Chem. Theory*

Comput. 14.5 (2018), pp. 2439–2445. ISSN: 1549-9618. DOI: 10.1021/acs.jctc.8b00022.

[83] F. M. Faulstich, M. Máté, A. Laestadius, M. A. Csirik, L. Veis, A. Antalík, J. Brabec, R. Schneider, J. Pittner, S. Kvaal, and Ö. Legeza. "Numerical and Theoretical Aspects of the DMRG-TCC Method Exemplified by the Nitrogen Dimer". In: *J. Chem. Theory Comput.* 15.4 (2019), pp. 2206–2220. ISSN: 1549-9618. DOI: 10.1021/acs.jctc.8b00960.

[84] K. Ghanem, A. Y. Lozovoi, and A. Alavi. "Unbiasing the Initiator Approximation in Full Configuration Interaction Quantum Monte Carlo". In: *J. Chem. Phys.* 151.22 (2019), p. 224108. ISSN: 0021-9606. DOI: 10.1063/1.5134006.

[85] H. Shull and G. Hall. "Atomic Units". In: *Nature* 184 (1959), pp. 1559–1560. DOI: 10.1038/1841559a0.

[86] W. Pauli. "Über den Zusammenhang des Abschlusses der Elektronengruppen im Atom mit der Komplexstruktur der Spektren". In: *Z. Phys.* 31.1 (1925), pp. 765–783.

[87] C. C. J. Roothaan. "New Developments in Molecular Orbital Theory". In: *Rev. Mod. Phys.* 23 (2 1951), pp. 69–89. DOI: 10.1103/RevModPhys.23.69.

[88] G. Hall. "The molecular orbital theory of chemical valency VIII. A method of calculating ionization potentials". In: *Proc. Roy. Soc. London A* 205.1083 (1951), pp. 541–552.

[89] F. Coester. "Bound states of a many-particle system". In: *Nucl. Phys.* 7 (1958), pp. 421–424. ISSN: 0029-5582. DOI: https://doi.org/10.1016/0029-5582(58)90280-3.

[90] F. Coester and H. Kümmel. "Short-range correlations in nuclear wave functions". In: *Nucl. Phys.* 17 (1960), pp. 477–485. ISSN: 0029-5582. DOI: https://doi.org/10.1016/0029-5582(60)90140-1.

[91] H. G. Kümmel. "A Biography of the Coupled Cluster method". In: *Int. J. Mod. Phys. B* 17.28 (2003), pp. 5311–5325. DOI: 10.1142/S0217979203020442.

[92] A. C. Hurley. In: *Electron correlation in small molecules*. Acad. Press, London, 1976.

[93] J. Pople, R. Krishnan, H. Schlegel, and J. Binkley. "Electron correlation theories and their application to the study of simple reaction potential surfaces". In: *Int. J. Quantum Chem.* 14.5 (1978), pp. 545–560. DOI: https://doi.org/10.1002/qua.560140503.

[94] R. J. Bartlett and G. D. Purvis. "Many-body perturbation theory, coupled-pair many-electron theory, and the importance of quadruple excitations for the correlation problem". In: *Int. J. Quantum Chem.* 14.5 (1978), pp. 561–581. DOI: https://doi.org/10.1002/qua.560140504.

[95] G. D. Purvis and R. J. Bartlett. "A full coupled cluster singles and doubles model: The inclusion of disconnected triples". In: *J. Chem. Phys.* 76.4 (1982), pp. 1910–1918. DOI: 10.1063/1.443164.

[96] J. C. Slater. "The Theory of Complex Spectra". In: *Phys. Rev.* 34 (10 1929), pp. 1293–1322. DOI: 10.1103/PhysRev.34.1293.

[97] E. U. Condon. "The Theory of Complex Spectra". In: *Phys. Rev.* 36 (7 1930), pp. 1121–1133. DOI: 10.1103/PhysRev.36.1121.

[98] B. H. Brandow. "Linked-cluster expansions for the nuclear many-body problem". In: *Rev. Mod. Phys.* 39.4 (1967), p. 771. DOI: https://doi.org/10.1103/RevModPhys.39.771.

[99] S. A. Kucharski and R. J. Bartlett. "Fifth-Order Many-Body Perturbation Theory and Its Relationship to Various Coupled-Cluster Approaches". In: Advances in Quantum Chemistry 18 (1986), pp. 281–344. DOI: https://doi.org/10.1016/S0065-3276(08)60051-9.

[100] R. J. Bartlett and M. Musiał. "Coupled-cluster theory in quantum chemistry". In: *Rev. Mod. Phys.* 79 (1 2007), pp. 291–352. DOI: 10.1103/RevModPhys.79.291.

[101] D. A. Matthews and J. F. Stanton. "Chapter 10 - Diagrams in coupled-cluster theory". In: *Mathematical Physics in Theoretical Chemistry*. Elsevier Inc., 2019, pp. 327–376.

[102] T. D. Crawford and H. F. Schaefer. "Chapter 2 - An introduction to coupled cluster theory for computational chemists". In: *Reviews in Computational Chemistry, Volume 14*. Vol. 14. Wiley, 1999, 2000, pp. 33–136.

[103] B. Adams, K. Jankowski, and J. Paldus. "Quasi-degeneracy and coupled-pair theories". In: Chem. Phys. Lett. 67 (1979), p. 144. DOI: 10.1016/0009-2614(79)87124-9.

[104] L. M. J. Huntington, A. Hansen, F. Neese, and M. Nooijen. "Accurate thermochemistry from a parameterized coupled-cluster singles and doubles model and a local pair natural orbital based implementation for applications to larger systems". In: *J. Chem. Phys.* 136.6 (2012), p. 064101. DOI: 10.1063/1.3682325.

[105] D. Kats. "Particle-hole symmetry in many-body theories of electron correlation". In: *Mol. Phys.* 116 (2018), p. 1496. DOI: 10.1080/00268976.2018.1448947.

[106] N. Metropolis and S. Ulam. "The Monte Carlo method". In: *J. Am. Stat. Assoc.* 44.247 (1949), pp. 335–341. DOI: https://doi.org/10.1080/01621459.1949.10483310.

[107] D. P. Kroese, T. Brereton, T. Taimre, and Z. I. Botev. "Why the Monte Carlo method is so important today". In: *WIREs Comput. Stat.* 6.6 (2014), pp. 386–392. DOI: https://doi.org/10.1002/wics.1314.

[108] K. Guther, R. J. Anderson, N. S. Blunt, N. A. Bogdanov, D. Cleland, N. Dattani, W. Dobrautz, K. Ghanem, P. Jeszenszki, N. Liebermann, G. L. Manni, A. Y. Lozovoi, H. Luo, D. Ma, F. Merz, C. Overy, M. Rampp, P. K. Samanta, L. R. Schwarz, J. J. Shepherd, S. D. Smart, E. Vitale, O. Weser, G. H. Booth, and A. Alavi. "NECI: N-Electron Configuration Interaction with an emphasis on state-of-the-art stochastic methods". In: *J. Chem. Phys.* 153.3 (2020), p. 034107. DOI: 10.1063/5.0005754.

[109] J. S. Spencer, N. S. Blunt, and W. M. Foulkes. "The sign problem and population dynamics in the full configuration interaction quantum Monte Carlo method". In: *J. Chem. Phys.* 136.5 (2012), p. 054110. DOI: 10.1063/1.3681396.

[110] D. Cleland, G. H. Booth, and A. Alavi. "A study of electron affinities using the initiator approach to full configuration interaction quantum Monte Carlo". In: *J. Chem. Phys.* 134 (2011), p. 024112. DOI: 10.1063/1.3525712.

[111] F. R. Petruzielo, A. A. Holmes, H. J. Changlani, M. P. Nightingale, and C. J. Umrigar. "Semistochastic projector monte carlo method". In: *Phys. Rev. Lett.* 109 (2012), p. 230201. DOI: 10.1103/PhysRevLett.109.230201.

[112] N. S. Blunt, S. D. Smart, J. A. F. Kersten, J. S. Spencer, G. H. Booth, and A. Alavi. "Semi-stochastic full configuration interaction quantum Monte Carlo: Developments and application". In: *J. Chem. Phys.* 142 (2015), p. 184107. DOI: 10.1063/1.4920975.

[113] T. Helgaker, P. Jørgensen, and J. Olsen. "Chapter 12 - Multiconfigurational Self-Consistent Field Theory". In: *Molecular Electronic-Structure Theory*. John Wiley & Sons, Ltd, 2000. Chap. 12, pp. 598–647. DOI: https://doi.org/10.1002/9781119019572.ch12.

[114] J. Olsen, B. O. Roos, P. Jörgensen, and H. J. A. Jensen. "Determinant based configuration interaction algorithms for complete and restricted configuration interaction spaces". In: *J. Chem. Phys.* 89.4 (1988), pp. 2185–2192. DOI: 10.1063/1.455063.

[115] D. Ma, G. Li Manni, and L. Gagliardi. "The generalized active space concept in multiconfigurational self-consistent field methods". In: *J. Chem. Phys.* 135.4 (2011), p. 044128. DOI: 10.1063/1.3611401.

[116] K. Andersson, P. Malmqvist, B. Roos, A. J. Sadlej, and K. Woliński. "Second-order perturbation theory with a CASSCF reference function". In: *J. Phys. Chem.* 94 (1990), pp. 5483–5488. DOI: 10.1021/J100377A012.

[117] K. Andersson, P.-Å. Malmqvist, and B. O. Roos. "Second-order perturbation theory with a complete active space self-consistent field reference function". In: *J. Chem. Phys.* 96.2 (1992), pp. 1218–1226. DOI: 10.1063/1.462209.

[118] H. Werner and P. J. Knowles. "An efficient internally contracted multiconfiguration-reference configuration interaction method". In: *J. Chem. Phys.* 89.9 (1988), pp. 5803–5814. DOI: 10.1063/1.455556.

[119] G. Li Manni, R. K. Carlson, S. Luo, D. Ma, J. Olsen, D. G. Truhlar, and L. Gagliardi. "Multiconfiguration Pair-Density Functional Theory". In: *J. Chem. Theory Comput.* 10.9 (2014), pp. 3669–3680. DOI: 10.1021/ct500483t.

[120] P.-O. Löwdin. "Quantum Theory of Many-Particle Systems. I. Physical Interpretations by Means of Density Matrices, Natural Spin-Orbitals, and Convergence Problems in the Method of Configurational Interaction". In: *Phys. Rev.* 97 (6 1955), pp. 1474–1489. DOI: 10.1103/PhysRev.97.1474.

[121] T. Helgaker, P. Jørgensen, and J. Olsen. "Chapter 13 - Coupled-Cluster Theory". In: *Molecular Electronic-Structure Theory*. John Wiley & Sons, 2000, pp. 648–723. DOI: https://doi.org/10.1002/9781119019572.ch13.

[122] T. Helgaker and P. Jørgensen. "Configuration-interaction energy derivatives in a fully variational formulation". In: *Theor. Chim. Acta* 75 (1989), 111–127. DOI: 10.1007/BF00527713.

[123] H.-J. Werner, P. J. Knowles, G. Knizia, F. R. Manby, M. Schütz, P. Celani, W. Györffy, D. Kats, T. Korona, R. Lindh, A. Mitrushenkov, G. Rauhut, K. R. Shamasundar, T. B. Adler, R. D. Amos, S. J. Bennie, A. Bernhardsson, A. Berning, D. L. Cooper, M. J. O. Deegan, A. J. Dobbyn, F. Eckert, E. Goll, C. Hampel, A. Hesselmann, G. Hetzer, T. Hrenar, G. Jansen, C. Köppl, S. J. R.

Lee, Y. Liu, A. W. Lloyd, Q. Ma, R. A. Mata, A. J. May, S. J. McNicholas, W. Meyer, T. F. Miller III, M. E. Mura, A. Nicklass, D. P. O'Neill, P. Palmieri, D. Peng, K. Pflüger, R. Pitzer, M. Reiher, T. Shiozaki, H. Stoll, A. J. Stone, R. Tarroni, T. Thorsteinsson, M. Wang, and M. Welborn. *MOLPRO, version 2019.2, a package of ab initio programs*. see https://www.molpro.net. Cardiff, UK, 2019.

[124] H.-J. Werner, P. J. Knowles, G. Knizia, F. R. Manby, and M. Schütz. "Molpro: a general-purpose quantum chemistry program package". In: *WIREs Comput. Mol. Sci.* 2 (2012), pp. 242–253. DOI: 10.1002/wcms.82.

[125] H.-J. Werner, P. J. Knowles, F. R. Manby, J. A. Black, K. Doll, A. Heßelmann, D. Kats, A. Köhn, T. Korona, D. A. Kreplin, Q. Ma, T. F. Miller, A. Mitrushchenkov, K. A. Peterson, I. Polyak, G. Rauhut, and M. Sibaev. "The Molpro Quantum Chemistry Package". In: *J. Chem. Phys.* 152.14 (2020), p. 144107. ISSN: 0021-9606. DOI: 10.1063/5.0005081.

[126] L. Z. Stolarczyk. "Complete active space coupled-cluster method. Extension of single-reference coupled-cluster method using the CASSCF wavefunction". In: *Chem. Phys. Lett.* 217 (1994), pp. 1–6. DOI: 10.1016/0009-2614(93)E1333-C.

[127] K. Jankowski and K. Kowalski. "Approximate coupled cluster methods based on a split-amplitude strategy". In: *Chem. Phys. Lett.* 256 (1996), pp. 141–148. DOI: 10.1016/0009-2614(96)00474-5.

[128] J. E. Deustua, J. Shen, and P. Piecuch. "Converging High-Level Coupled-Cluster Energetics by Monte Carlo Sampling and Moment Expansions". In: *Phys. Rev. Lett.* 119.22 (2017), p. 223003. ISSN: 0031-9007, 1079-7114. DOI: 10.1103/PhysRevLett.119.223003.

[129] J. E. Deustua, I. Magoulas, J. Shen, and P. Piecuch. "Communication: Approaching Exact Quantum Chemistry by Cluster Analysis of Full Configuration Interaction Quantum Monte Carlo Wave Functions". In: *J. Chem. Phys.* 149.15 (2018), p. 151101. DOI: 10.1063/1.5055769.

[130] D. I. Lyakh, V. F. Lotrich, and R. J. Bartlett. "The 'Tailored' CCSD(T) Description of the Automerization of Cyclobutadiene". In: *Chem. Phys. Lett.* 501.4 (2011), pp. 166–171. DOI: 10.1016/j.cplett.2010.11.058.

[131] M. Moerchen, L. Freitag, and M. Reiher. "Tailored coupled cluster theory in varying correlation regimes". In: *J. Chem. Phys.* 153 (2020), p. 244113. DOI: 10.1063/5.0032661.

[132] J. D. Watts, J. Gauss, and R. Bartlett. "Coupled cluster methods with noniterative triple excitations for restricted open-shell Hartree-Fock and other general single determinant reference functions. Energies and analytical gradients". In: *J. Chem. Phys.* 98.11 (1993), pp. 8718–8733. DOI: 10.1063/1.464480.

[133] Z. He and D. Cremer. "Analysis of coupled cluster methods. II. What is the best way to account for triple excitations in coupled cluster theory?" In: *Theor. Chim. Acta* 85.4 (1993), pp. 305–323. DOI: 10.1007/BF01129119.

[134] S. A. Kucharski and R. J. Bartlett. "Noniterative energy corrections through fifth-order to the coupled cluster singles and doubles method". In: *J. Chem. Phys.* 108.13 (1998), pp. 5243–5254. DOI: 10.1063/1.475961.

[135] M. Urban, J. Noga, S. J. Cole, and R. J. Bartlett. "Towards a full CCSDT model for electron correlation". In: *J. Chem. Phys.* 83.8 (1985), pp. 4041–4046. DOI: 10.1063/1.449067.

[136] D. Bohm and D. Pines. "A Collective Description of Electron Interactions: III. Coulomb Interactions in a Degenerate Electron Gas". In: *Phys. Rev.* 92 (3 1953), pp. 609–625. DOI: 10.1103/PhysRev.92.609.

[137] X. Ren, P. Rinke, C. Joas, and M. Scheffler. "Random-phase approximation and its applications in computational chemistry and materials science". In: *J. Mater. Sci.* 47 (2012), pp. 7447–7471. DOI: 10.1007/s10853-012-6570-4.

[138] G. E. Scuseria, T. M. Henderson, and D. C. Sorensen. "The ground state correlation energy of the random phase approximation from a ring coupled cluster doubles approach". In: *J. Chem. Phys.* 129.23 (2008), p. 231101. DOI: 10.1063/1.3043729.

[139] P. J. Knowles and N. C. Handy. "A determinant based full configuration interaction program". In: *Comput. Phys. Commun.* 54 (1989), 75–83. DOI: 10.1016/0010-4655(89)90033-7.

[140] T. Kato. "On the eigenfunctions of many-particle systems in quantum mechanics". In: *Comm. Pure Appl. Math.* 10.2 (1957), pp. 151–177. DOI: https://doi.org/10.1002/cpa.3160100201.

[141] E. F. Valeev. "Coupled-cluster methods with perturbative inclusion of explicitly correlated terms: a preliminary investigation". In: *Phys. Chem. Chem. Phys.* 10 (2008), pp. 106–113. DOI: 10.1039/B713938A.

[142] D. Kats and D. P. Tew. "Orbital-Optimized Distinguishable Cluster Theory with Explicit Correlation". In: *J. Chem. Theory Comput.* 15.1 (2019), p. 13. ISSN: 1549-9618. DOI: 10.1021/acs.jctc.8b01047.

[143] T. B. Adler, G. Knizia, and H.-J. Werner. "A simple and efficient CCSD(T)-F12 approximation". In: *J. Chem. Phys.* 127 (2007), p. 221106. DOI: 10.1063/1.2817618.

[144] G. Knizia, T. B. Adler, and H.-J. Werner. "Simplified CCSD(T)-F12 methods: Theory and benchmarks". In: *J. Chem. Phys.* 130 (2009), p. 054104. DOI: doi:10.1063/1.3054300.

[145] G. H. Booth, D. Cleland, A. Alavi, and D. P. Tew. "An Explicitly Correlated Approach to Basis Set Incompleteness in Full Configuration Interaction Quantum Monte Carlo". In: *J. Chem. Phys.* 137.16 (2012), p. 164112. ISSN: 0021-9606. DOI: 10.1063/1.4762445.

[146] J. a. F. Kersten, G. H. Booth, and A. Alavi. "Assessment of Multireference Approaches to Explicitly Correlated Full Configuration Interaction Quantum Monte Carlo". In: *J. Chem. Phys.* 145.5 (2016), p. 054117. ISSN: 0021-9606. DOI: 10.1063/1.4959245.

[147] E. Vitale, A. Alavi, and D. Kats. "FCIQMC-Tailored Distinguishable Cluster Approach". In: *J. Chem. Theory Comput.* 16 (2020), pp. 5621–5634. DOI: 10.1021/acs.jctc.0c00470.

[148] P. J. Hay, J. T. H. Dunning, and W. A. G. III. "Configuration interaction studies of O_3 and O_3^+. Ground and excited states". In: *J. Chem. Phys.* 62 (1975), p. 3912. DOI: 10.1063/1.430306.

[149] P. J. Hay and J. T. H. Dunning. "Geometries and energies of the excitedstates of O_3 from abinitio potential energysurfaces". In: *J. Chem. Phys.* 67 (1977), p. 2290. DOI: 10.1063/1.435064.

[150] W. D. Laidig and H. F. Schaefer. "Large multiconfiguration self-consistent-field wave functions for the ozone molecule". In: *J. Chem. Phys.* 74 (1980), p. 3411. DOI: 10.1063/1.441494.

[151] S. M. Adler-Golden, S. R. Langhoff, J. C. W. Bauschlicher, and G. D. Carney. "Theoretical calculation of ozone vibrational infrared intensities". In: *J. Chem. Phys.* 83 (1985), p. 255. DOI: 10.1063/1.449818.

[152] T. Shiozaki, G. Knizia, and H.-J. Werner. "Explicitly correlated multireference configuration interaction: MRCI-F12". In: *J. Chem. Phys.* 134 (2011), p. 034113. DOI: 10.1063/1.3528720.

[153] D. J. Coughtrie, R. Giereth, D. Kats, H.-J. Werner, and A. Köhn. "Embedded Multireference Coupled Cluster Theory". In: *J. Chem. Theory Comput.* 14.2 (2018), pp. 693–709. ISSN: 1549-9618. DOI: 10.1021/acs.jctc.7b01144.

[154] W. D. Laidig, P. Saxe, and R. J. Bartlett. "The description of N2 and F2 potential energy surfaces using multireference coupled cluster theory". In: *J. Chem. Phys.* 86.2 (1987), pp. 887–907. DOI: 10.1063/1.452291.

[155] K. A. Peterson and T. H. Dunning. "Intrinsic Errors in Several ab Initio Methods: The Dissociation Energy of N2". In: *J. Phys. Chem.* 99.12 (1995), pp. 3898–3901. DOI: 10.1021/j100012a005.

[156] D. Feller. "A comparison of techniques for predicting higher order correlation effects: Diatomic dissociation energies". In: *J. Chem. Phys.* 111.10 (1999), pp. 4373–4382. DOI: 10.1063/1.479202.

[157] X. Li and J. Paldus. "Full potential energy curve for N2 by the reduced multireference coupled-cluster method". In: *J. Chem. Phys.* 129.5 (2008), p. 054104. DOI: 10.1063/1.2961033.

[158] X. Li and J. Paldus. "Dissociation of N_2 triple bond: a reduced multireference CCSD study". In: *Chem. Phys. Lett.* 286.1-2 (1998), pp. 145–154. DOI: 10.1016/S0009-2614(97)01132-9.

[159] X. Li and J. Paldus. "Simultaneous handling of dynamical and nondynamical correlation via reduced multireference coupled cluster method: Geometry and harmonic force field of ozone". In: *J. Chem. Phys.* 110.6 (1999), pp. 2844–2852. DOI: 10.1063/1.477926.

[160] X. Li and J. Paldus. "Reduced multireference coupled cluster method: Rovibrational spectra of N_2". In: *J. Chem. Phys.* 113.22 (2000), pp. 9966–9977. DOI: 10.1063/1.1323260.

[161] R. J. Le Roy, Y. Huang, and C. Jary. "An accurate analytic potential function for ground-state N2 from a direct-potential-fit analysis of spectroscopic data". In: *J. Chem. Phys.* 125.16 (2006), p. 164310. DOI: 10.1063/1.2354502.

[162] D. Kats and A. Köhn. "On the Distinguishable Cluster Approximation for Triple Excitations". In: *J. Chem. Phys.* 150.15 (2019), p. 151101. ISSN: 0021-9606. DOI: 10.1063/1.5096343.

[163] G. Emerson, L. Watts, and R. Pettit. "Cyclobutadiene- and Benzocyclobutadiene-Iron Tricarbonyl Complexes". In: *J. Chem. Phys.* 87 (1965). ISSN: 131. DOI: https://doi.org/10.1021/ja01079a032.

[164] P. Reeves, J. Henery, and R. Pettit. "Further Experiments Pertaining to the Ground State of Cyclobutadiene". In: *J. Am. Chem. Soc.* 91 (1969). ISSN: 5888-5890. DOI: https://doi.org/10.1021/ja01049a042.

[165] P. Reeves, T. Devon, and R. Pettit. "Possible rectangular nature of cyclobutadiene". In: *J. Am. Chem. Soc.* 91 (1969). ISSN: 5890-5891. DOI: https://doi.org/10.1021/ja01049a043.

[166] N. C. Baird. "Quantum organic photochemistry. II. Resonance and aromaticity in the lowest $^3\pi\pi^*$ state of cyclic hydrocarbons". In: *J. Am. Chem. Soc.* 94 (1972). ISSN: 4941-4948. DOI: https://doi.org/10.1021/ja00769a025.

[167] T. Bally and S. Masamune. "Cyclobutadiene". In: *Tetrahedron* 36 (1980). ISSN: 343. DOI: https://doi.org/10.1016/0040-4020(80)87003-7.

[168] A. Balkova and R. J. Bartlett. "A multireference coupled-cluster study of the ground state and lowest excited states of cyclobutadiene". In: *J. Chem. Phys.* 101.10 (1994), pp. 8972–8987. DOI: 10.1063/1.468025.

[169] S. Levchenko and A. Krylov. "Equation-of-motion spin-flip coupled-cluster model with single and double substitutions: Theory and application to cyclobutadiene". In: *J. Chem. Phys.* 120 (2004). ISSN: 175. DOI: https://doi.org/10.1063/1.1630018.

[170] M. Eckert-Maksić, M. Vazdar, M. Barbatti, H. Lischka, and Z. B. Maksić. "Automerization reaction of cyclobutadiene and its barrier height: An ab initio benchmark multireference average-quadratic coupled cluster study". In: *J. Chem. Phys.* (2006). ISSN: 064310. DOI: https://doi.org/10.1063/1.2222366.

[171] X. Li and J. Paldus. "Accounting for the exact degeneracy and quasidegeneracy in the automerization of cyclobutadiene via multireference coupled-cluster methods". In: *J. Chem. Phys.* 131 (2009). ISSN: 114103. DOI: https://doi.org/10.1063/1.3225203.

[172] S. Sinha Ray, S. Manna, A. Ghosh, R. K. Chaudhuri, and S. Chattopadhyay. "Multireference perturbation theory with improved virtual orbitals for radicals: More degeneracies, more problems". In: *Int. J. Quantum Chem.* 119.4 (). DOI: https://doi.org/10.1002/qua.25776.

[173] D. W. Whitman and B. K. Carpenter. "Limits on the activation parameters for automerization of cyclobutadiene-1,2-d2". In: *J. Am. Chem. Soc.* 104 (1982). ISSN: 6473–6474. DOI: https://doi.org/10.1021/ja00387a065.

[174] B. K. Carpenter. "Heavy-atom tunneling as the dominant pathway in a solution-phase reaction? Bond shift in antiaromatic annulenes". In: *J. Am. Chem. Soc.* 105 (1983). ISSN: 1700–1701. DOI: https://doi.org/10.1021/ja00344a073.

[175] K. Bhaskaran-Nair, O. Demel, and J. Pittner. "Multireference state-specific Mukherjee's coupled cluster method with noniterative triexcitations". In: *J. Chem. Phys.* 129.18 (2008), p. 184105. DOI: 10.1063/1.3006401.

[176] G. E. Scuseria, T. J. Lee, A. C. Scheiner, and H. F. S. III. "Ordering of the O–O stretching vibrational frequencies in ozone". In: *J. Chem. Phys.* 90 (1989), p. 5635. DOI: 10.1063/1.456417.

[177] T. J. Lee and G. E. Scuseria. "The vibrational frequencies of ozone". In: *J. Chem. Phys.* 93 (1990), p. 489. DOI: 10.1063/1.459548.

[178] J. D.Watts, J. F.Stanton, and R. J.Bartlett. "A benchmark coupled-cluster single, double, and triple excitation (CCSDT) study of the structure and harmonic vibrational frequencies of the ozone molecule". In: *Chem. Phys. Lett.* 178 (1991), p. 471. DOI: 10.1016/0009-2614(91)87004-U.

[179] T. Müller, S. S. Xantheas, H. Dachsel, R. J. Harrison, J. Nieplocha, R. Shephard, G. S. Keziora, and H. Lischka. "A systematic ab initio investigation of the open and ring structures of ozone". In: *Chem. Phys. Lett.* 293 (1998), p. 72. DOI: 10.1016/S0009-2614(98)00798-2.

[180] O. Hino, T. Kinoshita, G. K.-L. Chan, and R. J. Bartlett. "Tailored Coupled Cluster Singles and Doubles Method Applied to Calculations on Molecular Structure and Harmonic Vibrational Frequencies of Ozone". In: *J. Chem. Phys.* 124.11 (2006), p. 114311. ISSN: 0021-9606. DOI: 10.1063/1.2180775.

[181] E. Miliordos and S. S. Xantheas. "On the Bonding Nature of Ozone (O_3) and Its Sulfur-Substituted Analogues SO_2,OS_2, and S_3: Correlation between Their Biradical Character and Molecular Properties". In: *J. Am. Chem. Soc.* 136 (2014), 2808-2817. DOI: 10.1021/ja410726u.

[182] S. Azadi, R. Singh, and T. D. Kühne. "Resonating valence bond quantum Monte Carlo: Application to the ozone molecule". In: *Int. J. Quantum Chem.* 115 (2015), pp. 1673–1677. DOI: 10.1002/qua.25005.

[183] D. Theis, J. Ivanic, T. L. Windus, and K. Ruedenberg. "The transition from the open minimum to the ring minimum on the ground state and on the lowest excited state of like symmetry in ozone: A configuration interaction study". In: *J. Chem. Phys.* 144 (2016), p. 104304. DOI: 10.1063/1.4942019.

[184] A. M. Sand, C. E. Hoyer, K. Sharkas, K. M. Kidder, R. Lindh, D. G. Truhlar, and L. Gagliardi. "Analytic Gradients for Complete Active Space Pair-Density Functional Theory". In: *J. Chem. Theory Comput.* 14 (2018), 126-138. DOI: 10.1021/acs.jctc.7b00967.

[185] S. Shih, R. Buenker, and S. Peyerimhoff. "Theoretical investigation of the cyclic conformer of ozone". In: *Chem. Phys. Lett.* 28 (1974), p. 463. DOI: 10.1016/0009-2614(74)80080-1.

[186] T. J. Lee. "On the energy separation between the open and cyclic forms of ozone". In: *Chem. Phys. Lett.* 169 (1990), p. 529. DOI: 10.1016/0009-2614(90)85642-P.

[187] A. D. Chien, A. A. Holmes, M. Otten, C. J. Umrigar, S. Sharma, and P. M. Zimmerman. "Excited States of Methylene, Polyenes, and Ozone from Heat-Bath Configuration Interaction". In: *J. Phys. Chem. A* 122.10 (2018), pp. 2714–2722. DOI: 10.1021/acs.jpca.8b01554.

[188] A. Melnichuk and R. J. Bartlett. "Relaxed Active Space: Fixing Tailored-CC with High Order Coupled Cluster. I". In: *J. Chem. Phys.* 137.21 (2012), p. 214103. DOI: 10.1063/1.4767900.

[189] A. Melnichuk and R. J. Bartlett. "Relaxed Active Space: Fixing Tailored-CC with High Order Coupled Cluster. II". In: *J. Chem. Phys.* 140.6 (2014), p. 064113. DOI: 10.1063/1.4862676.

[190] A. Köhn, M. Hanauer, L. A. Mück, T.-C. Jagau, and J. Gauss. "State-Specific Multireference Coupled-Cluster Theory". In: *WIREs Comput. Mol. Sci.* 3.2 (2013), pp. 176–197. DOI: 10.1002/wcms.1120.

[191] C. Duboc and M. Gennari. "Experimental Techniques for Determining Spin States". In: *Spin States in Biochemistry and Inorganic Chemistry*. John Wiley & Sons, Ltd, 2015. Chap. 4, pp. 59–83. ISBN: 9781118898277. DOI: https://doi.org/10.1002/9781118898277.ch4.

[192] C. Sousa and C. de Graaf. "Ab Initio Wavefunction Approaches to Spin States". In: *Spin States in Biochemistry and Inorganic Chemistry*. John Wiley & Sons, Ltd, 2015. Chap. 3, pp. 35–57. ISBN: 9781118898277. DOI: https://doi.org/10.1002/9781118898277.ch3.

[193] M. Costas and J. Harvey. "Discussion of an open problem". In: *Nature Chem.* 5 (2013), pp. 7–9. DOI: https://doi.org/10.1038/nchem.1533.

[194] G. Ganzenmueller, N. Berkaine, A. Fouqueau, M. E. Casida, and M. Reiher. "Comparison of density functionals for differences between the high- ($^5T_{2g}$) and low- ($^1A_{1g}$) spin states of iron(II) compounds. IV. Results for the ferrous complexes [Fe(L)('NHS4')]". In: *J. Chem. Phys.* 122.23 (2005), p. 234321. DOI: 10.1063/1.1927081.

[195] M. Swart, A. R. Groenhof, A. W. Ehlers, and K. Lammertsma. "Validation of Exchange-Correlation Functionals for Spin States of Iron Complexes". In: *J. Phys. Chem. A* 108.25 (2004), pp. 5479–5483. DOI: 10.1021/jp049043i.

[196] M. Swart. "Accurate Spin-State Energies for Iron Complexes". In: *J. Chem. Theory Comput.* 4.12 (2008), pp. 2057–2066. DOI: 10.1021/ct800277a.

[197] C. J. Cramer and D. G. Truhlar. "Density functional theory for transition metals and transition metal chemistry". In: *Phys. Chem. Chem. Phys.* 11 (46 2009), pp. 10757–10816. DOI: 10.1039/B907148B.

[198] A. Ghosh. "High-level ab initio calculations on the energetics of low-lying spin states of biologically relevant transition metal complexes: a first progress report". In: *Current Opinion in Chemical Biology* 7.1 (2003), pp. 113–124. ISSN: 1367-5931. DOI: https://doi.org/10.1016/S1367-5931(02)00023-6.

[199] J. Harvey. "DFT Computation of Relative Spin-State Energetics of Transition Metal Compounds". In: *Principles and Applications of Density Functional Theory in Inorganic Chemistry I. Structure and Bonding*. Vol. 112. Springer, 2004. DOI: https://doi.org/10.1007/b97939.

[200] A. Ghosh and P. R. Taylor. "Transition metal spin state energetics and noninnocent systems: challenges for DFT in the bioinorganic arena". In: *J. Biol. Inorg. Chem.* 11 (2006), pp. 712–724. DOI: 10.1007/s00775-006-0135-4.

[201] J. Harvey. "On the accuracy of density functional theory in transition metal chemistry". In: *Annu. Rep. Prog. Chem., Sect. C* 102 (2006), pp. 203–226. DOI: 10.1039/B419105F.

[202] E. Vitale, G. Li Manni, A. Alavi, and D. Kats. "FCIQMC-Tailored Distinguishable Cluster Approach: Open-Shell Systems". In: *J. Chem. Theory Comput.* 18 (2022), p. 3427. DOI: 10.1021/acs.jctc.2c00059.

[203] A. Fouqueau, M. E. Casida, L. M. L. Daku, A. Hauser, and F. Neese. "Comparison of density functionals for energy and structural differences between the high-$[^5T_{2g}:(t_{2g})^4(e_g)^2]$ and low- $[^1A_{1g}:(t_{1g})^6(e_g)^0]$ spin states of iron(II) coordination compounds. II. More functionals and the hexaminoferrous cation, $[Fe(NH_3)_6]^{2+}$". In: *J. Chem. Phys.* 122.4 (2005), p. 044110. DOI: 10.1063/1.1839854.

[204] K. Pierloot and S. Vancoillie. "Relative energy of the high-($^5T_{2g}$) and low-($^1A_{1g}$) spin states of $[Fe(H_2O)_6]^{2+}$, $[Fe(NH_3)_6]^{2+}$, and $[Fe(bpy)_3]^{2+}$: CASPT2 versus density functional theory". In: *J. Chem. Phys.* 125.12 (2006), p. 124303. DOI: 10.1063/1.2353829.

[205] M. Kepenekian, V. Robert, B. Le Guennic, and C. De Graaf. "Energetics of $[Fe(NCH)_6]^{2+}$ via CASPT2 calculations: A spin-crossover perspective". In: *J. Comput. Chem.* 30.14 (2009), pp. 2327–2333. DOI: https://doi.org/10.1002/jcc.21236.

[206] A. Domingo, M. Àngels Carvajal, and C. de Graaf. "Spin crossover in Fe(II) complexes: An ab initio study of ligand σ-donation". In: *Int. J. Quantum Chem.* 110.2 (2010), pp. 331–337. DOI: https://doi.org/10.1002/qua.22105.

[207] L. M. Lawson Daku, F. Aquilante, T. W. Robinson, and A. Hauser. "Accurate Spin-State Energetics of Transition Metal Complexes. 1. CCSD(T), CASPT2, and DFT Study of $[M(NCH)_6]^{2+}$ (M = Fe, Co)". In: *J. Chem. Theory Comput.* 8.11 (2012), pp. 4216–4231. DOI: 10.1021/ct300592w.

[208] A. Droghetti, D. Alfè, and S. Sanvito. "Assessment of density functional theory for iron(II) molecules across the spin-crossover transition". In: *J. Chem. Phys.* 137.12 (2012), p. 124303. DOI: 10.1063/1.4752411.

[209] M. Fumanal, L. K. Wagner, S. Sanvito, and A. Droghetti. "Diffusion Monte Carlo Perspective on the Spin-State Energetics of $[Fe(NCH)_6]^{2+}$". In: *J. Chem. Theory Comput.* 12.9 (2016), pp. 4233–4241. DOI: 10.1021/acs.jctc.6b00332.

[210] L. Wilbraham, P. Verma, D. G. Truhlar, L. Gagliardi, and I. Ciofini. "Multiconfiguration Pair-Density Functional Theory Predicts Spin-State Ordering in Iron Complexes with the Same Accuracy as Complete Active Space Second-Order Perturbation Theory at a Significantly Reduced Computational Cost". In: *J. Phys. Chem. Lett.* 8.9 (2017), pp. 2026–2030. DOI: 10.1021/acs.jpclett.7b00570.

[211] S. Song, M.-C. Kim, E. Sim, A. Benali, O. Heinonen, and K. Burke. "Benchmarks and Reliable DFT Results for Spin Gaps of Small Ligand Fe(II) Complexes". In: *J. Chem. Theory Comput.* 14.5 (2018), pp. 2304–2311. DOI: 10.1021/acs.jctc.7b01196.

[212] B. M. Floeser, Y. Guo, C. Riplinger, F. Tuczek, and F. Neese. "Detailed Pair Natural Orbital-Based Coupled Cluster Studies of Spin Crossover Energetics". In: *J. Chem. Theory Comput.* 16.4 (2020), pp. 2224–2235. DOI: 10.1021/acs.jctc.9b01109.

[213] L. A. Mariano, B. Vlaisavljevich, and R. Poloni. "Biased Spin-State Energetics of Fe(II) Molecular Complexes within Density-Functional Theory and the Linear-Response Hubbard U Correction". In: *J. Chem. Theory Comput.* 16.11 (2020), pp. 6755–6762. DOI: 10.1021/acs.jctc.0c00628.

[214] L. A. Mariano, B. Vlaisavljevich, and R. Poloni. "Improved Spin-State Energy Differences of Fe(II) Molecular and Crystalline Complexes via the Hubbard U-Corrected Density". In: *J. Chem. Theory Comput.* 17.5 (2021), pp. 2807–2816. DOI: 10.1021/acs.jctc.1c00034.

[215] J. Shee, M. Loipersberger, D. Hait, J. Lee, and M. Head-Gordon. "Revealing the nature of electron correlation in transition metal complexes with symmetry breaking and chemical intuition". In: *J. Chem. Phys.* 154.19 (2021), p. 194109. DOI: 10.1063/5.0047386.

[216] K. Pierloot, Q. M. Phung, and A. Domingo. "Spin State Energetics in First-Row Transition Metal Complexes: Contribution of (3s3p) Correlation and Its Description by Second-Order Perturbation Theory". In: *J. Chem. Theory Comput.* 13.2 (2017), pp. 537–553. DOI: 10.1021/acs.jctc.6b01005.

[217] Q. M. Phung, M. Feldt, J. N. Harvey, and K. Pierloot. "Toward Highly Accurate Spin State Energetics in First-Row Transition Metal Complexes: A Combined CASPT2/CC Approach". In: *J. Chem. Theory Comput.* 14.5 (2018), pp. 2446–2455. DOI: 10.1021/acs.jctc.8b00057.

[218] D. Zhang and D. G. Truhlar. "Spin Splitting Energy of Transition Metals: A New, More Affordable Wave Function Benchmark Method and Its Use to Test Density Functional Theory". In: *J. Chem. Theory Comput.* 16.7 (2020), pp. 4416–4428. DOI: 10.1021/acs.jctc.0c00518.

[219] M. Radón. "Spin-State Energetics of Heme-Related Models from DFT and Coupled Cluster Calculations". In: *J. Chem. Theory Comput.* 10.6 (2014), pp. 2306–2321. DOI: 10.1021/ct500103h.

[220] G. Li Manni and A. Alavi. "Understanding the Mechanism Stabilizing Intermediate Spin States in Fe(II)-Porphyrin". In: *J. Phys. Chem. A* 122.22 (2018), pp. 4935–4947. DOI: 10.1021/acs.jpca.7b12710.

[221] G. Li Manni, D. Kats, D. P. Tew, and A. Alavi. "Role of Valence and Semicore Electron Correlation on Spin Gaps in Fe(II)-Porphyrins". In: *J. Chem. Theory Comput.* 15.3 (2019), pp. 1492–1497. ISSN: 1549-9618. DOI: 10.1021/acs.jctc.8b01277.

[222] O. Weser, L. Freitag, K. Guther, A. Alavi, and G. Li Manni. "Chemical insights into the electronic structure of Fe(II) porphyrin using FCIQMC, DMRG, and generalized active spaces". In: *Int. J. Quantum Chem.* 121.3 (2020), e26454. DOI: https://doi.org/10.1002/qua.26454.

[223] Q. M. Phung, M. Feldt, J. N. Harvey, and K. Pierloot. "Toward Highly Accurate Spin State Energetics in First-Row Transition Metal Complexes: A Combined CASPT2/CC Approach". In: *J. Chem. Theory Comput.* 14.5 (2018), pp. 2446–2455. DOI: 10.1021/acs.jctc.8b00057.

[224] Y. Guo, C. Riplinger, U. Becker, D. G. Liakos, Y. Minenkov, L. Cavallo, and F. Neese. "Communication: An improved linear scaling perturbative triples correction for the domain based local pair-natural orbital based singles and doubles coupled cluster method [DLPNO-CCSD(T)]". In: *J. Chem. Phys.* 148.1 (2018), p. 011101. DOI: 10.1063/1.5011798.

[225] O. Weser, K. Guther, K. Ghanem, and G. Li Manni. "Stochastic Generalized Active Space Self-Consistent Field: Theory and Application". In: *J. Chem. Theory Comput.* 18.1 (2022), 251–272. DOI: 10.1021/acs.jctc.1c00936.

[226] J. Hachmann, W. Cardoen, and G. Chan. "Multireference correlation in long molecules with the quadratic scaling density matrix renormalization group". In: *J. Chem. Phys.* 125.14 (2006), p. 144101. DOI: 10.1063/1.2345196.

[227] W. A. Al-Saidi, S. Zhang, and H. Krakauer. "Bond breaking with auxiliary-field quantum Monte Carlo". In: *J. Chem. Phys.* 127.14 (2007), p. 144101. DOI: 10.1063/1.2770707.

[228] T. Tsuchimochi and G. E. Scuseria. "Strong correlations via constrained-pairing mean-field theory". In: *J. Chem. Phys.* 131.12 (2009), p. 121102. DOI: 10.1063/1.3237029.

[229] A. V. Sinitskiy, L. Greenman, and D. A. Mazziotti. "Strong correlation in hydrogen chains and lattices using the variational two-electron reduced density matrix method". In: *J. Chem. Phys.* 133.1 (2010), p. 014104. DOI: 10.1063/1.3459059.

[230] N. Lin, C. A. Marianetti, A. J. Millis, and D. R. Reichman. "Dynamical Mean-Field Theory for Quantum Chemistry". In: *Phys. Rev. Lett.* 106 (9 2011), p. 096402. DOI: 10.1103/PhysRevLett.106.096402.

[231] L. Stella, C. Attaccalite, S. Sorella, and A. Rubio. "Strong electronic correlation in the hydrogen chain: A variational Monte Carlo study". In: *Phys. Rev. B* 84 (24 2011), p. 245117. DOI: 10.1103/PhysRevB.84.245117. URL: https://link.aps.org/doi/10.1103/PhysRevB.84.245117.

[232] M. Motta, D. M. Ceperley, G. K.-L. Chan, J. A. Gomez, E. Gull, S. Guo, C. A. Jiménez-Hoyos, T. N. Lan, J. Li, F. Ma, A. J. Millis, N. V. Prokof'ev, U. Ray, G. E. Scuseria, S. Sorella, E. M. Stoudenmire, Q. Sun, I. S. Tupitsyn, S. R. White, D. Zgid, and S. Zhang. "Towards the Solution of the Many-Electron Problem in Real Materials: Equation of State of the Hydrogen Chain with State-of-the-Art Many-Body Methods". In: *Phys. Rev. X* 7 (3 2017), p. 031059. DOI: 10.1103/PhysRevX.7.031059.

[233] J. J. Eriksen and J. Gauss. "Many-Body Expanded Full Configuration Interaction. II. Strongly Correlated Regime". In: *J. Chem. Theory Comput.* 15.9 (2019), pp. 4873–4884. DOI: 10.1021/acs.jctc.9b00456.

[234] D. Vollhardt. "The Rich Inner Life of the Hydrogen Chain". In: *Phys.* 13.142 (2020). DOI: 10.1103/Physics.13.142.

[235] M. Motta, C. Genovese, F. Ma, Z.-H. Cui, R. Sawaya, G. K.-L. Chan, N. Chepiga, P. Helms, C. Jiménez-Hoyos, A. J. Millis, U. Ray, E. Ronca, H. Shi, S. Sorella, E. M. Stoudenmire, S. R. White, and S. Zhang. "Ground-State Properties of the Hydrogen Chain: Dimerization, Insulator-to-Metal Transition, and Magnetic Phases". In: *Phys. Rev. X* 10 (3 2020), p. 031058. DOI: 10.1103/PhysRevX.10.031058.